DER MATERIALS QUARTERLY PROGRESS REPORT

For the Period
October 1, 2003 to December 31, 2003

Prepared by:

David P. Stinton, Manager, and
Roxanne A. Raschke
DER Materials Research
Oak Ridge National Laboratory

For:

Department of Energy
Office of Distributed Energy

DER MATERIALS QUARTERLY PROGRESS REPORT

October—December 2003

TABLE OF CONTENTS

Mechanical Characterization of Monolithic Silicon Nitride Si_3N_4
R. R. Wills, S. Hilton, and S. Goodrich
University of Dayton Research Institute, Dayton, Ohio

Microstructural Characterization of CFCCs and Protective Coatings
K. L. More
Oak Ridge National Laboratory, Oak Ridge, Tennessee

DEVELOPMENT OF MONOLITHIC CERAMICS AND HIGH-TEMPERATURE COATINGS

Kennametal's Hot-Section Materials Development
R. Yeckley
Kennametal, Inc., Latrobe, Pennsylvania

Saint-Gobain Hot Section Materials Development
R. H. Licht
Saint-Gobain Ceramics & Plastics, Inc., Northboro, Massachusetts

Environmental Protection Systems for Ceramics in Microturbines and Industrial Gas Turbine Applications, Part A: Conversion Coatings
S. D. Nunn and R. A. Lowden
Oak Ridge National Laboratory, Oak Ridge, Tennessee

Environmental Protection Systems for Ceramics in Microturbines and Industrial Gas Turbine Applications, Part B: Slurry Coatings and Surface Alloying
B. L. Armstrong, K. M. Cooley, M. P. Brady, H-T Lin, and J. A. Haynes
Oak Ridge National Laboratory, Oak Ridge, Tennessee

Polymer Derived EBC for Monolithic Silicon Nitride
R. Raj
University of Colorado at Boulder
Boulder, Colorado

Failure Mechanisms in Coatings
J. P. Singh, Kedar Sharma, and P. S. Shankar
Argonne National Laboratory, Argonne, Illinois

High-Temperature Diffusion Barriers for Ni-Base Superalloys
B. A. Pint, J. A. Haynes, K. L. More, and I. G. Wright
Oak Ridge National Laboratory, Oak Ridge, Tennessee

POWER ELECTRONICS

High Temperature Heat Exchanger
E. Lara-Curzio
Oak Ridge National Laboratory, Oak Ridge, Tennessee

MATERIALS FOR ADVANCED RECIPROCATING ENGINES

RECUPERATORS

Recuperator Alloys – Composition Optimization for Corrosion Resistance

B. A. Pint
Metals and Ceramics Division
Oak Ridge National Laboratory
Oak Ridge, TN 37831-6156
Phone: (865) 576-2897, E-mail: pintba@ornl.gov

Objective

In order to provide a clear, fundamental understanding of alloy composition effects on corrosion resistance of stainless steel components used in recuperators, the oxidation behavior of model alloys is being studied. The first phase of this study narrowed the range of Cr and Ni contents required to minimize the accelerated corrosion attack caused by water vapor at 650°-800°C. Other factors that continue to be investigated include the effects of temperature, alloy grain size, phase composition and minor alloy additions. These composition and microstructure effects also will provide data for life-prediction models and may suggest a mechanistic explanation for the effect of water vapor on the oxidation of steels. This information will be used to select cost-effective alloys for higher temperature recuperators.

Highlights

The oxidation behavior of model austenitic alloys is being studied in order to better understand the role of minor alloy additions on the accelerated attack (AA) observed in exhaust gas at 650°C-700°C. In order to predict long-term behavior and differentiate the performance of the best alloys in shorter test times, accelerated testing is being explored with higher temperatures (800°C) or higher cycle frequency (1h instead of 100h). Higher temperature testing of commercial alloy foil materials shows the benefit of higher Cr and Ni contents such as those found in alloy 120 or 625. At 800°C, the benefit of an Al addition also is evident.

Technical Progress

Experimental Procedure

As outlined in previous reports, model alloys were vacuum induction melted and cast in a water-chilled copper mold, followed by hot forging and rolling to 2.5mm. The sheets were then cold rolled to 1.25mm and annealed under Ar + 4%H_2 for 2 min at 1000°C. Sheet specimens (12mm x 17mm x 1.2mm) were polished to 600 grit SiC finish. Chemical compositions were measured by combustion and plasma analysis after casting, Table I. The oxidation tests were done in air + 10 vol.% water vapor with 100h cycles at 800°C or 1h cycles at 700°C with 10 min cooling between cycles. After oxidation, selected specimens were Cu-plated, sectioned and polished to examine the oxide scale.

Results of oxidation testing

In an attempt to simulate longer times at lower temperatures and differentiate the performance of the best alloys, exposures at 800°C are being conducted. As reported in previous reports, results at 800°C show beneficial effects of Mn and Si additions for the model alloys with 20%Cr and/or 20%Ni, Figure 1a. Unlike testing at 650° or 700°C, all of the model alloys eventually showed AA. The

Table 1. Alloy chemical compositions (mass %) and average grain sizes (μm)

Material	Cr	Ni	Mn	Si	C	N	Nb	Ti	Mo	Other	aver. grain size
Fe-20Cr-20Ni	19.7	20.1	<	0.01	<	<	<	<	<		14μm
Fe-16Cr-15Ni	15.8	14.8	<	<	0.002	<	<	<	<		24
Fe-16Cr-15Ni+MS	15.8	14.8	1.76	0.24	<	<	<	<	<		21
Fe-16Cr-20Ni+MS	15.8	19.7	1.72	0.24	0.003	0.001	<	<	<		26
Fe-20Cr-15Ni+MS	19.8	14.9	1.70	0.24	0.001	0.007	<	<	<		20
Fe-20Cr-20Ni+Mn	20.0	19.8	1.47	0.01	0.002	0.001	<	<	0.01		16
Fe-20Cr-20Ni+Si	19.9	19.7	<	0.23	0.001	0.005	<	<	<		30
Fe-20Cr-20Ni+La	20.3	19.7	<	<	0.001	0.001	<	<	<	0.10 La	12
Fe-20Cr-20Ni+MS	19.8	19.8	1.69	0.25	<	0.003	<	<	<		25
Fe-20Cr-20Ni+MSL	20.2	19.9	1.61	0.22	0.001	0.011	<	<	<	0.12 La	14
Fe-20Cr-20Ni+etc.	20.9	20.8	3.8	0.24	0.08	0.18	0.25	<	0.31	0.3Cu,0.3Co	55
Fe-15Cr-16Ni-4Al	15.1	15.8	4.8	0.21	0.10	0.19	0.37	<	0.31	3.8Al,4Cu,0.3Co	30
20/25/Nb	22.3	25.0	1.02	0.42	0.02	0.18	0.21	0.04	1.46	0.1Co,0.1V	17
Alloy 120	24.7	37.6	0.73	0.24	0.06	0.20	0.61	0.02	0.28	0.1Al,0.1Co	13
Alloy 625	21	bal.					4		9		

< indicates below the detectability limit of <0.01% or <0.001% for interstitials

specimen of Fe-16Cr-15Ni+Mn,Si showed AA after 200h. A cross-section of the scale after 500h is shown in Figure 2a. A relatively thick oxide is observed despite the large mass losses shown in Figure 1a. Once AA begins, thick oxide forms during each cycle and the mass loss is due to spallation of this reaction product. By increasing both the Cr and Ni contents to 20%, the time to AA was

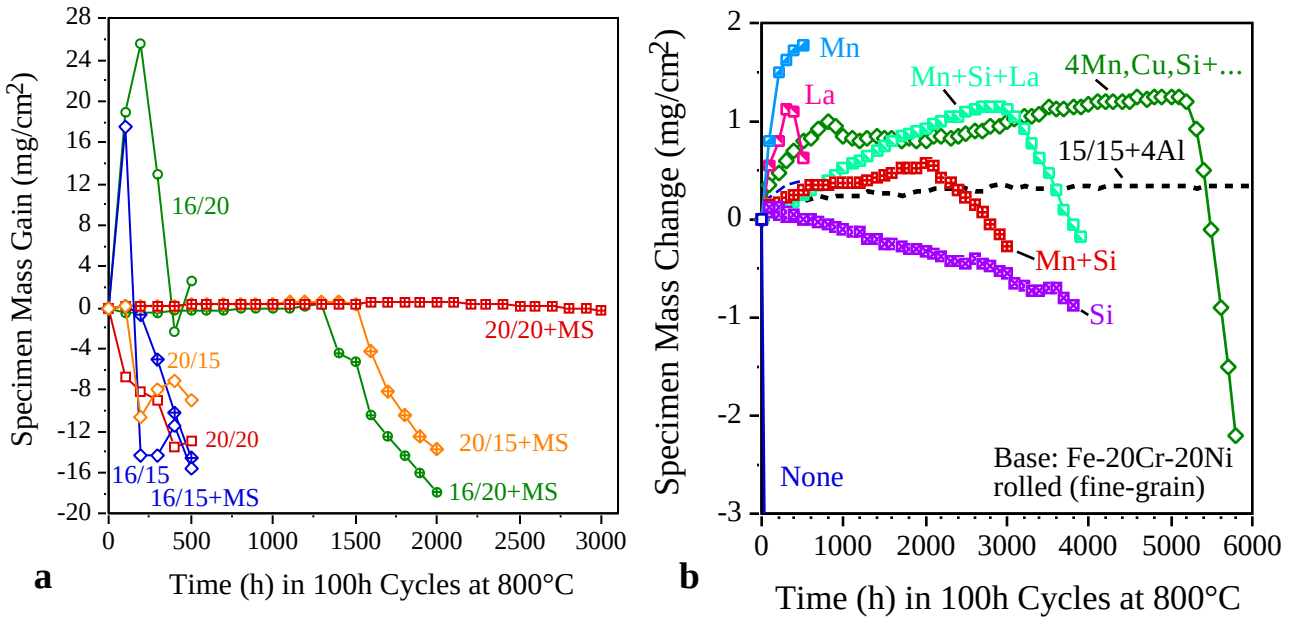

Figure 1. Specimen mass changes for model Fe-Cr-Ni alloys (designated by [Cr]/[Ni]) during 100h cycles at 650°C in air plus 10%H_2O, (a) alloys with and without Mn and Si additions and (b) alloys with a base composition of Fe-20Cr-20Ni. Designations with "+MS" indicate Mn and Si additions.

increased to over 2000h. (The onset of mass losses for this alloy is clearly seen with the expanded y-axis in Figure 1b.) A cross-section of the scale formed on Fe-20Cr-20Ni+Mn,Si after 3000h is shown in Figure 2b. Even after 3000h, the extent of AAwas less on the more highly alloyed material. The specimen of Fe-16Cr-20Ni+Mn,Si began to show AA after 1300h and the scale after 2,000h is shown in Figure 2c. The specimen of Fe-20Cr-15Ni+Mn,Si began to show AA after 1500h and its scale after 2000h is shown in Figure 2d. To illustrate the change between protective scale formation and AA, the scale formed on Fe-20Cr-15Ni+Mn,Si after 500h is shown in Figure 2e. Note the change in magnification as the ≈3μm thick scale after 500h increases to >40μm after 2000h, Figure 2d.

Figure 1b shows the performance of the various versions of Fe-20Cr-20Ni tested at 800°C. Similar to previously reported results at lower temperatures, the single additions of Mn and La did not provide a substantial benefit and the specimen with only Si added showed a continuous mass loss but no AA after 3,500h. As noted above, the specimen with Mn and Si began to show mass loss associated with the onset of AA after 2,000h. Interestingly, the alloy with La in addition to Mn and Si did not show AA until 3,000h. The scale formed on this alloy after 500h is shown in Figure 2f. The scale is thinner than that formed on Fe-20Cr-15Ni+Mn,Si after 500h suggesting a beneficial effect of La at this higher temperature. The addition of La also reduced the alloy grain size (Table I) which has been shown to produce beneficial effects in these alloys. An experimental creep resistant version of Fe-20Cr-20Ni with Mn, Cu, Si and Nb (Table I) did not show AA until 5,000h at 800°C. The initial thicker Mn-rich scale formed on this alloy (indicated by the higher mass gain) may have been beneficial under these conditions by reducing the evaporation of the protective Cr_2O_3 layer. The mass change for another experimental alloy, Fe-15Cr-16Ni-4Al (Table I) also is shown by a dashed line in Figure 1b. The Al was added to improve the oxidation resistance and this alloy has not shown AA after more than 6,000h of testing at 800°C.

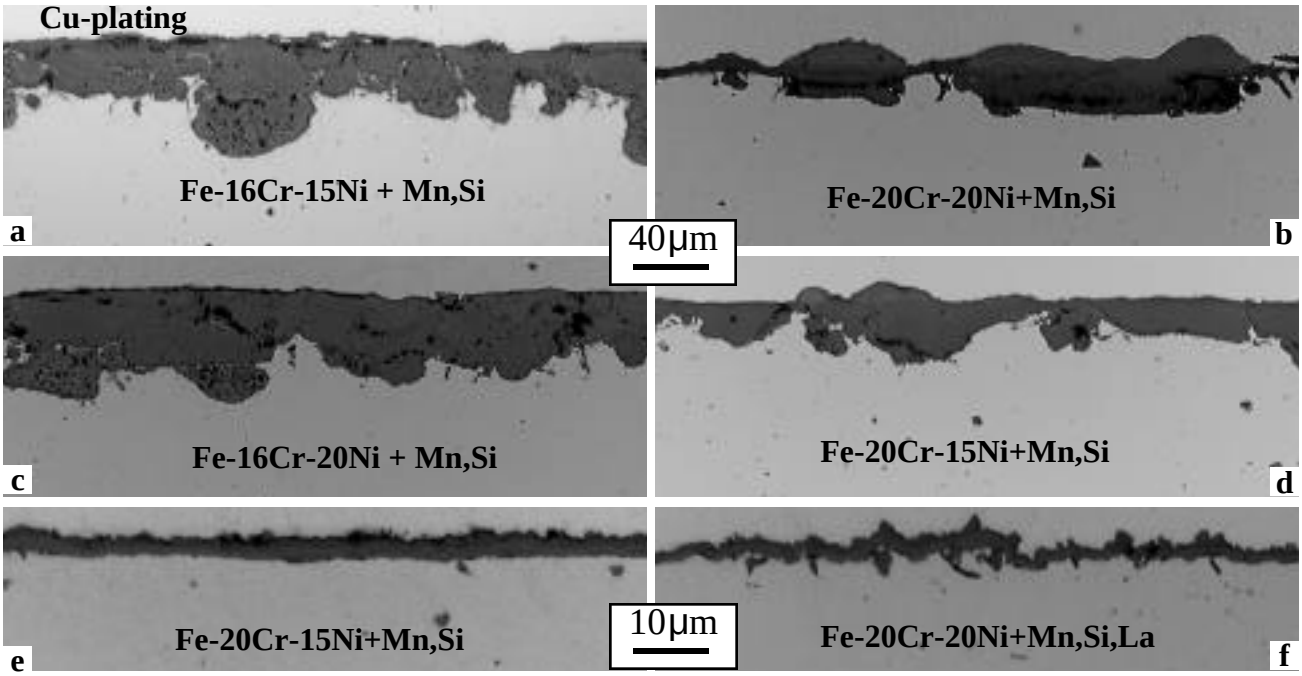

Figure 2. Light microscopy of polished cross-sections of model alloys oxidized for at 800°C in humid air (a) Fe-16Cr-15Ni+Mn,Si after 500h, (b) Fe-20Cr-20Ni+Mn,Si after 3000h, (c) Fe-16Cr-20Ni+Mn,Si after 2000h, (d) Fe-20Cr-15Ni+Mn,Si after 2000h, (e) Fe-20Cr-15Ni+Mn,Si after 500h and (f) Fe-20Cr-20Ni+Mn,Si,La after 500h.

Foil specimens also are being tested at 800°C, Figure 3. This temperature is beyond the capability of type 347 stainless steel from a creep strength standpoint and AA was observed for several types of 347 foils in less than 1,000h. Several 20/25/Nb foil specimens have yielded varying results. In one case, the mass gain remained relatively low while in the other cases discrete jumps in the mass gain were observed followed by low mass gains or slight losses. These rapid increases appear to be localized nodule formation where the nodules did not continue to grow. One foil specimen was removed after 5,000h while 2 others have continued to 6,000 and 7,000h, respectively, where they began to exhibit a continuous increase in mass gain suggesting the onset of AA, Figure 3. Foil specimens of the developmental Fe-20Cr-20Ni-4Mn alloy also are being tested. Like the sheet specimens of this composition, the foil specimens have shown a high mass gain after only 1,500h of testing. With 2 mg/cm^2 mass gain corresponding to >10µm of oxide, the expected lifetime of this material at 800°C appears limited.

Foil specimens of alloy 625 and 120 have exhibited better oxidation resistance during testing at 800°C. They have shown relatively low mass gains or slight losses typical of the combination of scale growth and evaporation. The foil specimen of alloy 120 has just begun to show signs of AA after 8,000h. Compared to 20/25/Nb foil, the longer time before AA for this alloy was expected because of its higher Cr and Ni contents. Exposure of the alloy 625 specimen was stopped after 6,000h for characterization. (A number of foil specimens currently are being characterized to study Cr depletion and oxide formation to gain a better mechanistic understanding of oxidation in these environments.)

Because the various competing mechanisms (Cr diffusion, evaporation and scale growth) are all temperature dependent, increasing the test temperature to 800°C is a questionable strategy. Another

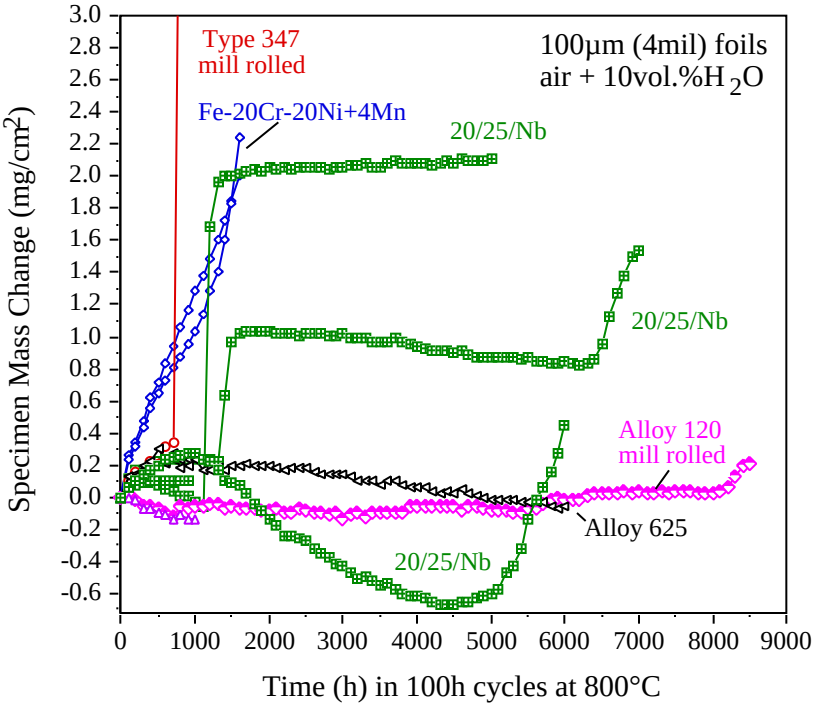

Figure 3. Specimen mass gains for various foil (100µm thick) materials during 100h cycles in humid air at 800°C.

possibility for accelerated testing is to increase the cycle frequency (i.e. decrease the time of each cycle) of the test at a more realistic (lower) temperature. Figure 4 shows results for these model alloys during 1h cycles at 700°C in humid air. Using 1h cycles has led to the onset of AA in several alloys that did not show similar attack during 100h cycles at this temperature. In particular, Fe-16Cr-20Ni+Mn,Si showed AA after ≈300h and Fe-20Cr-15Ni showed AA after 500h, first with a mass increase followed by spallation of the thicker scale. These alloys did not show AA after 50, 100h cycles at 700°C in humid air. Surprisingly, the Fe-20Cr-20Ni+Si specimen also began to show AA in less than 500h. To confirm this result, a second specimen also was tested and showed similar behavior, Figure 4. As at 800°C, the specimens showing the longest life all have Fe-20Cr-20Ni with Mn and Si additions. The specimen of Fe-20Cr-20Ni-4Mn has shown no clear indication of AAafter more than 3,500, 1h cycles. The specimen of Fe-20Cr-20Mn+Mn,Si,La has begun to show a mass increase after 2,000h. However, the specimen with only Mn and Si additions began to show some mass gains and losses after 1,500h and showed consistent mass losses after 3,000h indicating the onset of AA. Thus, earlier failure could be obtained at a lower temperature by increasing the cycle frequency. However, more study is required to determine if these accelerated test results can be correlated with performance in exhaust gas/recuperator environments.

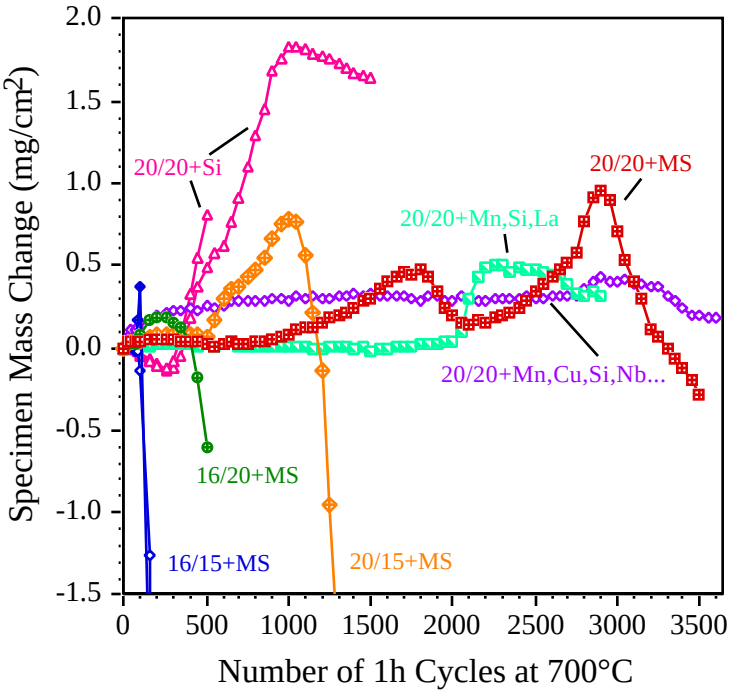

Figure 4. Specimen mass changes for model Fe-Cr-Ni alloys (specified by their Cr/Ni contents) during 1h cycles at 700°C in air plus 10%H_2O. Designations with "+MS" indicate Mn and Si additions.

Status of Milestones

Submit an open literature publication on the development of low cost, oxidation resistant stainless steels for exhaust gas environments. (September, 2004)

Industry Interactions

Discussed materials selection issues with Ingersoll Rand in November 2003.

Discussed materials selection issues with Capstone in December 2003.

Problems Encountered

None.

Publications/Presentations

None.

Recuperator Materials Testing and Evaluation

Edgar Lara-Curzio, Rosa Trejo and K. L. More
Metals and Ceramics Division
Oak Ridge National Laboratory
P.O. Box 2008, Oak Ridge, TN 37831-6069
Phone: (865) 574-1749, E-mail: laracurzioe@ornl.gov

Objective

The objective of this sub-task is to screen and evaluate candidate materials for the next generation of advanced microturbine recuperators. To attain this objective, a commercially-available microturbine was acquired and in coordination and collaboration with its manufacturer, it was modified to operate at recuperator inlet temperatures as high as 843°C. The durability of candidate recuperator materials will be determined by placing test specimens at a location upstream of the recuperator, followed by determination of the evolution of the material's physical and mechanical properties as a function of time of exposure. During exposure tests inside the microturbine, it will be possible to subject test specimens to various levels of mechanical stress by using a specially-designed sample holder and pressurized air. The selection of materials to be evaluated in the modified microturbine will be made in coordination and collaboration with other tasks of this program and with manufacturers of microturbines and recuperators.

Highlights

The first two 500-hr test campaigns to evaluate foils of 347 stainless steel and Haynes 230® Alloy have been completed. A test campaign is in progress to evaluate Haynes 230® and Haynes 120® alloys.

Technical progress

In this document we report the results from the evaluation and characterization of foils of Haynes 230® alloy after a 500-hr test campaign in ORNL's recuperator testing facility. This alloy has been considered a potential candidate material for the manufacture of advanced microturbine recuperators[1] because it "combines excellent high-temperature strength and oxidation resistance with superior long term stability and good fabricability[2]". Tables I and II list the composition and tensile properties of Haynes 230®.

Table I. Composition of Haynes 230® alloy (wt. %)[2]

Element	Concentration	Element	Concentration	Element	Concentration
Ni	57	Mo	2	Al	0.3
Cr	22	Mn	0.5	C	0.1
W	14	Si	0.4	La	0.02
Co	5 (max)	Fe	3 (max)	B	0.015 (max)

[1] Omatete, O., O., Maziasz, P. J., Pint, A. B., and Stinton, D. P., "Assessment of Recuperator Materials for Microturbines," ORNL TM-2000/304
[2] Haynes International, Kokomo, IN 46904

Table II. Tensile Properties of Haynes 230® alloy hot-rolled at 1232°C and solution annealed[2]

Yield strength (MPa)	Tensile strength (MPa)	Elongation (%)
395	865	49

Evaluation of baseline properties of Haynes 230® alloy foils.

The foil materials used in this investigation were supplied by Capstone Turbine Corporation in the form of 20.3-cm wide rolls with thicknesses of 0.089 mm and 0.102 mm. Figure 1 shows micrographs of polished cross-sections of as-received foils of Haynes 230® alloy. Large tungsten carbide particles are evident in these micrographs. It was also found that smaller tungsten carbide particles tended to be aligned. Also included in Figure 1 are equalized images of the micrographs, which reveal the grain structure of the material.

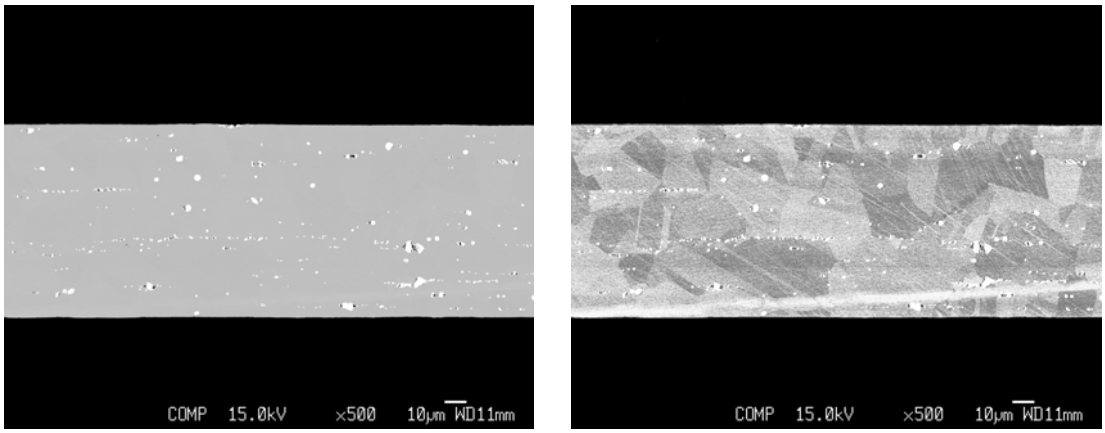

(a)

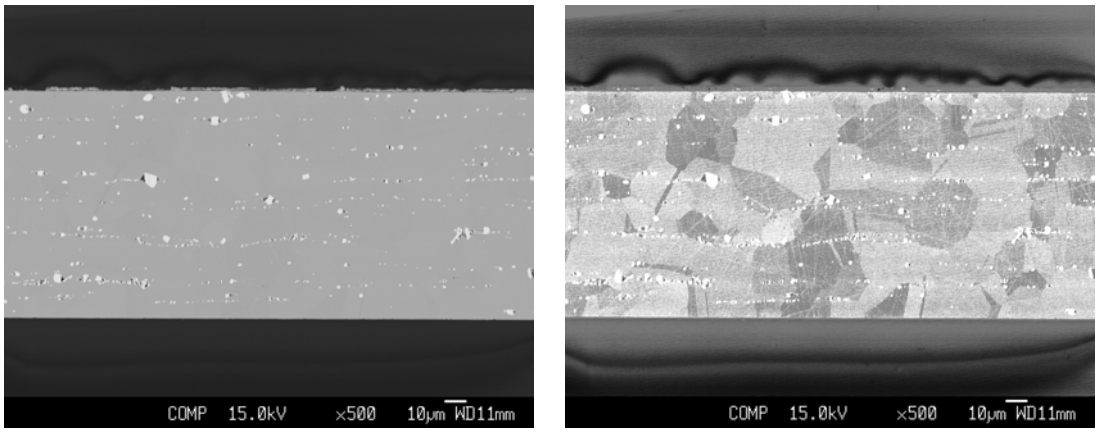

(b)

Figure 1. Cross-sectional micrographs of as-received Haynes 230® alloy: (a) 0.089-mm thick; (b) 0.102-mm thick. Equalized images are included on the right side to reveal grain structure.

Miniature dog-bone shaped test specimens with their principal axis aligned either parallel or perpendicular to the rolling direction, were obtained from the foil rolls by electric discharge

machining (Figure 2). The tensile behavior of the miniature test specimens was determined at ambient conditions using a procedure that has been described in detail elsewhere[3]. The tensile tests were carried out at a constant crosshead displacement rate and both the load and crosshead displacement were recorded during the test. Because of the small dimensions of the test specimens it was not possible to measure directly the tensile strain of the test specimens, but values of strain were determined from the crosshead displacement data after applying a correction for the compliance of the load train.

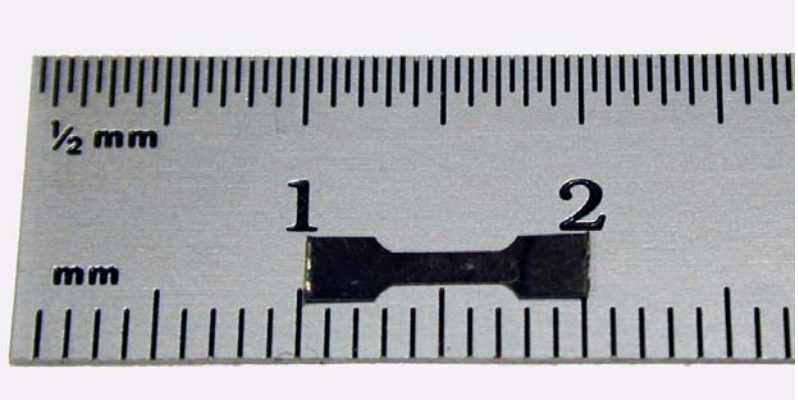

Figure 2. Miniature test specimen used for determination of tensile properties of Haynes 230® alloy.

Figures 3 and 4 show stress versus strain curves obtained from the tensile evaluation of test specimens that had been cut with their main axis either parallel or perpendicular to the rolling direction. The tensile stress-strain curves are characterized by a linear region associated with elastic deformation, a well-defined transition to plastic deformation at a high yield stress and failure strains near to 40%.

Table III summarizes the results of these tests and lists values for the 0.2% yield strength, ultimate tensile strength and strain at failure. An analysis of variance showed that the differences between the ultimate tensile strength of specimens cut either parallel or perpendicular to the rolling direction were not significant at the 95% confidence level. However, it was also found the ultimate tensile strength of 0.102-mm thick foils was significantly higher, at the 95% confidence level, than the ultimate tensile strength of 0.089-mm thick foils. Although the 0.2% yield strength values obtained are about 10% higher than those reported by Haynes[2], the ultimate tensile strength results are in good agreement with those reported by the manufacturer (See Table II).

[3] E. Lara-Curzio, "Recuperator Materials Testing and Evaluation" in DER Materials Program Quarterly Report, June-September, 2003

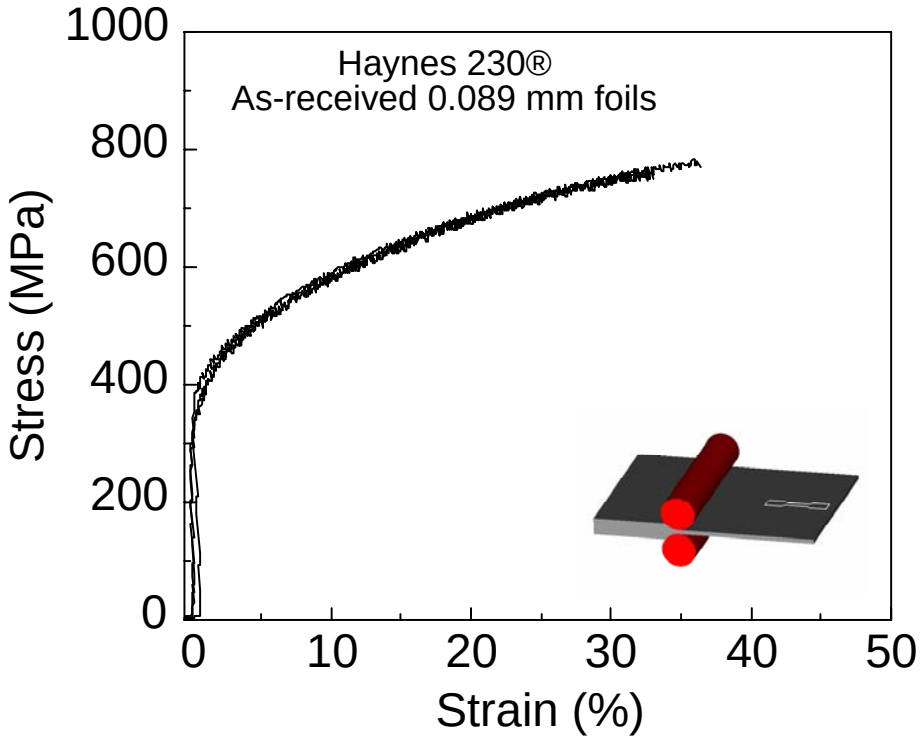

(a)

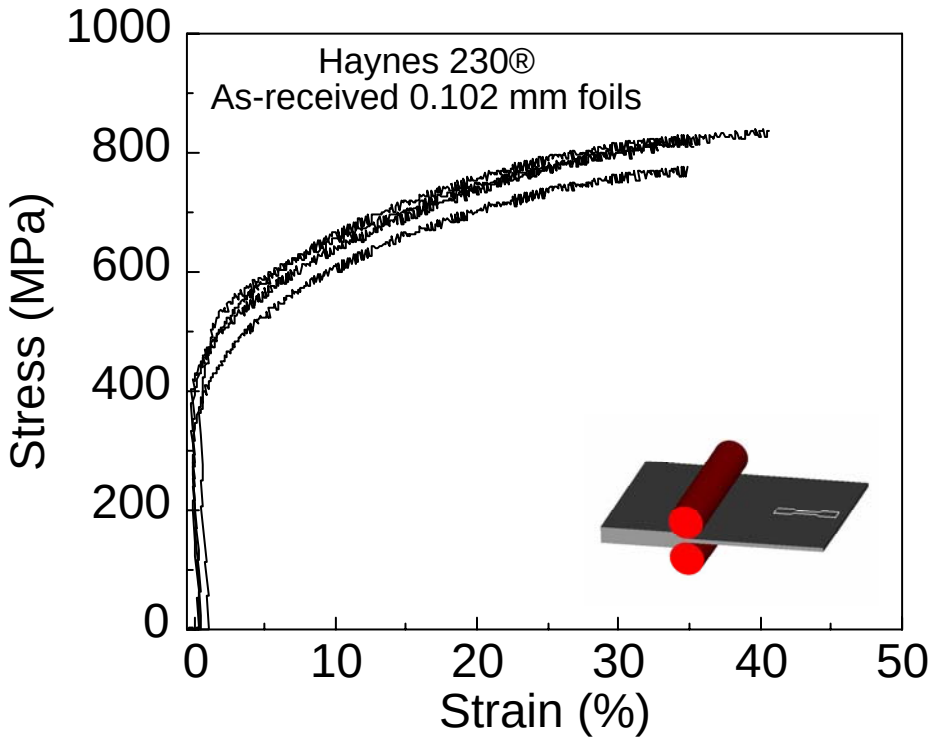

(b)

Figure 3. Stress-strain curves obtained from the tensile evaluation of miniature test specimens of Haynes 230® alloy with their main axis parallel to the rolling direction. (a) 0.089-mm thick specimens; (b) 0.102-mm thick specimens.

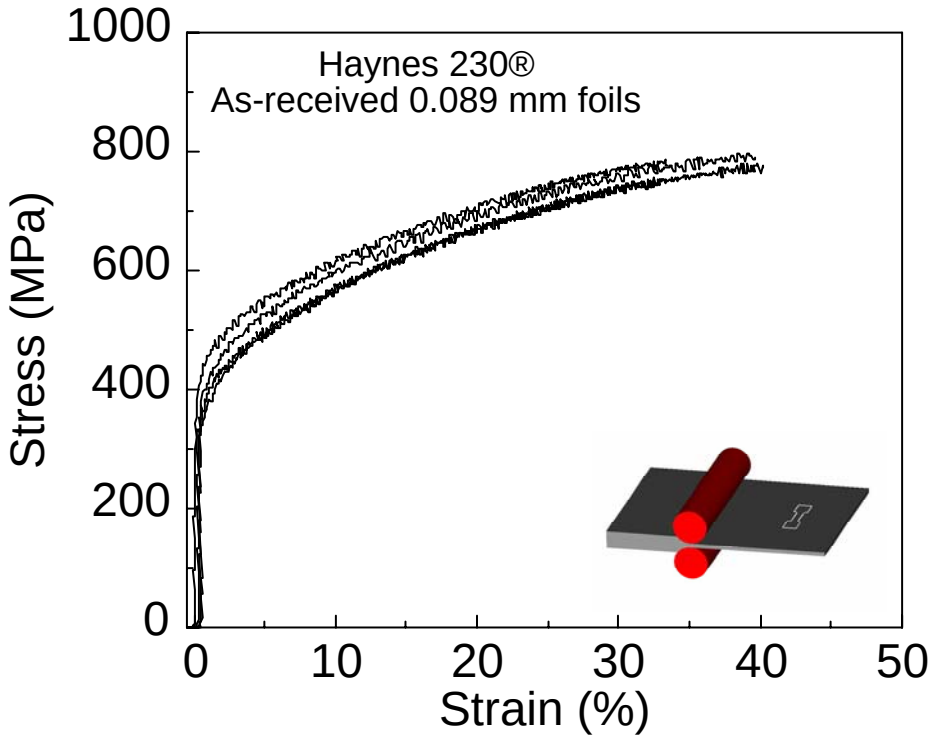

(a)

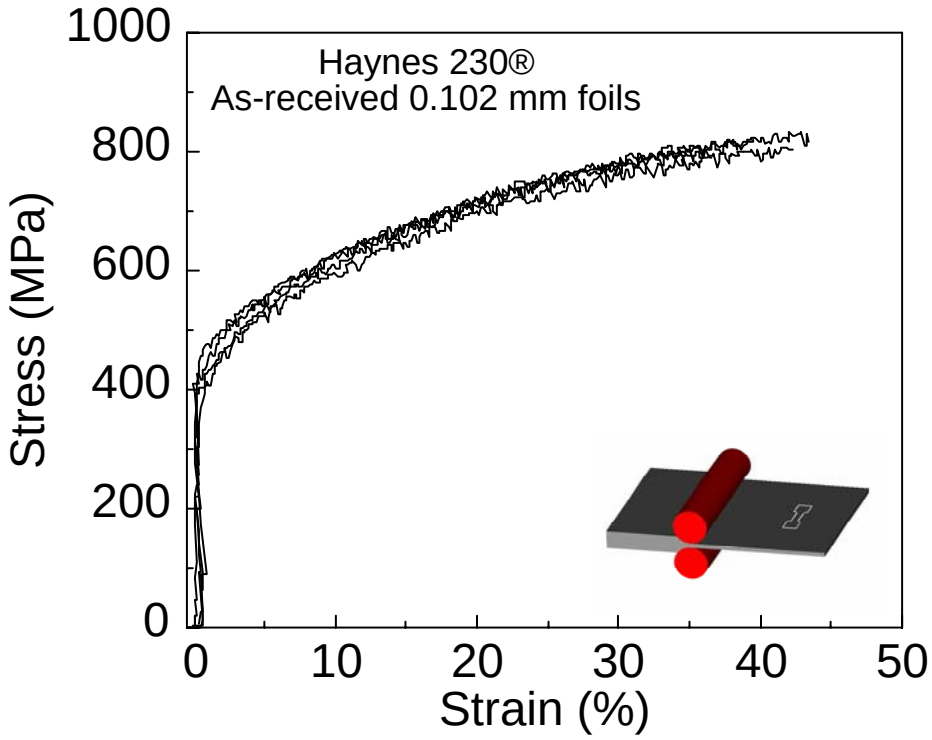

(b)

Figure 4. Stress-strain curves obtained from the tensile evaluation of miniature test specimens of Haynes 230® alloy with their main axis perpendicular to the rolling direction. (a) 0.089-mm thick specimens; (b) 0.102-mm thick specimens.

Table III. Summary of tensile results for as-received materials.

Haynes 230® alloy	0.2% Yield Strength (MPa)	Ultimate Tensile Strength (MPa)	Failure Strain (%)
0.089-mm thick			
⊥ to rolling direction	452± 24	780 ± 18	36 ± 4
|| to rolling direction	422 ± 12	770 ± 11	34 ± 2
0.102-mm thick			
⊥ to rolling direction	466 ± 23	817 ± 12	40 ± 4
|| to rolling direction	489 ± 45	818 ± 27	36 ± 3

Evaluation of Haynes 230® alloy foils in ORNL's microturbine test facility.
Foil strips 75-mm long and 14-mm wide were laser-welded onto a Haynes 230® alloy sample holder as described in detail elsewhere[3]. The diameter of the sample holder onto which the foils were welded was 23.1 mm. Foils of two different thicknesses were evaluated and Table IV lists the positioning of the foils in the sample holder.

Table IV. Thickness of foils

Position in Sample Holder	1	2	3	4
Thickness (mm)	0.089	0.102	0.089	0.102

The sample holder was internally pressurized using plant air at 60 psi and subjected to a 500-hour exposure in ORNL's modified microturbine operating with the settings listed in Table V. The temperature of each foil was monitored during the test using type-K thermocouples that had been placed inside the sample holder.

Table V. Microturbine settings for 500-hr test.

Engine Speed	45,000 RPM
Turbine Exit Temperature	800°C
Fuel	natural gas

In addition to the magnitude of air pressure inside the sample holder, the temperature of the four foils and the turbine exit temperature were recorded during the test, as illustrated by the temperature history in Figure 5. The maximum and minimum temperatures were 752°C and 679°C, respectively. Unfortunately faulty contacts prevented the recording of the temperature of foils 2 and 3, but previously obtained information on temperature distribution along the sample holder was used to determine these values.

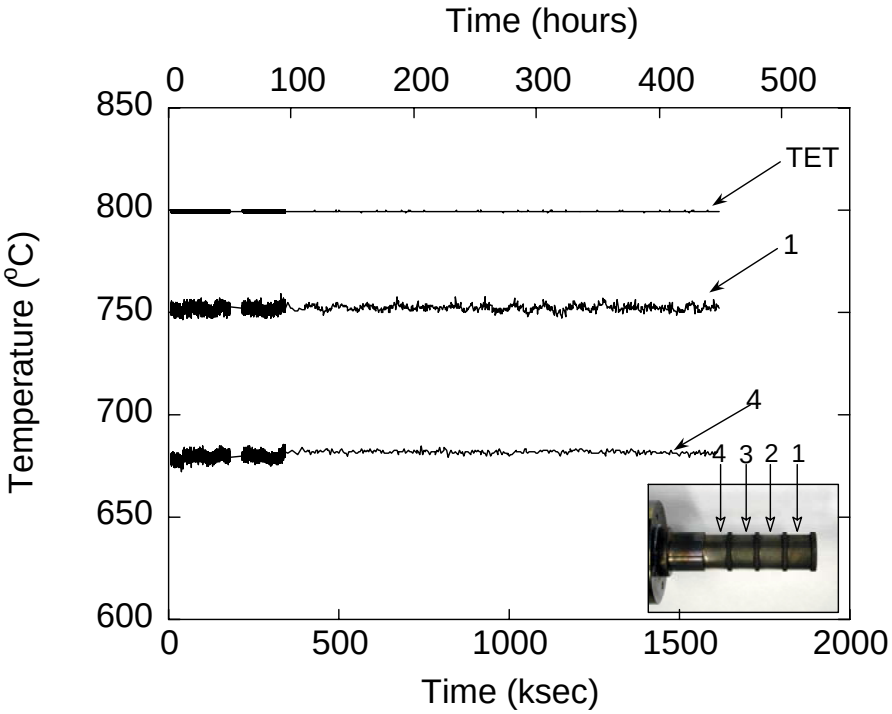

Figure 5. Temperature history for 500-hr test to evaluate the behavior of 0.089-mm and 0.102-mm thick foils of Haynes 230® alloy.

Post-test analysis

Figures 6 and 7 show the sample holder and Haynes 230® foils at the end of the 500-hr exposure. The foils were removed from the sample holder using a lathe and a diamond tool. About 12 miniature test specimens were obtained from each foil by electric discharge machining for subsequent tensile evaluation and microstructural characterization.

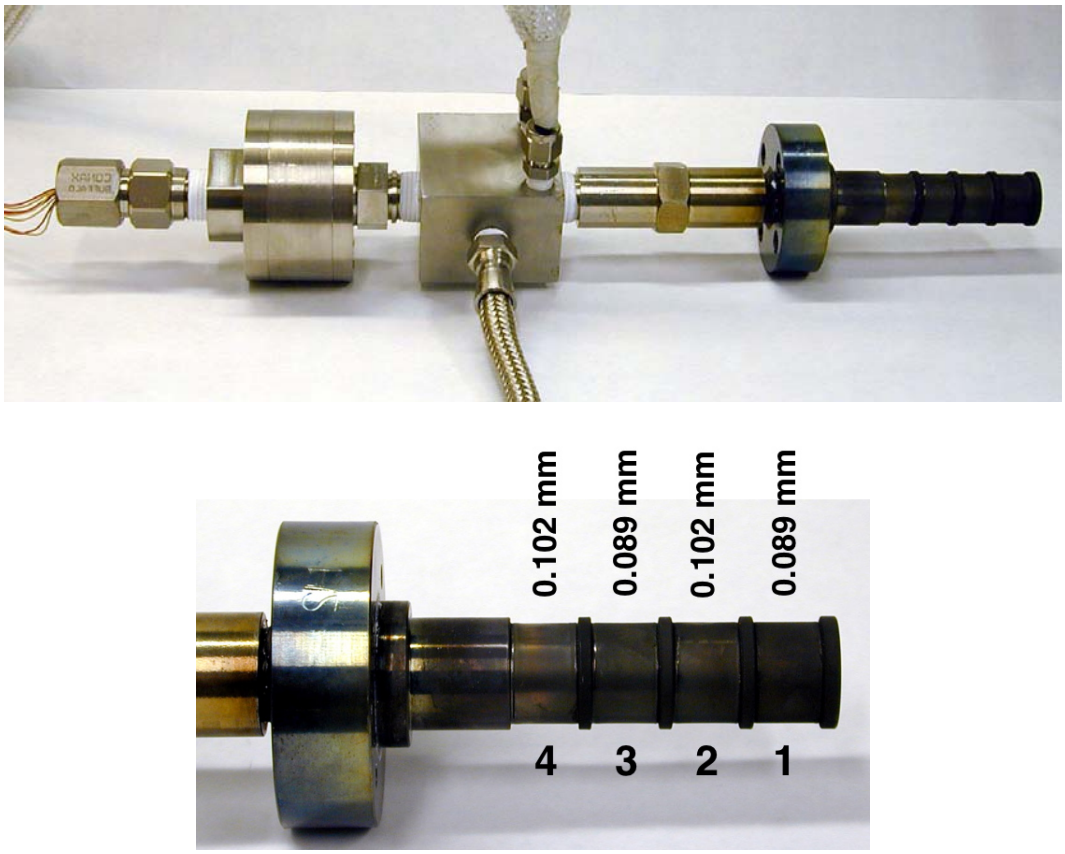

Figure 6. Photographs of sample holder with 0.089-mm and 0.102-mm thick Haynes 230® foils after 500-hr test at TET=800°C and internal pressure of 60 psi.

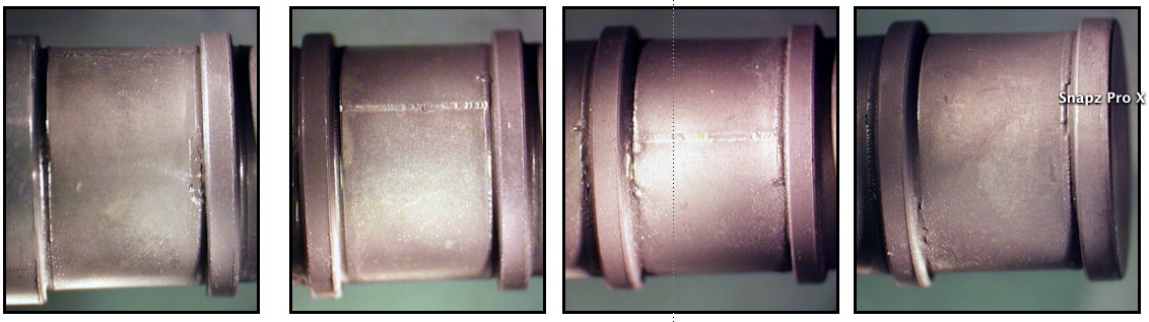

(a) (b) (c) (d)

Figure 7. Photographs of Haynes 230® alloy foils after 500-hr test at TET=800°C and internal pressure of 60 psi; (a) 0.089-mm thick 752°C; (b) 0.102-mm thick 736°C; (c) 0.089-mm thick 700°C; (d) 0.102-mm thick 679°C.

Figures 8-11 present the stress versus strain curves obtained from the tensile evaluation of the miniature test specimens. It was found that the ultimate tensile strength and ductility of Haynes 230® alloy decreased by 30% and 60%, respectively, after 500 hours exposure at 752°C. At the lowest exposure temperature of 679°C the ultimate tensile strength and ductility decreased by 10% and 25%, respectively. Table VI summarizes the tensile results.

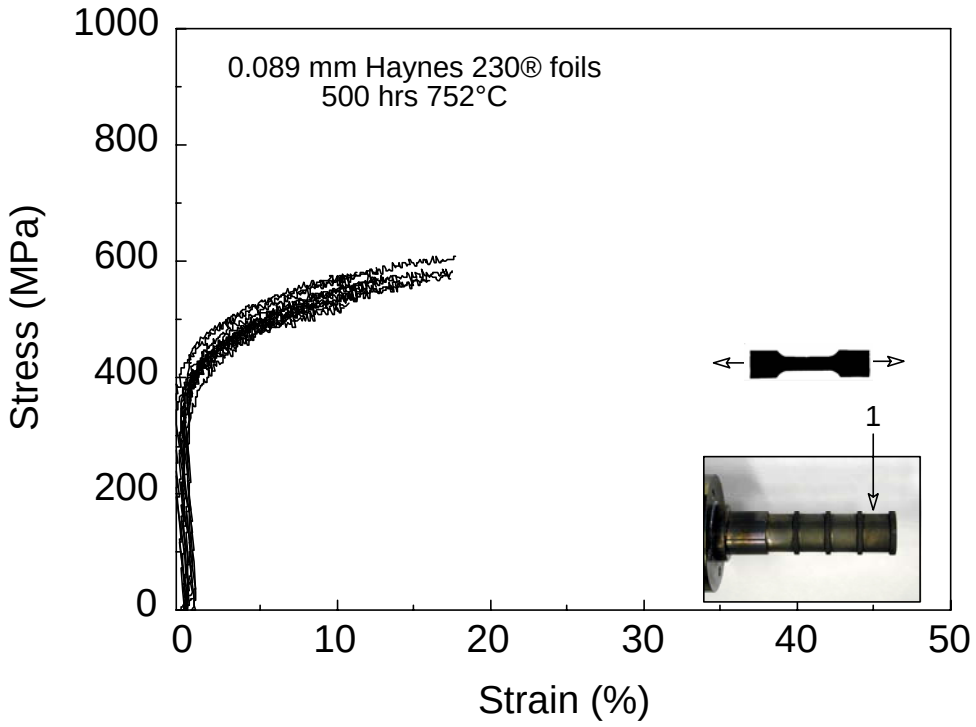

Figure 8. Stress versus strain curves obtained from the tensile evaluation of miniature test specimens obtained from 0.089-mm thick Haynes 230® alloy exposed at 752°C for 500 hours.

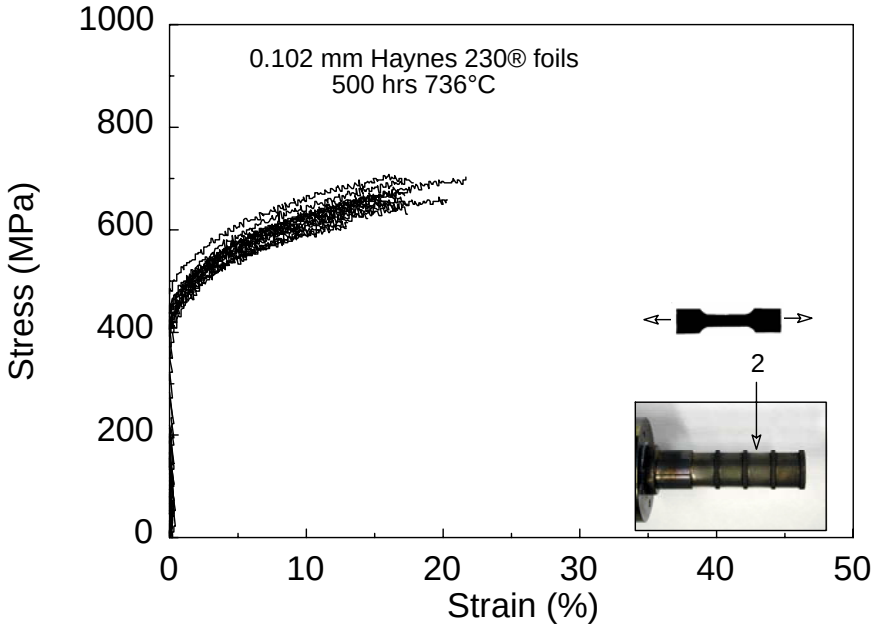

Figure 9. Stress versus strain curves obtained from the tensile evaluation of miniature test specimens obtained from 0.102-mm thick Haynes 230® alloy exposed at 736°C for 500 hours.

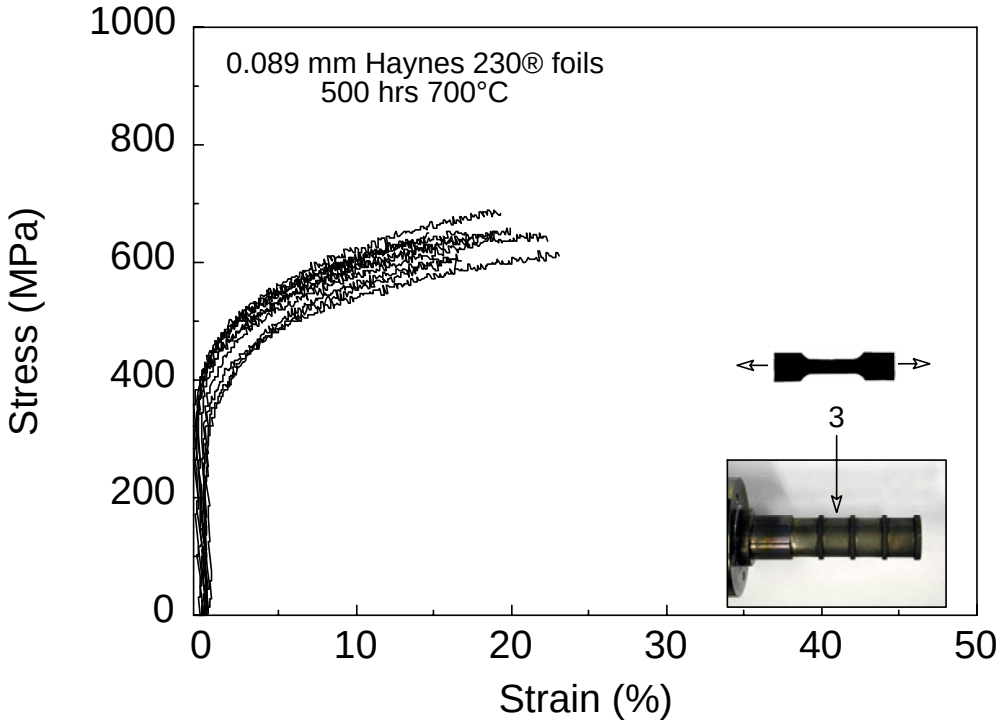

Figure 10. Stress versus strain curves obtained from the tensile evaluation of miniature test specimens obtained from 0.089-mm thick Haynes 230® alloy exposed at 700°C for 500 hours.

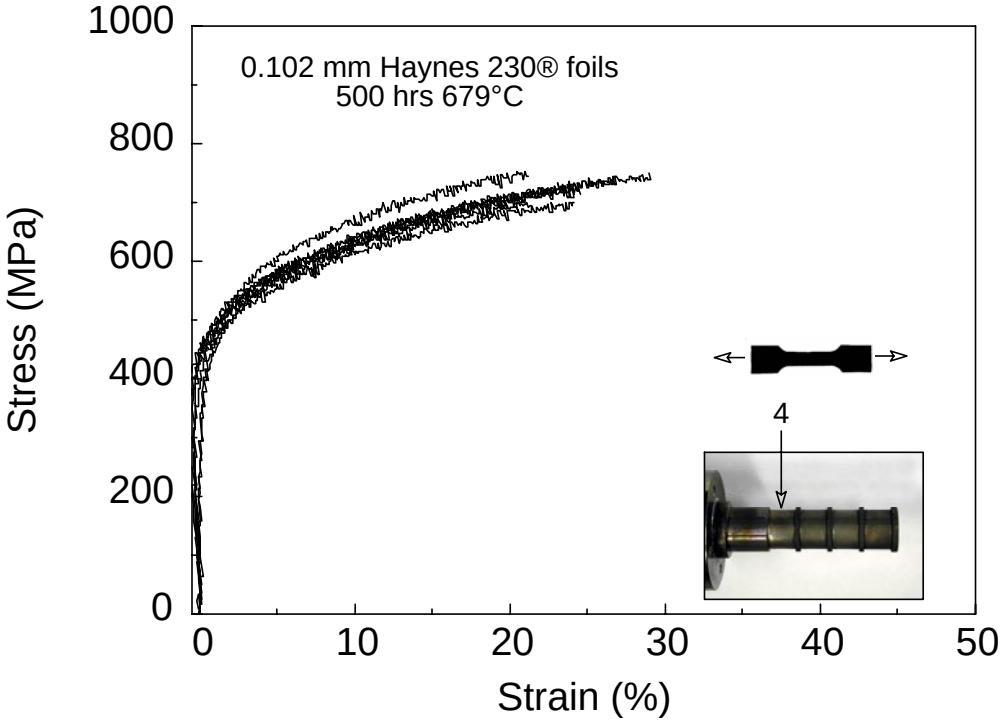

Figure 11. Stress versus strain curves obtained from the tensile evaluation of miniature test specimens obtained from 0.102-mm thick Haynes 230® alloy exposed at 679°C for 500 hours.

Table VI. Summary of tensile results for Haynes 230® alloy.

Foil	Thickness (mm)	T (°C)	0.2% σ_y (MPa)	UTS (MPa)	Failure strain (%)
1	0.089	752	415 ± 12	561 ± 28	13.0 ± 3.0
2	0.102	736	457 ± 15	660 ± 34	19.0 ± 3.4
3	0.089	700	418 ± 41	644 ± 24	19.0 ± 2.9
4	0.102	679	481 ± 7.1	728 ± 22	27.0 ± 6.3

Figures 12 and 13 present scanning electron micrographs of cross-sections obtained from foil 1, which had been exposed at 752°C for 500 hours. It was found that only a very thin layer of chromium oxide had formed on the surfaces. It was also found that a series of intergranular cracks that were several micrometers long and had spanned more than one grain had developed on the side of the foil that had been exposed to the microturbine exhaust gases. A chemical analysis revealed that the surface of those cracks was rich in oxygen and poor in chromium. Smaller cracks were also observed on the surface of the foils that had been exposed to compressed air.

Figures 14 to 17 present scanning electron micrographs of the cross-sectional area of foils that had been exposed for 500 hours in positions 2, 3 and 4 of the sample holder. The average values of the temperatures recorded at these locations were 736°C, 700°C and 679°C, respectively. It was found that, similarly to the foil that had been exposed to the highest temperature in position 1 of the sample holder (752°C), short cracks had formed along the grain boundaries on the surface of the foil that had been exposed to the microturbine exhaust gases. Smaller cracks were also evident on the edge exposed to compressed plant air. Elemental maps showed that the surfaces of those cracks were rich in oxygen and deficient in chromium.

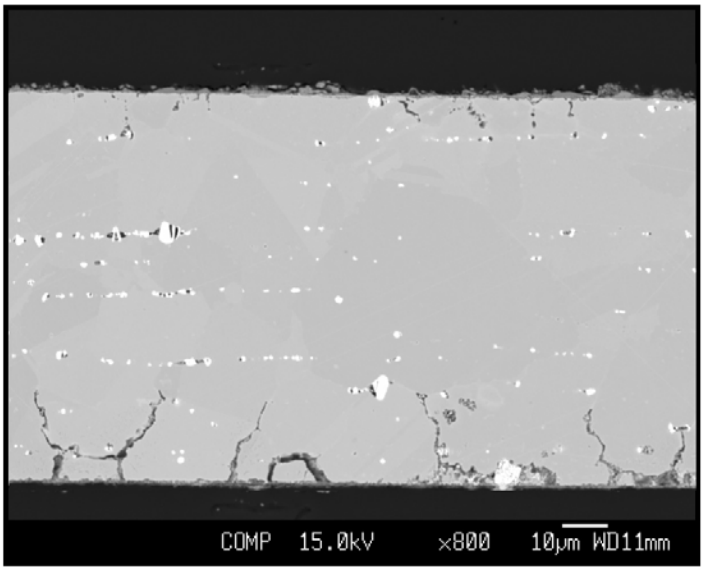

Figure 12. Scanning electron micrograph of cross-section obtained from 0.089-mm thick Haynes 230® alloy foil after 500-hr exposure at 752°C. The lower surface in the micrograph had been exposed to the microturbine exhaust gases.

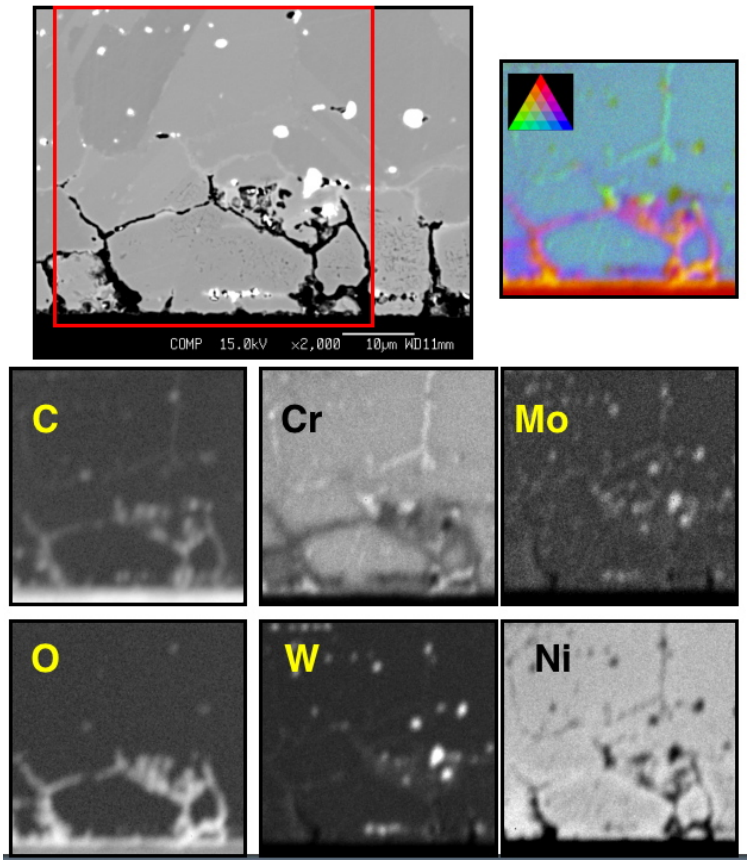

Figure 13. Scanning electron micrograph of cross-sectional area of 0.089-mm thick Haynes 230® alloy foil that had been exposed for 500 hours at 752°C. The lower surface in the micrograph had been exposed to the microturbine exhaust gases. Atomic composition maps of the area in the inset are also included.

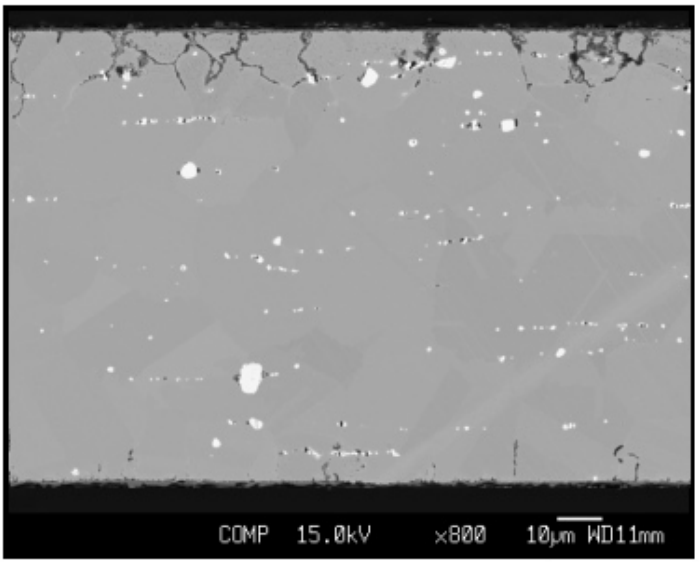

Figure 14. Scanning electron micrograph of cross-sectional area obtained from 0.102-mm thick Haynes 230® alloy exposed for 500 hours at an average temperature of 736°C and internal pressure of 60 psi. Top surface in micrograph was exposed to microturbine exhaust gases.

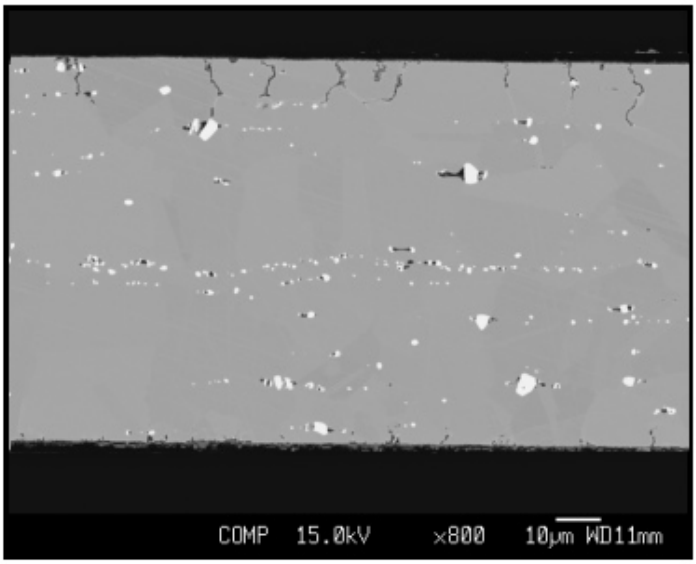

Figure 15. Scanning electron micrograph of cross-sectional area obtained from 0.089-mm thick Haynes 230® alloy exposed for 500 hours at an average temperature of 700°C and internal pressure of 60 psi. Top surface in micrograph was exposed to microturbine exhaust gases.

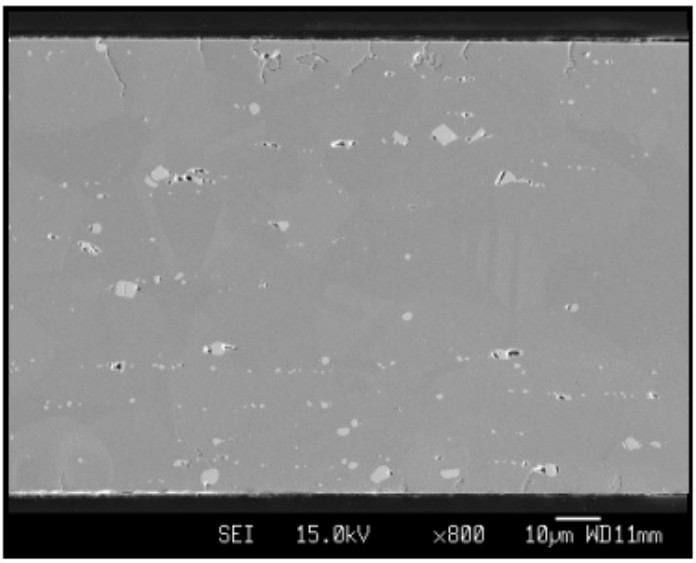

Figure 16. Scanning electron micrograph of cross-sectional area obtained from 0.102-mm thick Haynes 230® alloy exposed for 500 hours at an average temperature of 679°C and internal pressure of 60 psi. Top surface in micrograph was exposed to microturbine exhaust gases.

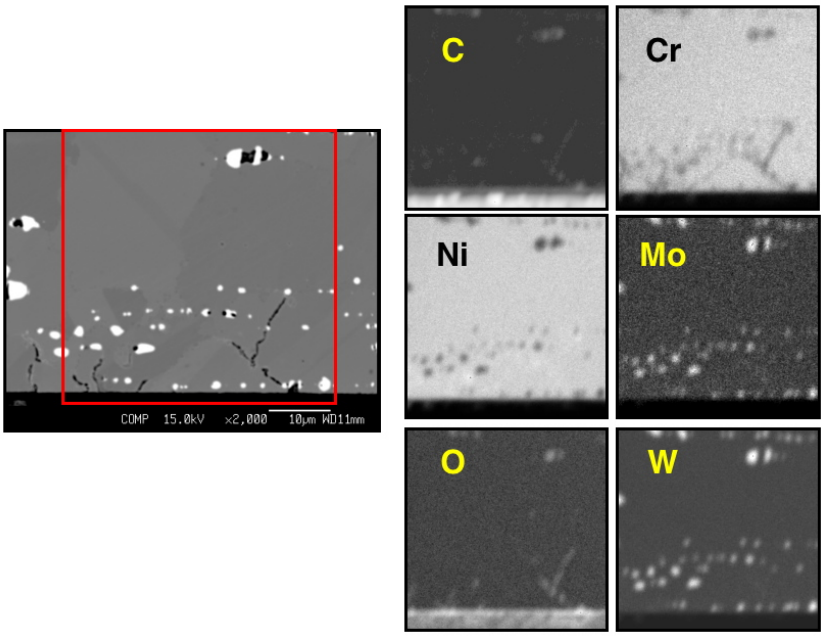

Figure 17. Scanning electron micrograph of cross-sectional area obtained from 0.102-mm thick Haynes 230® alloy exposed for 500 hours at an average temperature of 679°C and internal pressure of 60 psi. Bottom surface in micrograph was exposed to microturbine exhaust gases. Atomic composition maps of the area in the inset are also included.

When these results are compared with those obtained for 347 stainless steel when evaluated under similar circumstances, it is clear that Haynes 230® possesses much better corrosion resistance and retention of strength and ductility. The mechanisms responsible for the preferential cracking of the material on the surface that was exposed to the microturbine exhaust gases are currently being investigated.

Status of Milestones

Complete study of how the mechanical properties, microstructure and corrosion products of Haynes-214 and HR230 alloys evolve as a function of exposure time and applied stress in recuperator testing facility**.** (September 2004)

Complete evaluation of residual properties of five decommissioned microturbine recuperators.

Industry Interactions

The foils used in this investigation were provided by Capstone Turbine Corporation.

Problems encountered

None

Publications/Presentations

None

Advanced Alloys for High-Temperature Recuperators

P. J. Maziasz, B. A. Pint, K. L. More,
J. P. Shingledecker, and N. D. Evans
Metals and Ceramics Division
Oak Ridge National Laboratory
P.O. Box 2008, Oak Ridge, TN 37831-6115
Phone: (865) 574-5082, E-mail: maziaszpj@ornl.gov

Objective

The main objective of this program is to work with commercial materials suppliers (foil and thin sheet) and recuperator manufacturers to enable manufacture and evaluation of upgraded recuperators from cost effective alloys with improved performance and temperature capability. The near term goal is better performance to or above 704°C (1300°F), and the longer-term goal is reliable performance at 760°C (1400°F) and higher.

Highlights

Materials for use to about 704°C (1300°F)

A joint project between ORNL and Allegheny-Ludlum Technical Center (ALTC) concluded last year produced commercial sheets and foils of standard composition 347 stainless steel with modifying process that produced significantly better creep rupture resistance. This new product, designated AL347HP, is now commercially available. Recent laboratory oxidation/corrosion testing (in 10% water vapor) has indicated that severe moisture-enhanced oxidation can occur in 347 steel after 1000-1500h at 650-700°C. New ORNL modified 347 steels with added Mn and N, and more oxidation-resistant commercial alloys like HR120, NF709 and alloy 625, all show little or no effects of such moisture enhanced oxidation after similar testing for well beyond 8000h.

Materials for use to 760°C (1400°F) or higher

Foils of commercial alloys (0.003-0.005 in.) HR120, NF709 and alloy 625 all show good creep rupture resistance at 750°C and 100 MPa. Commercial recuperator sheet (0.010 in.) of alloy 625 obtained from Ingersoll Rand Energy Systems is now also being creep tested at this condition this quarter.

Technical Progress

Recuperator Component Analysis

Several different microturbine OEMs have provided pieces of fresh and engine-tested PFR and PSR recuperators made from standard 347 stainless steel for analysis, testing, and characterization, which was completed last quarter. ORNL has expanded analysis of PFR recuperator air cells and related manufacturing process specimens with Ingersoll Rand Energy Systems this quarter. Detailed component analyses data are reported to each OEM. Collaborative efforts between ORNL and the recuperator makers to support

making recuperators with more temperature capability and reliability from advanced alloys (i.e. HR120, 20-25Nb or alloy 625) continued this quarter.

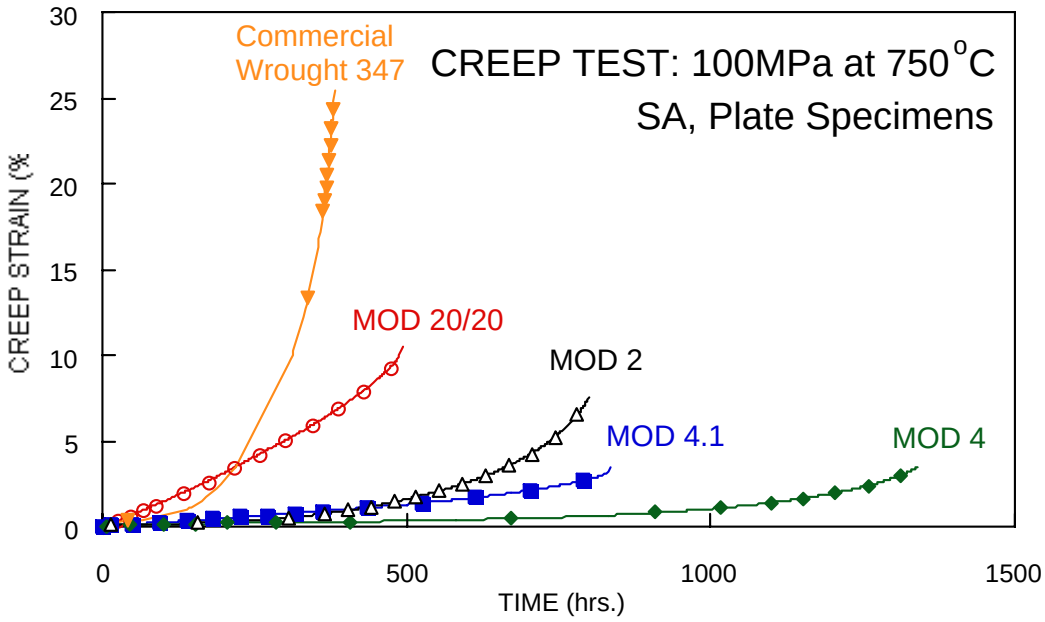

Figure 1 – ORNL creep rupture testing of standard 347 steel and ORNL modified 347 steel plate (0.020 – 0.060 in.) specimens at 750°C and 100 MPa (14.5 ksi) in air.

Selection and Commercial Scale-Up of Advanced Recuperator Materials:
a) Materials for use to about 704°C (1300°F)

Testing of standard 347 steel with modified commercial processing for improved creep rupture resistance as sheet and foil has been completed by ORNL and Allegheny Ludlum Technical Center (ALTC). Allegheny Ludlum has made this material commercially available as AL347HP, and commercial quantities appropriate for recuperator air cell manufacturing have been supplied to Capstone Turbines and Ingersoll Rand Energy Systems.

This quarter creep testing of specimens from plate stock was completed to measure improvements of the initial series of 347 stainless steels with modified compositions relative to standard 347 steel. Results of creep at 750°C and 100 MPa are shown in Fig. 1. Both the mod. 2 and mod. 4, 347 steels have significantly longer rupture life and lower secondary creep rates than standard 347 stainless steel ORNL previously creep tested various standard commercial 347 steel foil and sheet at 700-750°C to establish the baseline behavior for current recuperators.

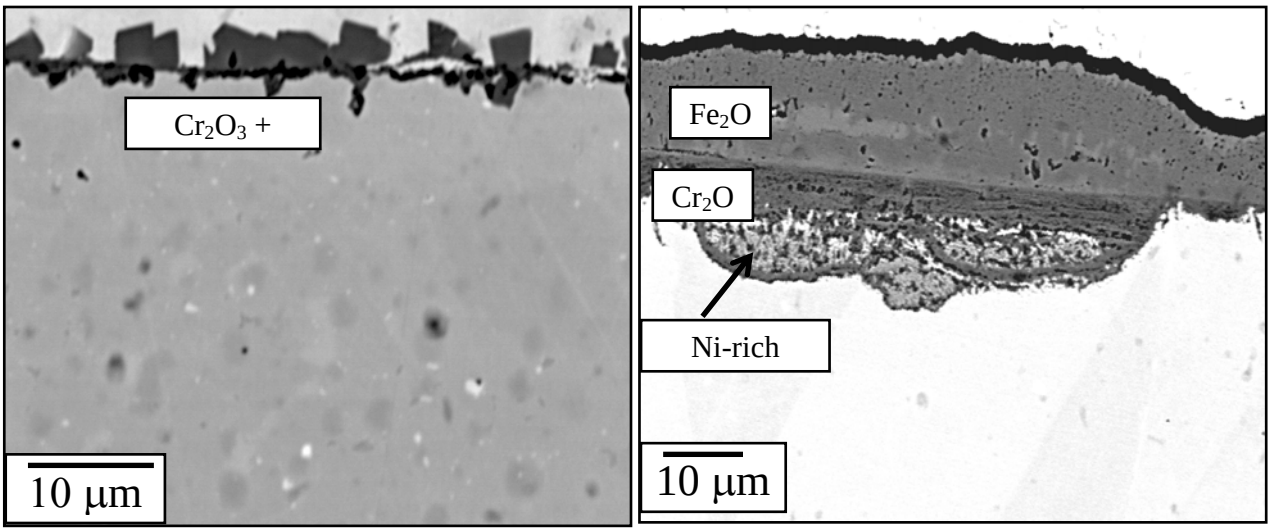

Figure 2 – Backscattered SEM analysis of the oxidized surface of polished cross-sections of 347 stainless steel foils (0.1 mm) tested in air + 10% water vapor at 700°C for 1,000 h. a) ORNL developmental modified 347 stainless steel (mod.4), and b) standard, commercial 347 stainless steel. The Fe-rich surface oxide on top of the chromia scale and corresponding subsurface attack are the microstructural signatures of moisture enhanced break-away oxidation attack in b). By contrast the modified 347 steel (mod.4) has a mixed oxide scale and is more resistant to such break-away oxidation.

Previous oxidation testing in 10% water vapor at 650-750°C also shows a significant benefit of the modified 347 steels that contain Mn and N additions relative to standard 347 steel particularly the mod. 4 steel. Cross section microstructural analysis of standard 347 and modified 347 (mod. 4) tested at 700°C are shown at lower magnification in Figure 2, and clearly the modified 347 is showing resistance to breakaway oxidation, with none of the characteristic thick, non-protective outer iron oxide layer seen on standard 347 steel. More detailed microanalysis using analytical electron microscopy of the modified 347 (mod. 4) steel specimen in Figure 3 shows complex surface oxides rich in Mn and Cr on top of a thinner chromia layer at the metal-oxide scale interface. There is a clear role of Mn that helps form a protective oxide to resist moisture-enhanced oxidation, in addition to its role in improved creep resistance.

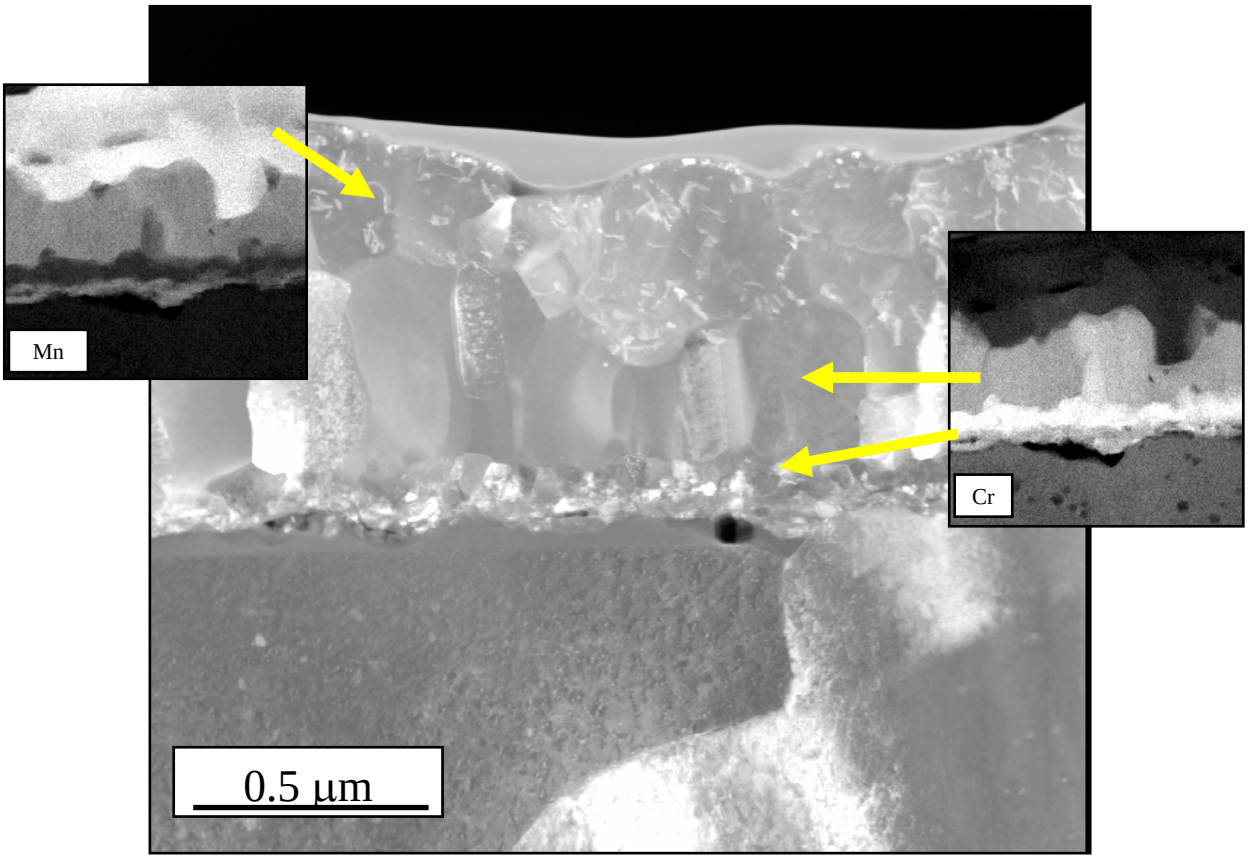

Figure 3 – Higher resolution microanalysis of the oxidized surface of the ORNL modified 347 (mod.4) stainless steel foil tested in air + 10% water vapor at 700°C for 1000 h (shown in Fig. 2) is obtained from analytical electron microscopy of a cross-section specimen, electropolished so that the surface oxides and subsurface metal are electron transparent. The background picture is a transmission electron microscopy (TEM) image, while the two insets are high resolution X-ray maps using the characteristic Kα peak of the elements indicated. This analysis reveals that there is a Mn-rich oxide scale on top of the Cr-rich oxides that forms on the metal surface. This is likely an important feature in the stability of these oxide scales and the relative resistance of this Mn-modified 347 steel to moisture enhanced oxidation compared to standard 347 stainless steel.

b) Materials for use at 760°C (1400°F) or higher

HR 120 (Fe-25Cr-35Ni) is one of the more promising commercially available material with significantly better creep-resistance and corrosion-resistance in this temperature range at 3-4 times the cost of 347 stainless steel. Commercial 3.5 mil foil of HR120 was obtained by ORNL from Elgiloy Specialty Metals (Elgin, IL) and creep-tested at 704°C/152 MPa, and at 750°C/100 MPa. The HR 120 foil lasted 900h at 704°C, and lasted for 3300 h at 750°C, both with good rupture ductility. The creep resistance of HR 120 at 750°C is about 13 times better than standard 347 steel foil with standard commercial processing (Fig. 4). Creep data is also included for NF709 (Fe-20Cr-25Ni,

Nb,N), from boiler tubing that was split and rolled into foil at ORNL. The NF709 shows about 50% longer rupture life than HR120. Alloys 625 and HR214 show roughly similar creep rupture resistance, but have much lower creep rates.

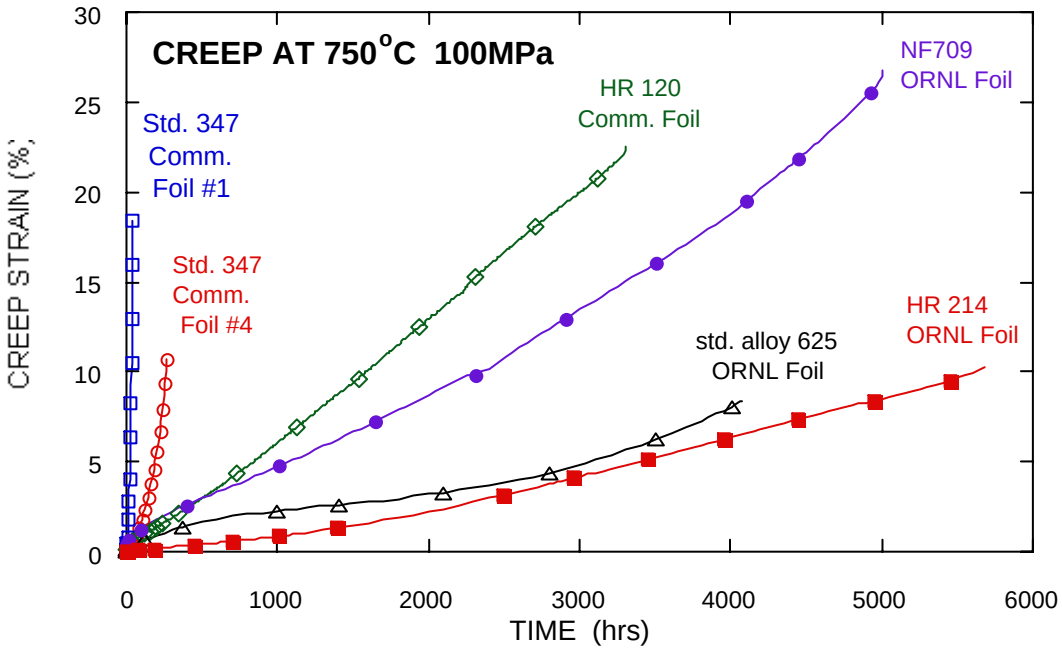

Figure 4 – Comparison of creep rupture curves for testing of commercial or ORNL processing of 4 mil foils of high performance alloys at 750°C and 100 MPa (14.5 ksi). Foils include commercial HR120, and ORNL processed foils of NF709, alloy 625 and HR 214.

The commercial HR 120 foil and ORNL foils of alloy 625 and NF709 have also been incorporated into the oxidation testing matrix, and at 650-750°C are resistance to water-vapor enhanced oxidation, at least to about 8000 h. Oxidation testing will continue next quarter, and many of these steels and alloys will also be incorporated into the ORNL recuperator testing facility next quarter.

Status of Milestones

In collaboration with Allegheny-Ludlum, produce a 5000 lb. commercial heat of corrosion-resistant 20/25 Nb foil for high-temperature recuperators (August 2004)

Industry Interactions

Microturbine OEM Ingersoll-Rand Energy Systems took delivery of the new AL347HP sheet and foils processed by Allegheny-Ludlum and ORNL for improved creep resistance for recuperator manufacturing. Capstone Turbines also took delivery of some 5 mil foil

of the AL347HP for testing and evaluation. Ingersoll Rand sent ORNL pieces of several engine tested and fresh recuperators (mainly 347 steel, but also some alloy 625) for microcharacterization analysis and evaluation. ORNL and Ingersoll Rand have also begun braze alloy studies in support of their advanced recuperator manufacturing efforts.

Problems Encountered

None

Publications/Presentations

P. J. Maziasz, R. W. Swindeman, J. P. Shingledecker, K. L. More, P. A. Bint, E.Lara-Curzio, and N. D. Evans, "Improving High-Temperature Performance of Austenitic Stainless Steels for Advanced Microturbine Recuperators," paper was presented at the 6th International Charles Parsons Turbine Conference, held September 16-18, 2003 in Dublin, Ireland; paper is pp. 1057-1073 of Parsons 2003: Engineering Issues in Turbine Machinery, Power Plants and Renewables, Institute for Materials, Minerals and Mining, Maney Publishing, London, UK (2003).

DEVELOPMENT OF MONOLITHIC CERAMICS AND HIGH-TEMPERATURE COATINGS

Kennametal's Hot-Section Materials Development

R. Yeckley, J. R. Hellmann, K. M. Fox, D. J. Green, and E. C. Dickey
Kennametal Inc.
1600 Technology Way, P.O. Box 231, Latrobe, PA 156-0231
Phone: (724) 539-4822, E-mail: Russ.yeckley@kennametal.com

Objective

Determine potential of an existing structural SiAlON that is being manufactured for other applications that, commensurate with the requirements of advanced microturbines shows potential for strength, environmental stability, and manufacturability for complex shapes.

Highlights

The SiAlON compositions selected for screening are centered on Kennametal's Ky1540 product. The SiAlON selected have the desired variation in composition and grain boundary structure to study effect on mechanical behavior and oxidation resistance. Mechanical testing is complete. Two SiAlON are selected further mechanical evaluation encompassing flexure testing of the ground and as processed surface and tensile testing.

Technical Progress

Table 1 summarizes the flexure testing completed along with toughness, α-SiAlON content, the α-SiAlON 'x' value and the β SiAlON 'z' value. The 'x' and 'z' value were determined by x-ray diffraction. The SiAlON ab831 and ab832 have similar 'z' values of 0.25. The SiAlON ab582, ab581, ab531, ab532 are SiAlON with a 'z' value of .77 to .84. SiAlON ab131 and ab132 are located between the first two groups with a 'z' value of ~0.6. The α-SiAlON content has a narrower range than expected. The rare earth substitution into the α-SiAlON crystal structure exhibits a correlation with β-SiAlON solid solution as shown in Figure 1. Two rare earth levels are used, those SiAlON with the ID ending in 2 have the higher rare earth content. The two SiAlON selected for further development are ab831 and ab531 because of their good strength and lower rare earth level.

Strength dependence on stress rate has been measured for three SiAlON with the high rare earth contents. The slow crack growth exponent for ab532 is excellent.

Table 1 SiAlON Property Summary

	Hvn	st dev	Kic	st dev	Fracture Strength				α	α sialon	β sialon
Sialon	GPa		MPa m1/2		RT	m	1204	m	%	x'	z'
ab831	18.35	0.13	6.89	0.26	960	8.5	607	10.5	32	0.26	0.33
ab582	19.48	0.25	4.95	0.51	567	7.2	331	8.9	58	0.40	0.79
ab581	18.19	0.24	4.59	0.30	455	8.3	383	6.7	36	0.42	0.78
ab581	18.31	0.33	4.09	0.13					37	0.42	0.77
ab531	17.62	0.33	5.83	0.26	801	10.7	497	24.0	28	0.41	0.92
ab832	18.72	0.35	7.36	0.22	783	6.1	540	6.3	44	0.25	0.38
ab532	17.38	0.58	5.73	0.16	651	5.9	393	9.8	36	0.41	0.84
ab132	18.21	0.25	6.91	0.11	878	6.4	507	8.6	39	0.35	0.57
ab131	17.39	0.20	6.58	0.16	733	6.3	466	10.3	28	0.37	0.64

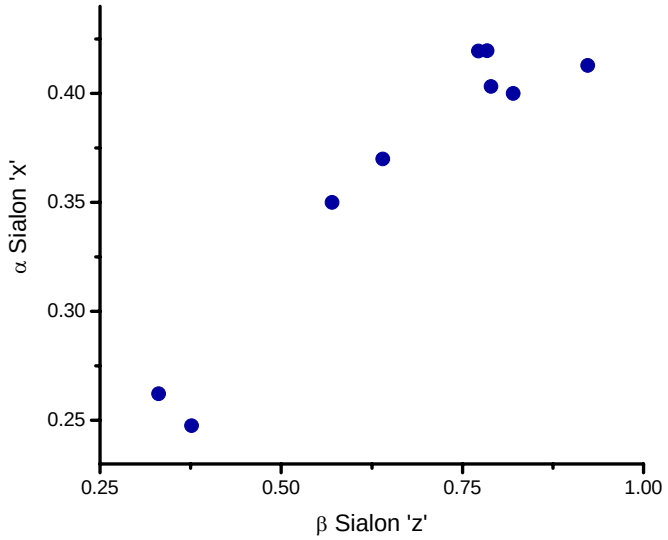

Figure 1. Rare earth in the α-SiAlON increases with increasing β-SiAlON z value.

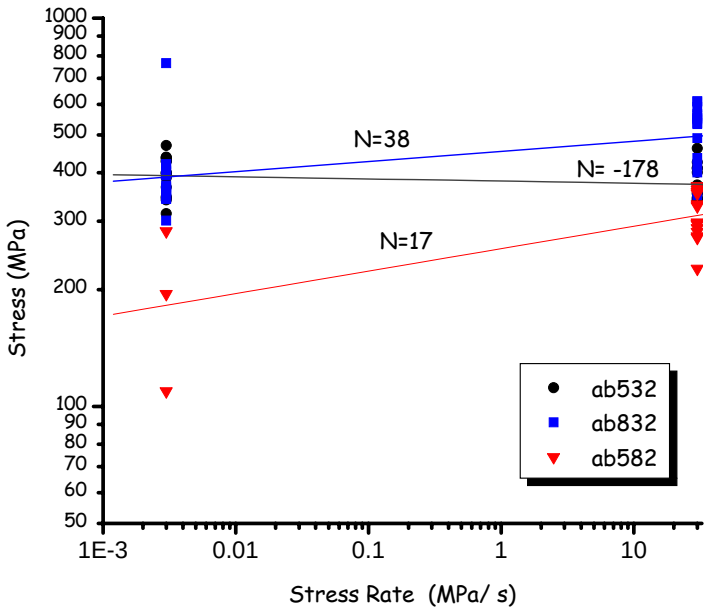

Figure 2. Strength dependence on stress rate at 1200 C.

The excellent fatigue resistance of the SiAlON may be explained by the characterization work under way at the Pennsylvania State Univeristy.
High-resolution TEM work is underway to determine the extent to which the glassy phase wets the grain boundaries in compositions ab831 and ab582. Quantitative compositional work will begin once a suitable standard of Yb-containing α-Sialon is prepared.

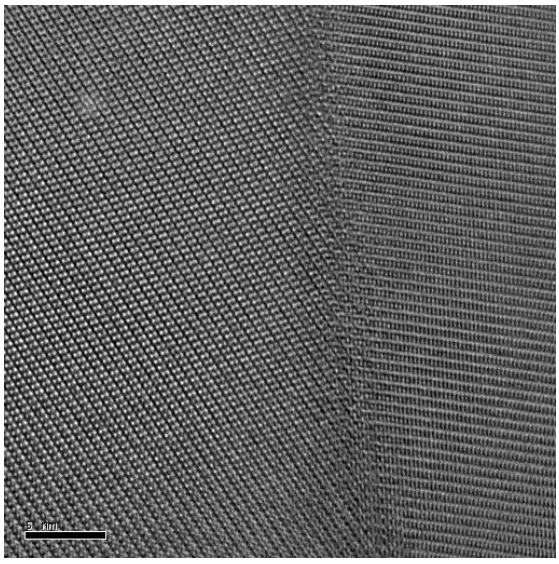

Figure 3. High resolution TEM image of composition ab582, showing the lack of an amorphous phase at a grain boundary.

Impression creep testing is a method that may enable comparison of the creep behavior changes of ceramic turbine components after operation. Construction of the impression creep testing system is complete. Transducer calibration and heating/loading tests are finished. A 2 mm diameter, flat-ended SiC cylinder is being used as the indenter. The first run has been completed on composition ab582, and data analysis is underway. The initial review of the data showed that the transducers are more dependent on temperature than was first expected. A calibration factor will be calculated and used to correct the data on future runs.

Figure 4. Overview of the impression creep test equipment.

Figure 5. Close-up view of the specimen, loading and support rods, and transducer rods inside the furnace.

Status of Milestones

Tensile and flexure bar preparation of ab531 and ab831 in process.
Prepare ab531 and ab831 tile for Kaiser rig testing.
Complete impression creep runs on two SiAlON.

Problems Encountered

None

Publications/Presentations

SiAlON Materials Development, R. Yeckley Kennametal Inc, J. Hellmann, K Fox, The Pennsylvania State University. presented at the EBC Workshop, Nashville TN, Nov. 03.

Saint-Gobain Hot -Section Materials Developement

R. H. Licht, Vimal K. Pujari, William T. Collins, James M. Garrett, Ara M. Vartabedian
Saint-Gobain Ceramics & Plastics, Inc.
Goodard Road, Northboro, MA 01532
Phone: (508) 351-7815, E-mail: Robert.h.licht@saint-gobain.com

Objective

The goal of this Phase I program was to develop and optimize a high temperature silicon nitride based ceramic material and process suitable for microturbine hot-section component applications.

Highlights

The technical effort focused on the optimization of the as-processed (AP) surface properties of NT154. A proprietary hot isostatic press (HIP) process mentioned in the previous report was utilized. The proprietary process continued to show expected improvements in AP strength. During this period, effort was directed toward its implementation in the production HIP. Through a well laid out set of experiments, HIP parameters were evaluated for their impact on AP strength. Based on this study, modified HIP conditions were identified and improved AP strength of NT154 was realized. Phase I was completed this period and the Phase II program is scheduled to start at the beginning of January 2004.

Technical Progress

The technical effort involved a two-pronged approach:

1. Material Development
2. Net Shape Forming Development (NSFD) Involving the Machining and Direct Casting (DC) Approaches

1. MATERIAL DEVELOPMENT:

During this period, effort was directed toward duplicating the excellent AP strength of NT154, as reported previously, in a production HIP unit. Key HIP process parameters (temperature, time, and heating rate) were systematically examined through a well laid out set of experiments in the production HIP. Based on this study, the AP strength has been found to be effected by both surface flaws and the near surface microstructure. These factors appear to be controlled by both the initial green surface finish and the HIP conditions, which, due to the glass encapsulation, are dependent on the size of the HIP and, potentially, on the load.

Adjustments to the HIP schedule have resulted in a steady improvement in AP strength. The improved results, which approach those reported previously for the smaller HIP unit, are shown in Figure 1. It is important to note that the new, proprietary HIP process continues to result in higher AP strengths than the old process, regardless of the conditions. Another experiment to study the effect of the green and dense surface finish on the AP strength is underway and will

extend into Phase II. Anticipated improvements from this study are expected to result in AP strength close to the target of 700 MPa.

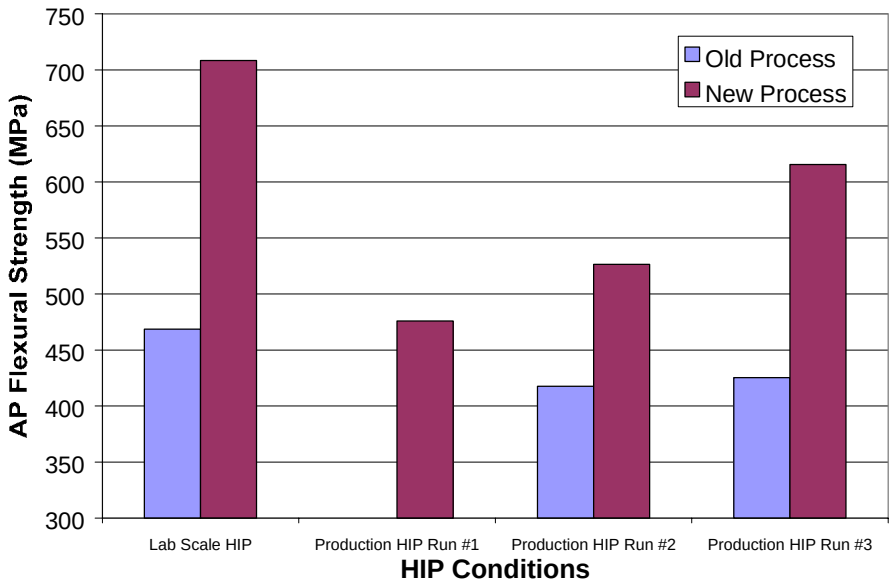

Figure 1: AP Strength as a Function of HIP Conditions

Baseline (uncoated) NT154 tiles have been supplied to ORNL for Keiser Rig testing to evaluate the environmental stability in the Microturbine environment. Silica scale thickness data for 1000 hours of testing at 1200°C is shown in Figure 2. Micrographs showing the silica scale after 500 hours of testing are shown in Figure 3. The microstructural differences between the samples appear to impact the silica scale thickness.

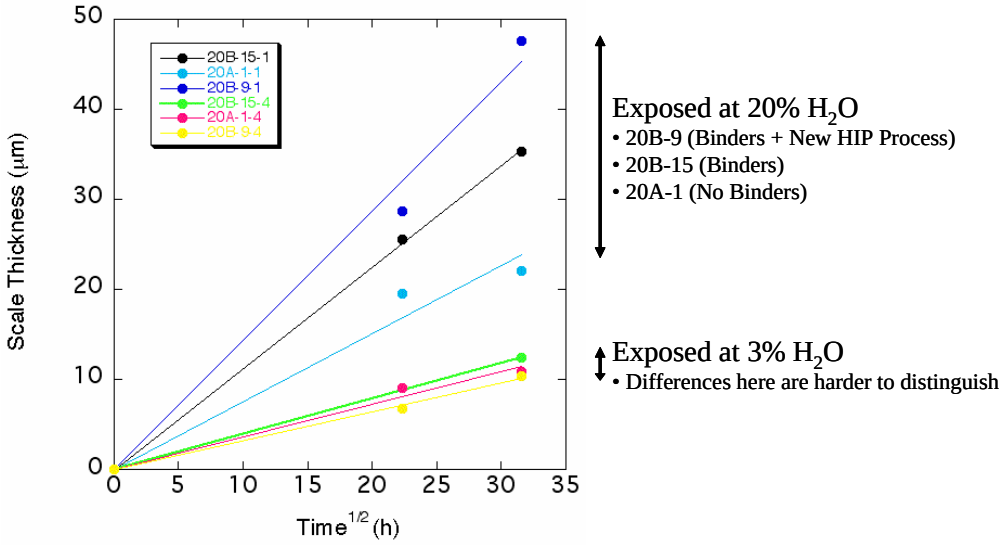

Figure 2: Keiser Rig Data for NT154

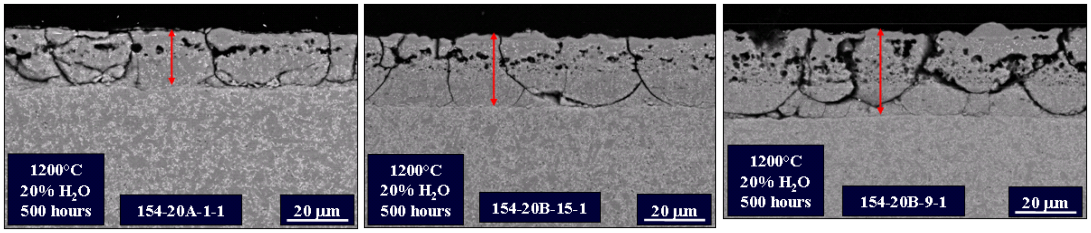

Figure 3: Micrographs of Silica Scale Formation on NT154

2. NET SHAPE FORMING DEVELOPMENT (NSFD):

As mentioned in the previous quarterly report, four fully featured green machined rotors have been fabricated. In Phase II, the optimized AP strength HIP condition described in Section 1 above will be utilized to densify these rotors. Dense rotors will be fully characterized for dimensional accuracy, AP surface finish, and mechanical properties. Test samples will be machined out of a rotor for mechanical properties evaluation at ORNL. This data will be compared with the already established data from test tiles.

Status of Milestone

Industry Interactions

- Vimal Pujari and Ara Vartabedian attended the EBC Workshop held in Nashville, TN on November 18-19, 2003.
- Robert Licht and William Donahue attended the DOE Distributed Energy Peer Review meeting, Washington, December 2-4, 2003. There were several side meetings with DOE, ORNL, and industry regarding Advanced Microturbine Systems and hot section materials.
-

Problems Encountered

None

Publications/Presentations

Ara Vartabedian, "Hot Section Silicon Nitride Materials Development for Advanced Microturbines Applications," presented at the EBC Workshop held in Nashville, TN on November 18, 2003.

Robert H. Licht, "Silicon Nitride Materials Development at Saint-Gobain", Poster Presentation at the DOE Distributed Energy Peer Review meeting, Washington, December 2, 2003.

Environmental Protection Systems for Ceramics in Microturbines and Industrial Gas Turbine Applications Part A: Conversion Coatings

S. D. Nunn and R. A. Lowden
Metals and Ceramics Division
Oak Ridge National Laboratory
Oak Ridge, TN 37831

Objective

Monolithic silicon nitride ceramics are currently the primary ceramic material being used in combustion engine environments and are under consideration as hot-section structural materials for microturbines as well as other advanced combustion systems. Under oxidizing conditions, silicon nitride will typically form a surface oxidation (silicate) layer. In a combustion environment, this silicate layer can undergo rapid degradation because of the corrosive and erosive effects of high temperature, high pressure, and the presence of water vapor. This degradation can severely limit the useful life of the ceramic in this environment. Thus, the development of an environmental protection system for the ceramic has become an essential goal for enabling the long-term utilization of these materials in advanced combustion engine applications.

One approach that is being pursued to produce an environmental protection system for silicon nitride is the formation of a surface conversion layer using the pack cementation process. Pack cementation has been used for many years to develop an oxidation protection coating on nickel-based superalloys that are used for hot-section components in gas turbine engines. A reactive gas atmosphere is used to change the composition and microstructure of the metal alloy at the surface of the component so that it will form a protective oxide film under normal operating conditions. The same approach can be used to form a modified surface region on silicon nitride ceramic components. By selecting an appropriate reactive atmosphere for the pack cementation process, the surface region can be modified to form ceramic compounds that may provide enhanced corrosion and erosion resistance in the combustion engine environment.

Highlights

The results of a study comparing the effects of pack composition, substrate composition, and furnace atmosphere on pack cementation coating products were presented at the EBC Workshop in Nashville, TN. For a given pack composition, the furnace atmosphere generally had a more significant influence on the coating composition than did the silicon nitride substrate composition. Stable oxide compounds, such as rare earth silicates, were among the phases identified in the coatings that were formed in the study.

Technical Progress

A series of silicon nitride samples was coated using the pack cementation process. Three different silicon nitride compositions were evaluated: Honeywell AS800, St. Gobain/Norton NT154, and Kyocera SN281. Each silicon nitride contains different additives to aid densification and to control the microstructure of the ceramic. The AS800 contains La, Y, and Sr; the NT154 contains Y; and the SN281 contains Lu. These elements contribute to the coating product that is formed during pack cementation. For this study, four reactive pack components were compared; these included: $AlCl_3$, $Sr(NO_3)_2$, $Y(NO_3)_3$, and $ZrCl_4$. The coating was done at 1200ºC for 2 hours. Coating furnace atmospheres of air, argon, or nitrogen were compared. These processing variables are summarized in Table 1.

Table 1. Processing variations for the pack cementation coating study.

Silicon Nitride Substrate	Reactive Pack Component	Coating Furnace Atmosphere
AS800	$AlCl_3$	Air
NT154	$Sr(NO_3)_2$	Argon
SN281	$Y(NO_3)_3$	Nitrogen
	$ZrCl_4$	

In most cases, the composition of the Si_3N_4 substrate affected the characteristics of the coating that was formed. The different additives that are used by the ceramic manufacturers can react differently with the active chemicals in the pack composition during the coating process. However, for some of the specimens with the packs containing $Sr(NO_3)_2$ or $ZrCl_4$, the coating product was unaffected by the substrate composition. The coating furnace atmosphere had a more profound affect on the coating that was formed. In almost all cases, the coating composition was different in each of the coating atmospheres.

Many of the specimens formed stable oxide coating phases in the pack cementation process. These included phases such as Y_2SiO_5, $Y_2Si_2O_7$, Lu_2SiO_5, $SrSiO_3$, $Sr_3Al_2O_6$, and $ZrSiO_4$. The coatings often showed two distinct layers: an additive coating on the surface of the substrate and a diffusion coating that penetrated into the surface of the silicon nitride. An example is shown in Fig. 1. In this case, the additive layer on the NT154 silicon nitride was only 1-2 μm thick, while the diffusion layer was 10-15 μm in depth. X-ray diffraction analysis showed the additive layer to be $SrSiO_3$. Examination of this layer by scanning electron microscopy (Fig. 2) showed that the $SrSiO_3$ had formed elongated crystals which lay flat on the surface of the substrate. Several other samples also showed prismatic crystals on the surface. Samples of promising coatings will be selected for environmental testing to evaluate the protective character of the coatings.

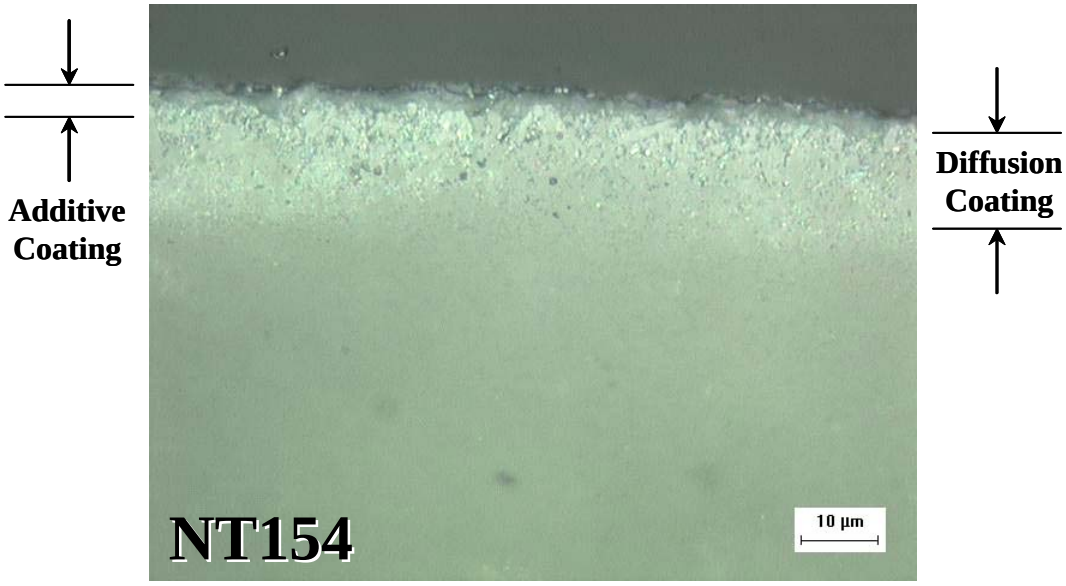

Figure 1. Optical micrograph of specimen cross-section showing the morphology of the conversion coating formed on NT154 Si_3N_4 after pack cementation at 1200ºC in nitrogen. The reactive component in the pack composition was $Sr(NO_3)_2$. The principal coating product identified by XRD analysis was $SrSiO_3$.

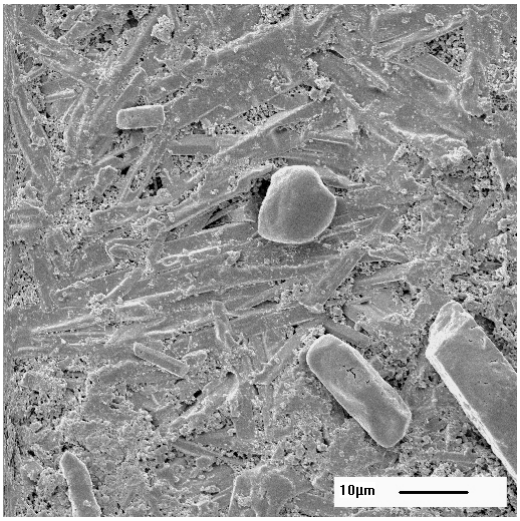

Figure 2. SEM micrograph of the coated surface of the specimen shown in Fig.1. The $SrSiO_3$ formed lath-type crystals on the surface of the silicon nitride substrate.

Status of Milestones

Evaluate the corrosion resistance of strontium aluminate-type and ytterbium-containing surface conversion coatings on silicon nitride in a simulated combustion atmosphere. (Sept. 2004)

Industry Interactions

Discussed with St. Gobain Ceramics, GE Aircraft Engines, and Kennametal collaborative efforts to produce pack cementation coatings for protection of specific materials of interest to each individual company.

St. Gobain Ceramics has agreed to supply NT154 silicon nitride material from new production runs for development and evaluation of pack cementation coatings.

Met with UTRC to identify coating compositions that may be produced by pack cementation to protect silicon nitride-based substrates.

Problems Encountered

None

Publications and Presentations

A technical presentation entitled “Pack Cementation: The Effect of Atmosphere and Substrate on Coating Composition” was given at the Environmental Barrier Coating Workshop in Nashville, TN in November 2003.

Environmental Protection Systems for Ceramics in Microturbines and Industrial Gas Turbine Applications, Part B: Slurry Coatings and Surface Alloying

B. L. Armstrong, M. P. Brady, K. M. Cooley, G. H. Kirby, and H. T. Lin
Metals and Ceramics Division
Oak Ridge National Laboratory
P. O. Box 2008, Oak Ridge, Tennessee 37831-6063
Phone: (865) 241-5862, E-mail: armstrongbl@ornl.gov

Objectives

Silicon-based monolithic ceramics are candidate hot-section structural materials for microturbines and other combustion systems. The performance of silica-forming ceramic materials in combustion environments is, however, severely limited by rapid environmental attack caused by the combination of high temperature, high pressure, and the presence of water vapor. Thus, the development of environmental protection systems has become essential for enabling the long-term utilization of these materials in advanced combustion applications.

Similar to thermal barrier coatings for nickel-based super alloys that utilize a specialized oxide surface layer and a metallic bond coat, successful environmental protection systems for ceramics and ceramic composites will likely utilize multiple layers and complex combinations of materials. Most recent efforts have focused on the selection and deposition of the oxide surface layer, and due to numerous factors, the majority of the candidates have been from the aluminosilicate family of oxide ceramics. Stable rare-earth silicate deposits have been found on component surfaces after recent engine and rig tests, indicating there may be other stable oxide compositions that have not been fully investigated. Thin coatings of selected silicate compositions will be deposited on test coupons using a variety of techniques. The specimens will then be exposed to simulated high-pressure combustion environments and materials that demonstrate good potential will be investigated further

Highlights

Concentrated Y_2SiO_5 and $Y_2Si_2O_7$ suspensions (ϕ = 0.45) that exhibit long-term stability have been fabricated for use in a dip-coating process.

Technical Progress

Characterization of the Yttrium Silicate Slurries

The behavior of aqueous suspensions comprised of yttrium silicate (Y_2SiO_5) and yttrium disilicate ($Y_2Si_2O_7$) particles was studied. Zeta potential experiments were carried out in order to characterize the surface of the particles in aqueous suspension. In addition, concentrated suspensions (~ 45 vol%) suitable for a dip-coating process were fabricated using a cationic polyelectrolyte dispersant.

Zeta Potential Analysis

Zeta potential measurements were carried out as a function of pH for dilute Y_2SiO_5 and $Y_2Si_2O_7$ suspensions (10^{-3} vol%) using capillary electrophoresis (Zetasizer 3500HS, Malvern Instruments Ltd.) and the results are shown in Fig. 1. The isoelectric point (IEP) was observed at a pH of 3.5 and 5.5 for Y_2SiO_5 and $Y_2Si_2O_7$, respectively, which is near the IEP reported for pure SiO_2 (pH 2-3).[1] Furthermore, a characteristic pH value of 9.5 was observed for both systems where a sharp decline in zeta potential occurred. This pH correlates with the IEP of Y_2O_3,[2] suggesting its coexistence with SiO_2 on the surface.

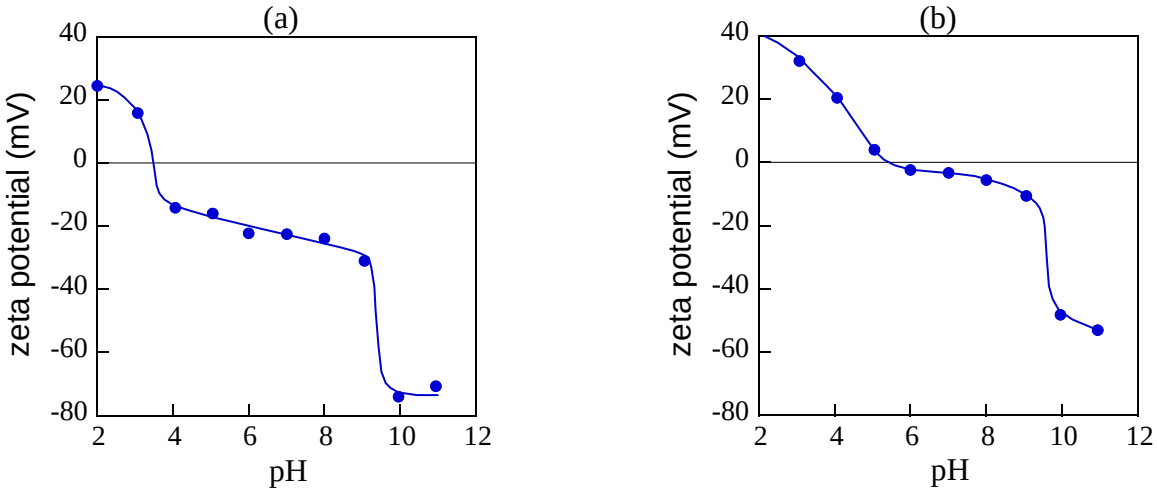

Fig. 1. Zeta potential as a function of pH for (a) Y_2SiO_5 and (b) $Y_2Si_2O_7$ suspensions (10^{-3} vol%).

Development of Concentrated Y_2SiO_5 and $Y_2Si_2O_7$ Suspensions

The ability to fabricate concentrated ceramic suspensions and optimize their rheological behavior for dip-coating is governed by interparticle forces. Long-range, attractive van der Waals forces are ubiquitous and must be nearly balanced by one or more repulsive forces to obtain slightly shear-thinning flow behavior. Polyelectrolyte dispersants, e.g., poly(acrylic acid), poly(methacrylic acid), and polyethylenimine, are commonly used to modify ceramic particle surfaces in order to impart repulsive electrosteric forces.[3, 4] PEI, a cationic polyelectrolyte, was used as the dispersant in this study. The PEI had a weight average molecular weight of 10,0000 g/mole and one protonizable amine group (NH) per monomer unit. The fraction of protonated amine groups, α, plotted as a function of pH is shown in Fig. 2. This plot indicates that PEI is negligibly protonated at pH 11, but fully protonated at pH 5.5. Favorable conditions for adsorption of the PEI onto the ceramic particle surface existed at pH conditions between 3.5 and 8.8 and between 5.5 and 8.8 for Y_2SiO_5 and $Y_2Si_2O_7$, respectively, where the PEI was highly positively charged ($1 > \alpha > 0.5$) and the ceramic powders were negatively charged.

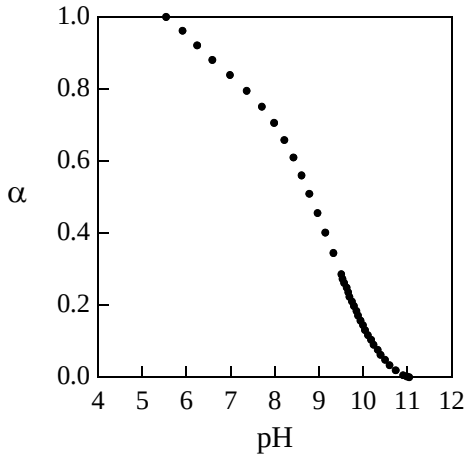

Fig. 2. Fraction of protonated amine groups, α, as a function of pH in dilute PEI solutions (10^{-3} *M*). Note, $\alpha = [NH_2^+]/([NH] + [NH_2^+])$.

Concentrated Y_2SiO_5 and $Y_2Si_2O_7$ suspensions (45 vol% solids) suitable for a dip-coating process were fabricated with the use of PEI. Rheological experiments are underway to measure the apparent viscosity (η_a), linear elastic shear modulus (G'), and yield stress (τ_Y) of such suspensions in order to optimize the dip-coating process. Future work will explore how coating uniformity and thickness may vary with the linear elastic modulus and yield stress, which can be tailored by adjusting the PEI concentration, pH, and ionic strength (salt content).

Development of a Sacrificial Coating

The presentation, "Feasibility Assessment of Self-Grading Metallic Bond Coat Alloys to Protect Si-Based Ceramics" by M.P. Brady, B.L. Armstrong, H.T. Lin, M.J. Lance, and L. R. Walker was given by M. Brady on November 19, 2003 at the 2nd Annual Environmental Barrier Coatings Workshop at the Gaylord Resort and Convention Center in Nashville, Tennessee. No further work to report this quarter.

Industry Interactions

Discussions with UTRC, Honeywell, and GE have continued. This project has also collaborated with an ARTD Fossil Energy project on Corrosion Resistant Coatings.

Problems Encountered

None

Publications

None

References

1. Reed, J.S., *Principles of Ceramic Processing*. 2nd ed. 1995, New York, NY: John Wiley & Sons. 658.

2. Parks, G. A., "The Isoelectric Points of Solid Oxides, Solid Hydroxides, and Aqueous Hydroxo Complex Systems," *Chem. Rev.*, **65** 177-198 (1965).

3. Cesarano III, J. and I.A. Aksay, "Processing of Highly Concentrated Aqueous α-Alumina Suspensions Stabilized with Polyelectrolyte," *J. Am. Ceram. Soc.*, **71** [12] (1988).

4. Cesarano III, J., I.A. Aksay, and A. Bleier, "Stability of Aqueous α-Al_2O_3 Suspensions with Poly(methacrylic acid) Polyelectrolyte," *J. Am. Ceram. Soc.*, **71** [4] 250-55 (1988).

Polymer Derived EBC for Monolithic Silicon Nitride

Rishi Raj and Sudhir Brahmandam
University of Colorado
Boulder, Co
Phone: (303)492-1029, E-mail: Rishi.Raj@Colorado.EDU

Background and Objective

Thermal barrier coating studies have shown that yttria stabilized zirconia (YSZ) shows excellent corrosion resistance in hydrothermal environments that are encountered during the operating cycle of turbine engines. However, YSZ cannot be directly used as an environmental barrier coating (EBC) over silicon nitride turbine blades, primarily because of its high thermal expansion coefficient and poor adhesion to silicon nitride. Therefore, a functionally graded multilayer, with zirconia as the outer layer and a bond coat as the inner layer, is proposed as a means of utilizing the beneficial properties of zirconia.

A candidate material for the bond coat is polymer derived silicon carbonitride (SiCN) because it has a thermal expansion coefficient that is comparable to silicon nitride and also good adhesion to it. Further, preliminary studies reveal two other attractive features (i) it exhibits good oxidation resistance and (ii) it adheres strongly to zirconia.

The objective of the present study was to explore the possibility of using SiCN – zirconia ceramics as environmental barrier coatings for silicon nitride turbine blades. The study is proposed to be conducted in two phases:

Phase (I)

(i) Developing a methodology to prepare dense SiCN – zirconia composites.
(ii) Testing the thermal shock, thermal expansion and oxidation behaviour.

Phase (II)

(i) Extending the processing technique to make dense three phase composites of SiCN, silicon nitride and zirconia.
(ii) Testing the thermal shock, thermal expansion and oxidation behaviour.

Issues Involved

The densification behaviour and thermo-mechanical properties can depend on the length scale and architecture of SiCN and zirconia in the composite microstructure. For instance, two microstructural architectures are possible (Fig. 1): Type 1 with a continuous phase of SiCN, with the zirconia particles embedded in it. Type 2, with a random distribution of grains of zirconia and SiCN.

In view of the fact that SiCN exhibits a better thermal shock resistance than zirconia, it is anticipated that Type 1 microstructure would exhibit better thermo-mechanical properties than

Type 2. However, there are additional issues in this architecture: the particle size of zirconia, the thickness of SiCN around zirconia particles and the volume fraction of the two can be varied, and these would change the properties of the resultant composite. Hence, these are potential parameters which can be changed to tailor the properties of the composite.

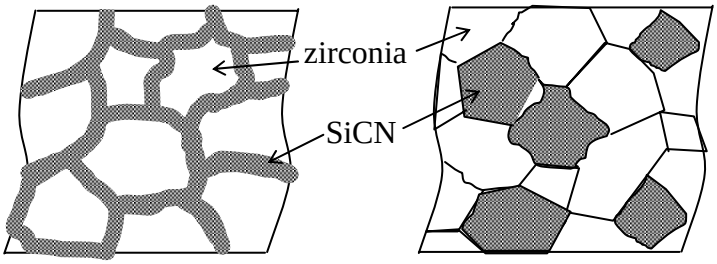

Figure 1(a) The two architectures of SiCN – Zirconia composites.

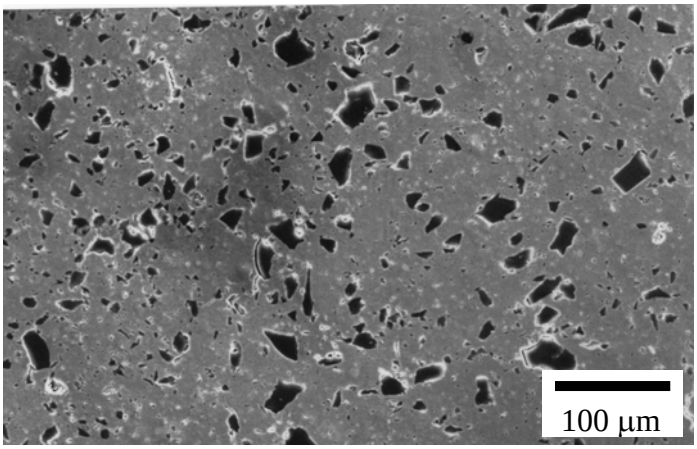

Figure 1(b) An example of Type 2 composite: Zirconia – 15 vol% SiCN. The dark phase is SiCN and the white phase is polycrystalline zirconia.

Approach

In order to design SiCN – zirconia composites with different length scales, two approaches are possible: the particle size of zirconia can be varied at a particular volume fraction of SiCN or the volume fraction of SiCN can be varied at a particular particle size of zirconia. A relationship between the zirconia particle size (P), thickness of SiCN (δ) and the volume fraction of SiCN (V_{SiCN}) can be easily derived by assuming the zirconia particles to be cubes and the SiCN to form a uniform coating on these particles. Figure 2 gives the derivation as well as a graphic representation of the relation between volume fraction of SiCN and particle size of zirconia for SiCN layers with thickness in the range of 0.01 to 1 μm.

In the present study, 10 mol% yttria stabilized cubic zircona (10YCZ) powders with two different particle sizes of 0.5 and 12 μm were procured. Initial studies were aimed at obtaining dense composites with a continuous coating of SiCN on the zirconia particles at 20 vol% SiCN. As seen in Fig. 2, the expected SiCN thickness for the 0.5 and 12 μm particles is 30 nm and 1 μm, respectively.

$$V_{SiCN} = \frac{(P+\delta)^3 - P^3}{(P+\delta)^3} = 1 - \frac{1}{\left(1+\frac{\delta}{P}\right)^3}$$

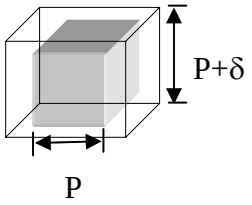

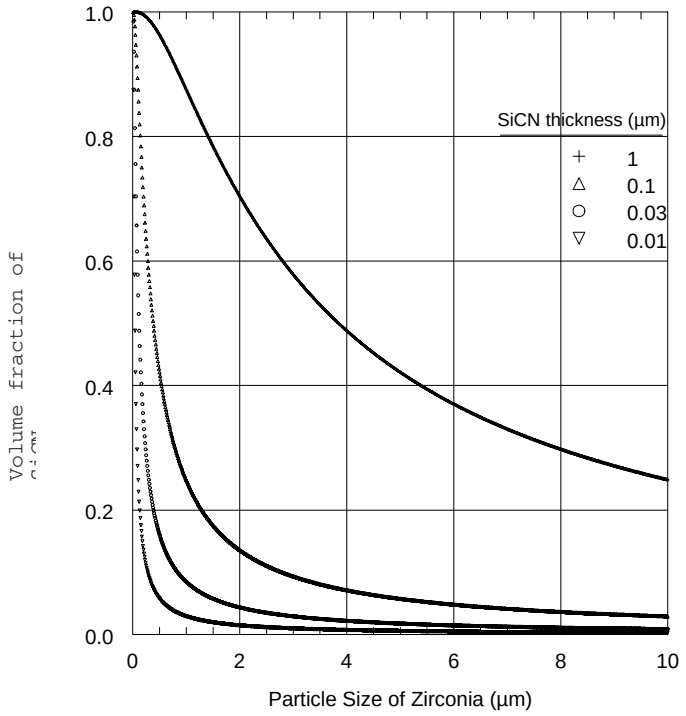

Figure 2 Variation in the volume fraction of SiCN with particle size of zirconia at various thicknesses of SiCN.

Highlights and Technical Progress

A methodology was developed for obtaining dense 10YCZ(0.5 μm) – 20 vol% SiCN and 10YCZ(12 μm) – 20 vol% SiCN composites with Type 1 microstructure. The processing involved three steps: (a) weighed amounts of zirconia powder and ceraset polymer were mixed thoroughly using acetonitrile as an extender to get a viscous slurry. The slurry was cross-linked at 673 K for 5 hr. in flowing nitrogen. This resulted in a hard porous cake. (b) the cake was ball

milled to a fine powder using zirconia balls. The fine powder was then pyrolyzed at 1273 K for 3 hr., again in flowing nitrogen. This 'ceramizes' the cross-linked polymer. (c) The pyrolyzed powder was hot-pressed in a graphite die at 1623 K at a stress of 25 MPa for a duration till the densification strain of the compact saturated, which was 11 hr. in the case of 10YCZ(0.5) – 20 v% SiCN, and 15 hr. in the case of 10YCZ(12) – 20 v% SiCN. The hot-pressing was also carried out in flowing nitrogen.

Density measurements and microstructural studies revealed that the compacts had a density of > 98%. The microstructural examination also revealed that the cubic zirconia grain size was same as the particle size of the starting powders, that is, the presence of SiCN as an interfacial phase had suppressed grain growth during densification (cubic zirconia, by itself, suffers extensive grain growth during densification). The absence of grain growth indicates that the SiCN has found a continuous coating around the zirconia particles.

Status of Milestones

Adequate progress has been made to achieve the goals of the research at this time.

Industry Interactions

Technical discussions with H. T. Lin, Karren More and Peter Tortorelli of Oak Ridge National Laboratories (ORNL). A synopsis of the recent discussion is given below:
Plan: H.T. Lin serves as the host for the post-doc (B. Sudhir), while the technical collaboration occurs with Peter, Karren and HT, as suggested by HT. Initial screening of samples to be done in HT's furnace (which can test in humid environments albeit at ambient pressure), followed by more rigorous testing in the Keiser Rig. The microstructural analysis is critical to the understanding of the oxidation process and mechanisms, which is expected to be done at HTML, possibly by Sudhir himself.

Problems Encountered

None

Publications and Presentations

Technical presentation titled "Polymer Derived EBCs for Protecting Si_3N_4 in Gas Turbine Environments" at the workshop on Polymer-Derived-Ceramics "NanoTechnology for UltraHigh Temperatures." ORNL, EBC meeting, November 18-19, 2003; Nashville, USA.

Failure Mechanisms in Coatings

J. P. Singh, K. Sharma, and P. S. Shankar
Energy Technology Division
Argonne National Laboratory
Argonne, IL 60439
Phone: (630) 252-5123, E-mail: jpsingh@anl.gov

Objective

The purpose of this research is to identify failure mode(s), understand and evaluate failure mechanisms, and to develop appropriate test methods and protocols to characterize the integrity and predict failure of environmental and thermal barrier coatings for advanced turbine applications.

Technical Highlights

Finite element analysis (FEA) was performed to evaluate the stress profile in an AS800 Si_3N_4 bar coated with an environmental barrier coating of pure Ta_2O_5 under four-point bend loading. The maximum stress at fracture was estimated to occur at the Ta_2O_5/Si_3N_4 interface. This result was consistent with fractographic observations of failed four-point specimens, which clearly indicated fracture initiation from the interface. Also, the value of maximum stress calculated by FEA was in good agreement with the experimentally measured flexure strength.

Technical Progress

Effort this quarter concentrated on a three dimensional FEA to evaluate the stress profile during four-point flexure loading of a rectangular bar specimen of AS800, coated with pure Ta_2O_5. The specimen dimensions were taken to be 2mm x 1.5mm x 26mm, and the thickness of the Ta_2O_5 coating was 200 μm. The outer and inner loading spans were taken to be 20 mm and 10 mm, respectively. The simulation of stress profile in the Si_3N_4 bar during flexure loading considered: (1) the effect of residual stresses due to coefficient of thermal expansion (CTE) mismatch between the Ta_2O_5 coating the Si_3N_4 substrate, and (2) the effect of elastic mismatch between the coating and substrate during mechanical loading.

All simulations were performed using ABAQUS standard FEA software program. The stresses were modeled on one-fourth ($1/4^{th}$) section of the sample in order to decrease computing time. This allowed the mesh to be tightened by four times, and also facilitated a denser cluster of data points to be acquired at the areas of interest. The Ta_2O_5 coating was assumed to be deposited at 1200°C and subsequently cooled to room temperature. Experimentally determined elastic modulus values of the Ta_2O_5 coating (E = 90 GPa) was used in the determination of stresses by finite element analysis. A value of 3.45 x

10^{-6}/K was used for the CTE of Ta_2O_5 coating. The elastic modulus and CTE of Si_3N_4 were taken to be 315 GPa and 3.9 x 10^{-6}/K, respectively.

Figure 1 shows the stress distribution in the Ta_2O_5 coating and Si_3N_4 substrate at fracture, as estimated by FEA. These stresses are directed in the longitudinal direction in a plane parallel to the substrate. It is clear from the figure that the maximum tensile stress is present at the Ta_2O_5/Si_3N_4 interface. The maximum tensile stress is expected to promote the propagation of inherent crack at the interface leading to failure of the coated Si_3N_4 substrate. This is consistent with the observed failure of a coated Si_3N_4 substrate as shown in Figure 2, which indicates fracture initiation from voids at the Ta_2O_5/Si_3N_4 interface. The average measured strength (458±80 MPa) of the coated Si_3N_4 substrate agrees reasonably well with the maximum stress (470 MPa) estimated by FEA. The strength measurement was based on the analysis of a composite beam in bending. Since the maximum stress occurs at the substrate/coating interface, a calculation was also made based on the simple beam bending equation using only the substrate thickness. The calculation resulted in an average measured strength of 432±82 MPa, which is also in a reasonable agreement with the maximum stress obtained by FEA. This agreement is believed to be due to the small thickness and low elastic modulus of the coating layer.

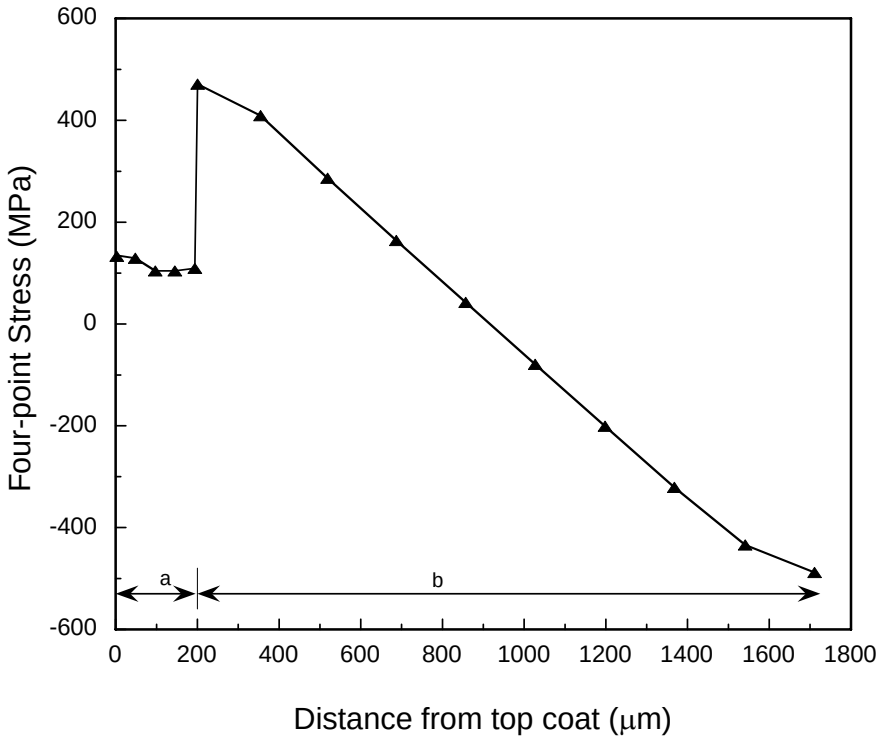

Fig. 1 Stress profile (obtained by FEA) at failure in a Ta_2O_5 coated AS800 Si_3N_4 substrate under four-point flexure loading. a and b, represent the thickness of the Ta_2O_5 coating and Si_3N_4 substrate, respectively.

Thus, the use of simple beam bending equation using only the substrate thickness can provide reliable strength data for coated Si_3N_4 substrates with thin coating layers having low elastic modulus. However, the stress profile and the location of maximum stress depend on various parameters, including the thickness and elastic modulus of EBC layers. Thus, each EBC system should be analyzed for stress distribution in order to judiciously select the bending equation and thickness parameter for strength evaluation.

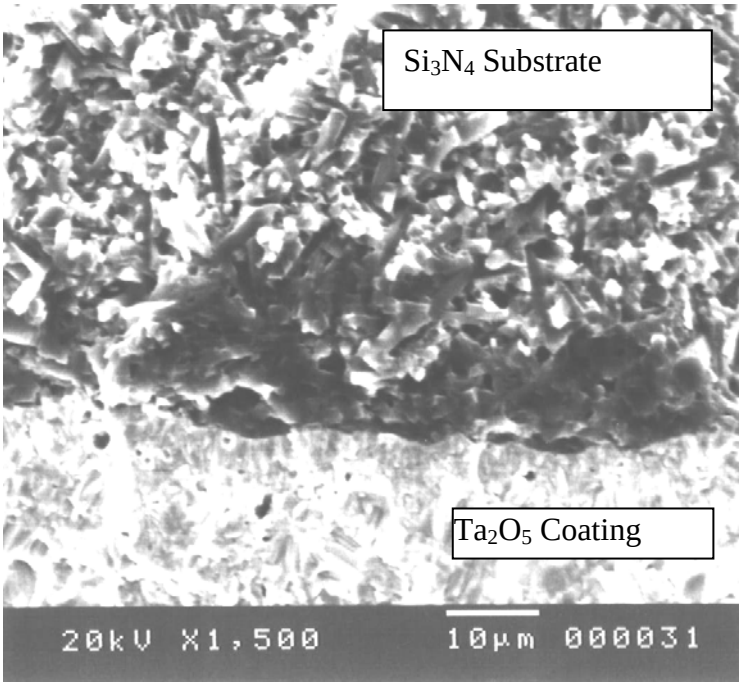

Fig. 2 Micrograph of a Ta_2O_5 - coated AS800 Si_3N_4 specimen showing the critical flaw (voids) causing fracture initiation at the coating/substrate interface.

Status of Milestones

Examine and estimate residual stresses and their effect on mechanical properties of coated specimens. November 2003. Completed.

Initiate mechanical and microstructural evaluation of Si_3N_4 specimens with novel EBCs obtained from Northwestern University/Honeywell. September 2004. On Schedule.

Industry Interactions

Discussion on the results of mechanical and microstructural evaluation of Ta_2O_5 coated AS800 Si_3N_4 specimens was continued with Northwestern University/Honeywell.

Problems Encountered

None

Publication

J. P. Singh will present James I. Mueller Award Lecture entitled, " Residual Stresses in Ceramic Composites and Coatings", at the 28th International Cocoa Beach Conference and Exposition on Advanced Ceramics and Composites, January 25-30, 2004.

High-Temperature Diffusion Barriers for Ni-Base Superalloys

B. A. Pint, K. M. Cooley and J. A. Haynes
Metals and Ceramics Division
Oak Ridge National Laboratory
Oak Ridge, TN 37831-6156
Phone: (865) 576-2897, E-mail: pintba@ornl.gov

Objective

Nickel-base superalloys require coatings to improve their high temperature oxidation resistance, particularly when a thermal barrier coating is employed. The underlying oxidation-resistant metallic coating or bond coat is degraded by the loss of Al due to oxidation, but much more Al is lost due to interdiffusion with the superalloy. Loss of Al causes diffusion aluminide coatings to undergo phase transformations, which likely cause deformation of the bond coat surface and subsequent loss of the protective alumina scale and the overlying thermal protection layer. The goal of this program is to fabricate and assess potential compounds for use as high-temperature diffusion barriers between coating and substrate. Ideally, the barrier would act to reduce the inward diffusion of Al, as well as the outward diffusion of substrate elements (such as Cr, Re, Ta, W), which generally degrade the oxidation resistance of the coating. The work is motivated by previous experimental results which suggested some compositions that exhibited diffusion-barrier capabilities. A secondary objective is to demonstrate routes to fabricating diffusion aluminide coatings incorporating a diffusion barrier using chemical vapor deposition (CVD).

Highlights

Aluminide coatings with a starting Hf-Pt coating are now being characterized. Pre-oxidized, Ni-plated superalloys also were aluminized to form CVD NiAl from a Ni plating. Although some of the Ni plating spalled prior to aluminizing, initial characterization showed that NiAl coatings with the target microstructure were formed in regions where the Ni plating remained intact. This result suggests that Ni-plating of specimens prior to aluminizing may be a feasible route to building a diffusion coating on top of an effective diffusion barrier.

Technical Progress

Pt-Hf coatings

Additional Pt+Hf plated specimens were heat treated and aluminized this quarter for characterization of Pt-Hf thin film behavior during aluminizing, and for oxidation testing. A series of these specimens is being analyzed by electron microprobe analysis to evaluate the influence of various heat treatments to promote the formation of $HfPt_3$, and to examine the stability of this phase in contact with NiAl.

Figure 1 shows a specimen with a 3 μm Pt layer and a 1 μm Hf layer after heat treatment at 500°C for 1h and 900°C for 2h. The original intent of the heat treatment was to prevent or reduce delamination of the coating during aluminizing. After heat treatment, three layers were evident, with little porosity and a total thickness of ≈10 μm. As reported previously, the central layer had a composition near $HfPt_3$, the outer layer was Pt-rich, and the inner layer was the due to interdiffusion with the substrate. There was some buckling of the coating in localized areas, but most of the coating was intact and adherent.

Figure 1b shows the same specimen after 1h aluminizing at 1100°C. The aluminizing was stopped after only one hour to determine the rate of diffusion of Al through the Hf-Pt phase shown in Figure

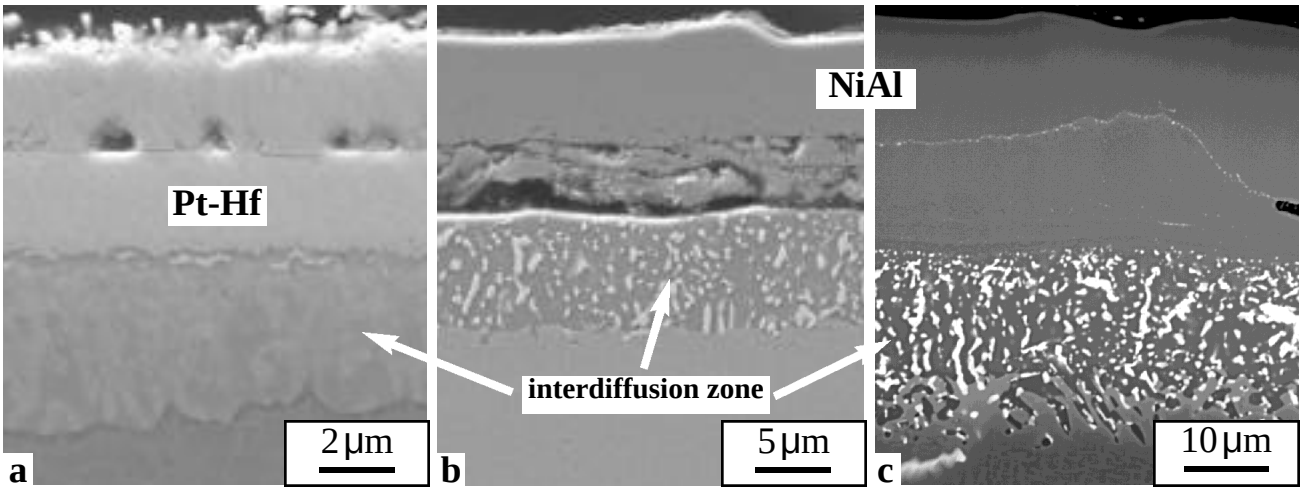

Figure 1. SEM secondary electron images of (a) polished cross-section of a specimen with a 3µm Pt and a 1µm Hf layer after heat treatment for 1h at 500°C and 2h at 900°C. (b) Same specimen after 1h aluminizing at 1100°C. (c) SEM back-scattered electron image of a similar specimen after 6h aluminizing. Note the different magnifications in each micrograph.

1a. After aluminizing, there was a significant increase in total coating thickness (18.4µm), as well as important changes in the microstructure. The outer β phase layer was 7 µm thick, similar to the inner interdiffusion zone. The middle layer appeared to be cracked and porous and may result from poor adhesion between the original coating and the substrate. Chemical composition profiles of this specimen are currently being measured by electron microprobe. For reference, Figure 1c shows a similar specimen after 6h aluminizing at 1100°C, with little porosity remaining between the outer layer and the interdiffusion layer

One interesting result of the various pre-aluminizing heat treatments is illustrated in Figure 2. This figure shows some unique areas from the annealed specimen in Figure 1a. In these regions, there were visible gaps between the two outer layers. In those regions, the surface of the coating was smooth, and there was less interdiffusion beneath the coating. However, in areas where the two layers

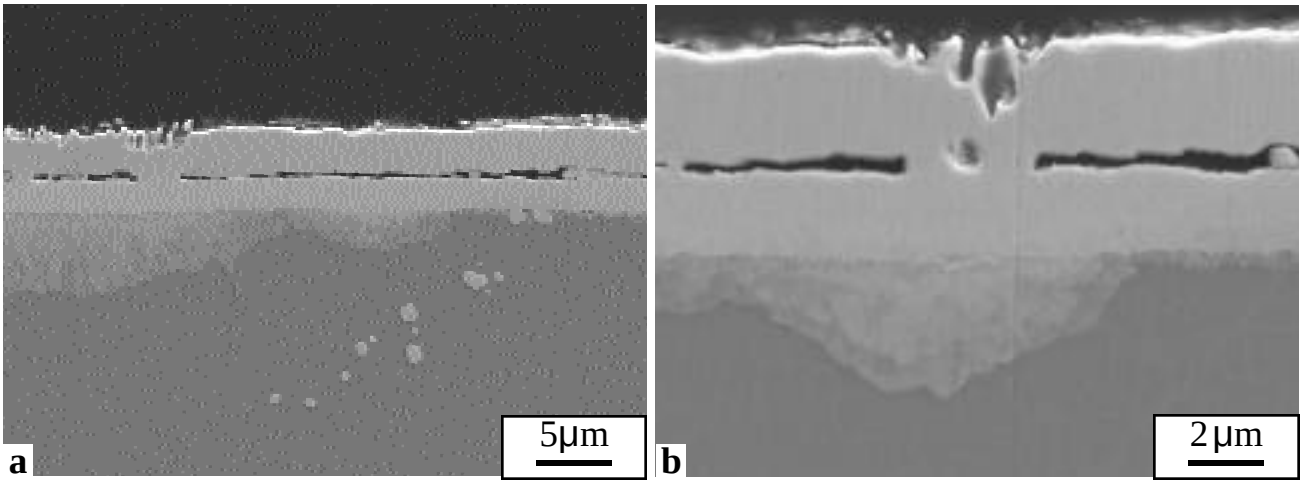

Figure 2. SEM secondary electron images of polished cross-sections of a specimen with a 3µm Pt and a 1µm Hf layer after heat treatment for 1h at 500°C and 2h at 900°C. Note the correlation between surface perturbation and sub-surface interdiffusion.

were in intimate contact and more diffusion had occurred, there were two visible changes in microstructure, Figure 2b. First, beneath the intact coatings a deeper interdiffusion zone formed in the superalloy. As shown previously, this zone is rich in Pt and a low concentration of Hf. Second, the surface of the outer Pt layer became very irregular, particularly in Figure 2b, possibly due to rapid Pt diffusion into the substrate.

Aluminizing Ni-plated specimens

In order to study the process of fabricating a coating over an effective diffusion barrier, René N5 superalloy substrates with an alumina scale acting as a model diffusion barrier were Ni-plated and aluminized. A commercial source was used for the Ni-plating and, in some cases, the Ni adhesion was poor. Two of the Ni-plated specimens were aluminized for 3h at 1100°C, and two others were aluminized under identical conditions for 6h. Figure 3 shows two different specimens aluminized for 3h with Ni plating over intact alumina layers. In both cases, patches of NiAl are visible on top of the alumina scale. The coating morphology was very non-uniform, possibly due to lateral diffusion of Ni across the alumina surface. No interdiffusion zone was visible beneath the alumina layers, suggesting that little if any Ni diffused outward and little Al diffused into the superalloy substrate.

Figure 4 compares an aluminized (6h, 1100°C) surface with no Ni-plating (plating spalled prior to aluminizing), with a location where most of the Ni remained intact. In Figure 4a, the microstructure and thickness (34 μm) of the single-phase NiAl coating and the inner multi-phase interdiffusion zone (29 μm) are very similar to that of a typical aluminized superalloy. Figure 4b shows a similar thickness of NiAl coating (36 μm), however, the underlying diffusion zone was much thicker (59 μm) and contained significant porosity and larger refractory-rich precipitates. Unfortunately, there was no evidence of the initial sub-micron layer of alumina beneath the Ni plating that was to serve as the model diffusion barrier. The alumina layer may have broken up into particles during aluminizing, or been otherwise disturbed. The results demonstrate that it is possible to form a single-phase NiAl coating from a Ni overlayer, although the experiment was not completely successful due to the lack of an intact diffusion barrier and the increased porosity. A new Ni plating vendor is now plating a second set of pre-oxidized substrates.

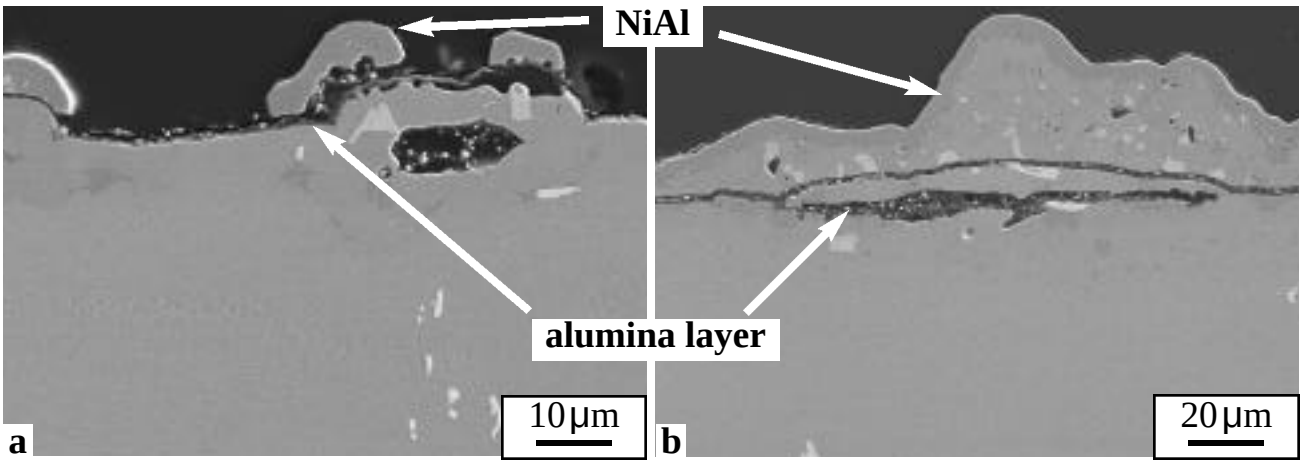

Figure 3. SEM secondary electron images of polished cross-sections of CVD aluminized (3h) pre-oxidized, Ni-plated superalloys. Because the Ni plating was not very adherent, only patches remained for aluminizing.

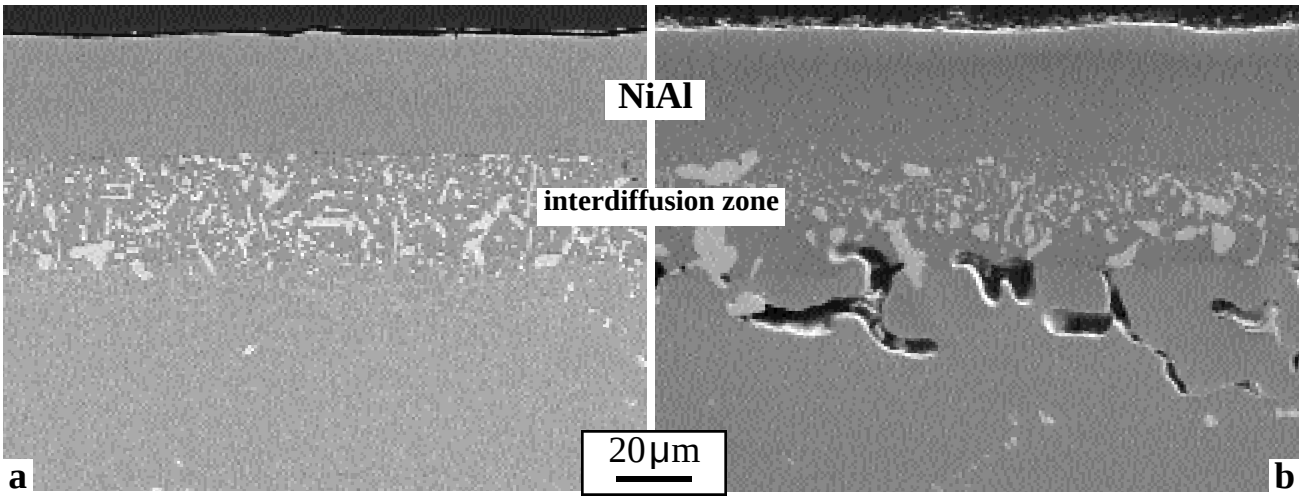

Figure 4. SEM secondary electron images of cross-sections of René N5 specimen after aluminizing for 6h. (a) location where Ni plating spalled away prior to aluminizing, (b) location with intact Ni-plating.

Status of Milestones

FY 2004
Complete characterization and testing of the first batch of precious metal-based diffusion barriers and report disclosable findings in an open literature publication.
(September 2004)

Industry Interactions

Discussed aluminide coatings on Ni-base alloys for advanced heat exchangers with Barry Yang from Velocys Inc. (Plain City, OH)

Problems Encountered

None

Publications

None

POWER ELECTRONICS

High Temperature Heat Exchanger

E. Lara-Curzio, J. G. Hemrick, A. Zaltash, N.C. Gallego, C.A. Walls
Oak Ridge National Laboratory
P.O. Box 2008, Oak Ridge, TN 37831-6069
Phone: (865) 574-1749, E-mail: laracurzioe@ornl.gov
B. E. Thompson
University of Western Ontario

Objective

As part of a collaborative effort between ORNL and the University of Western Ontario, graphite-based heat exchangers will be designed and evaluated for heat recovery systems in microturbine applications. In particular, it is desired to improve the efficiency of heat recovery systems based on aluminum fin heat exchangers that are currently being used in commercial units. In coordination with modeling efforts, the microstructure of graphite-based heat exchangers will be designed in order to maximize heat transfer while minimizing pressure drop. The efficiency of the new designs will be compared against currently used aluminum fin heat exchangers and eventually evaluated using a Unifin Microgen heat recovery unit couple to a Capstone C60 microturbine.
Work will be supplemented with experiments to gain a better understanding of the effect of heat exchanger material microstructure on gas flow penetration, pressure drop, and mechanical strength.

Technical Progress

Four scenarios have been formulated for the connection of the Unifin Microgen heat exchanger to the 60 kW Capstone microturbine. These scenarios compare the feasibility of running the heated hot water from the Unifin Microgen into a building hot water supply via an external holding tank, versus creating a closed loop system where hot water from the Unifin Microgen would be cooled via a secondary heat exchanger and recirculated continuously through the system. A comparison of water/water versus water/air secondary heat recovery systems is also underway. Cost estimates for each scenario are currently being performed.

The development and fabrication of a “miniature wind tunnel” device was initiated to determine the effect of material microstructure on the depth of gas penetration and pressure drop in carbon foam and fiber-based heat exchanger materials. An experimental prototype was constructed and the applicability of infrared imaging, fluorescent microsphere tracers, and sulfur containing tracer gases will be investigated to determine the depth of gas penetration into the heat exchanger materials. Information on the depth of gas penetration in these systems is important to optimize material usage.

Development and implementation of a method to evaluate and compare the mechanical properties of individual foam ligaments using X-ray tomography and rapid prototyping techniques has been initiated. Argonne National Laboratory has been identified as one

site for performing the tomography and estimates are being sought for file conversion and rapid prototyping services.

Alternate graphite fiber materials, with similar properties to that of the graphite foam, have been identified. Sources of these fibers and weaving methods are currently being investigated.

A study of thermal flow and pressure drop in carbon foam materials was performed at the University of Western Ontario. This study resulted in the formulation of an engineering model that provides thermal resistance and pressure drop in air-water heat exchangers with plate-fin and annular-fin configurations**.** Results are based on a combination of the following: measurements of bulk conductivity of porous carbon foam; well-established correlations for convective heat transfer from tubes, plates and fins; measured thermal resistance at the interface between aluminum and porous carbon foam with a number of different joints; and an engineering approximation for the effects of porosity on convective heat transfer.

Status of Milestones

- Installation of Unifin Microgen heat exchanger and connection to Capstone 60 kW microturbine. (June 2004)
- Fabrication of carbon-fiber perform prototypes. (September 2004)

Problems Encountered

None

Publications/Inventions/Meetings

B. E. Thompson and A. G. Straatman, “Modeling of Porous-Carbon-Foam Heat Exchangers”, AGS Scientific Inc. (2003).

Industrial Interactions

Technical discussions have been held with the following organizations:
Albany International Techniweave Inc.
Cytec Carbon Fibers
Javelin
Mo-Sci Corporation
Pheonix TPC
Unifin

Heat Exchange Concepts Utilizing Porous Carbon Foam

B. E. Thompson and A. G. Straatman
Faculty of Engineering
The University of Western Ontario
London, Ontario, Canada N6G 4K1
Phone: (519)850-2530, E-mail: Thompson@eng.uwo.ca

Objective

There is a need to produce engineering models for design of heat exchangers made from emerging porous carbon-foam materials. Knowledge and understanding of the effects of carbon foam on convective heat transfer is crucial to the development of appropriate engineering approximations for these design models. The overall objective is to explore new ideas for heat-exchanger configurations, especially for situations in which current technology is marginally cost effective. A thermo-economic model and a strategic design study are planned to provide new understanding for assessment in a stage-gate approach to further prototype development.

Highlights

A combination of engineering-design and computational activities have been initiated to obtain new understanding and knowledge about interstitial flow through carbon foam that affects the effective surface area for heat transfer and about the effects of roughness and pore size on flow over carbon foam. Preliminary results obtained on automotive radiators suggest heat transfer enhancement could be significant if the pores size, permeability and geometry of carbon-foam components were designed appropriately.

Technical Progress

A thermal engineering model for the design of air–water heat exchangers has been developed based on a unit cube of porous carbon foam. This model can quantify the surface roughness, exposed surface area, ratio of surface area to volume, permeability, and effective thermal conductivity based on local thermal equilibrium in porous carbon-foam components. The model was validated by comparison measured effective thermal conductivity for two carbon foam samples (Domestic Precursor Conoco Mesophase FOAM A; Foreign Presursor AR mesophase FOAM B) measured at ORNL (see “High thermal conductivity graphite foam” www.ms.ornl.gov/sections/mpst/cimtect/default.htm). The maximum differences between measured and calculated values were less than 2% for the FOAM A and less than 6.5% for FOAM B.

In addition, a thermal resistance model has been engineered to estimate the airside pressure drop in the pore channel (neglecting inertial term), the airside thermal resistance based on channel flow correlations, and the core geometry and tube configuration based

on an effectiveness-NTU method. An orthogonal design method was used with these models to predict an optimal pore diameter of about 300 to 350 um and an optimal porosity which is about 80% smaller than that of air-water radiator reported in R.D. Ott, A. Zaltash, J.W. Klett, "Utilization of a graphite foam radiator on a natural gas engine-driven heat pump", proceeding of IMECE'02, 2002 ASME International Mechanical Engineering Congress & Exposition, New Orleans, Louisiana Nov. 17-22, 2002. Calculated values of core performance rating at the test conditions for this radiator were about 0.89 and about 11% less than those measure so that the model is sensibly conservative. Using these models new design for the air radiator application were investigated and it was estimated that the use of porous carbon foam could result in performance improvements of about 35% increasing on the heat load, 67% reduction on the air pressure drop, 40% reduction on the tube number and 25% reduction on the bundle weight. Experimental validation of these calculated estimates is needed.

Two phenomena appear likely responsible for the enhanced convective heat transfer in flow over a porous carbon-foam surface: first, increased mixing in flow over the surface and, second, interstitial flow that increases the surface area on which convection transfers heat in an array of bubble pores. Computational Fluid Dynamics (CFD) is also being explored to predict convective heat transfer in flow over porous carbon foam and, after development is complete, will be used to provide insight into the two aforementioned phenomena that are expected to strongly influence these empirical values. In addition, additional experiments needed to make these constants more generally applicable have been designed and are under discussion with ORNL and Western technical personnel.

Status of Milestones

The next milestone is the design of air-water heat exchanger made of carbon foam in collaboration with ORNL technical personnel. The design philosophy for this heat exchanger will aim to show the benefits of the use of a carbon-foam replacement for a commercial recuperator in a microturbine, which has been chosen for detailed study.

Industry Interactions

Unifin continues to support Western efforts to obtain better understanding of heat-exchanger performance and selection issues for microturbine applications.

Problems Encountered

Experimental results from which the values of empirical constants for the thermal model porous-carbon foam can be obtained, are needed. The quantity of existing data is insufficient for the range of problems of practical interest in microturbines. A test program has been developed to obtain results in a practical range of porosity, pore size and fin geometries..

Publications/Presentations

Thompson, B.E. and Yu, Q.: Development of an ultra-efficient air to water heat exchanger using carbon foam. DOE/CETC Conference on Microturbine Applications, Los Angeles, CA, January 20-23, 2004.

Hemrick, J.G., Lara-Curzio, E., Zaltash, A., Gallego, N.C., Walls, C.A., Thompson, B.E.: Evaluation and Application of High Thermal Conductivity Materials for Microturbine Heat transfer Systems. DOE/CETC Conference on Microturbine Applications, Los Angeles, CA, January 20-23, 2004.

MATERIALS FOR ADVANCED RECIPROCATING ENGINES

SPARK PLUG EROSION AND FAILURE

M. P. Brady, H. T. Lin, J. H. Whealton, R. K. Richards, and J. B. Andriulli,
Oak Ridge National Laboratory
P.O. Box 2008, Oak Ridge, TN 37831-6115
Phone: (865) 574-5153, E-mail: bradymp@ornl.gov

In order to meet increased efficiency and decreased emissions goals in natural gas engines, the lean-limit will need to be extended through increasing cylinder pressures. Significant increases in pressure are often limited by the ignition system that already is the primary maintenance item in NG engines. The goal of this research is to increase our fundamental understanding of plug erosion and the relationships between plug life, costs, and the technical factors that can influence plug life. The ultimate objective of this work is improved spark plugs for natural gas engines. The spectral emission efforts and a portion of the metallurgical examinations are funded by the ARES Program.

Technical Progress and Results – Erosion and Failure of NG Spark Plugs

An intensive study has continued in the identification of the chemicals found in the spark plug arcs. The goal of this study is to identify an erosion mechanism based on this chemical identification through changes in the observation as the spark plugs age. Many of these chemicals have been identified by observation of spectral emission lines including molecular nitrogen, calcium, sodium, oxygen, nickel and hydrogen. So far, ***no*** spectral emission lines associated with either platinum or iridium have been identified. A new spectrometer has been added for these investigations that extends the spectral coverage both into the infrared and the ultraviolet. It is in the ultraviolet range that we expect to explore for line emissions from the metals. The time response of the spectral emissions during the electrical discharge is also being investigated. The time behavior of the spectral lines offers information on the source of the erosion process. Preliminary time evolution results are interesting in that the emissions lines persist beyond when the spark plug current terminates

With the new spectrometer exploring emissions from the spark in the ultraviolet, lines from nickel were identified. These were found when testing new spark plugs. For most of the used plugs, the nickel lines were not observed. In contrast, the calcium was observed in the used plugs but not found in the emissions from the new plugs. This can be seen in the spectra shown in Figure 1.

The change in the spectral emissions from nickel for a new plug to calcium for a used plug suggests that the erosion mechanism also changes as the plug is used. For a new spark plug the nickel is probably eroding due to sputtering. The platinum and iridium do not sputter as easily as nickel and are not observed in the emission spectrum. As the spark plug ages and becomes

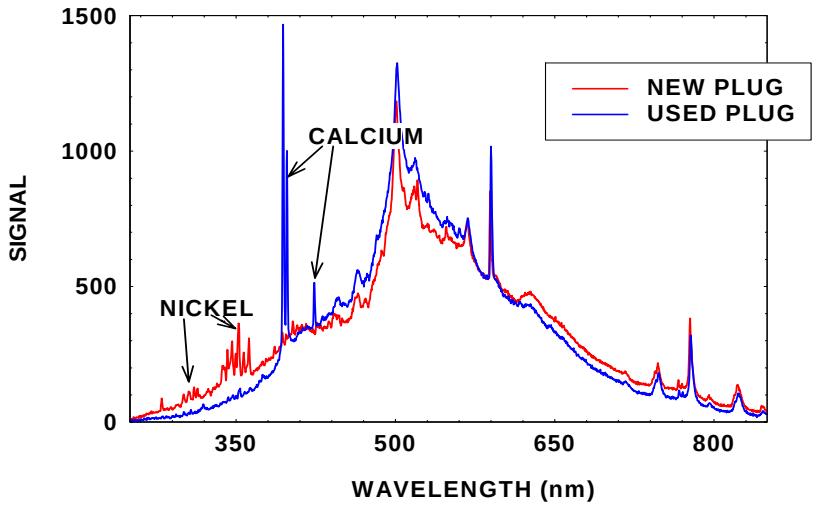

Figure 1. Comparison of spectral line emissions of a new spark plug (red curve) to a used plug (blue curve).

contaminated with calcium coming from the lubricant, the erosion changes. It is likely that the calcium bonds with the metals on the electrodes; this permits the electrodes to oxidize and produce cracking and flaking of surface material as the loss mechanism. These speculations are consistent with the metallurgical observations as seen in Figs. 2 and 3 below.

Characterization and Development of Spark Plug Materials and Components - H. T. Lin and M. P. Brady

Microstructure characterization for spark plugs after 4,386 h engine tests was continued this reporting period. Representative polished cross sections of these plugs are shown in Figure 3. Extensive intergranular cracking was observed in both Pt and Ir electrodes after engine service. In addition to surface erosion processes/material loss due to sputtering and related effects, the generation, growth, and coalescence of intergranular cracks in both electrodes would result in significant material loss and accelerated erosion during service. A Ca-containing oxide scale (< 1 μm thick) was also observed on both electrode surfaces. Efforts are underway to initiate a systematic joint study for characterization of spark plugs after defined intervals of engine service to elucidate the failure mechanism and the relative importance of the Ca-containing oxide scale formation to the onset of crack generation in the Pt and Ir electrodes, as well as other erosion mechanisms. An extensive literature research has also been initiated regarding impurity elements/conditions that lead to intergranular cracking and Pt and Ir alloys.

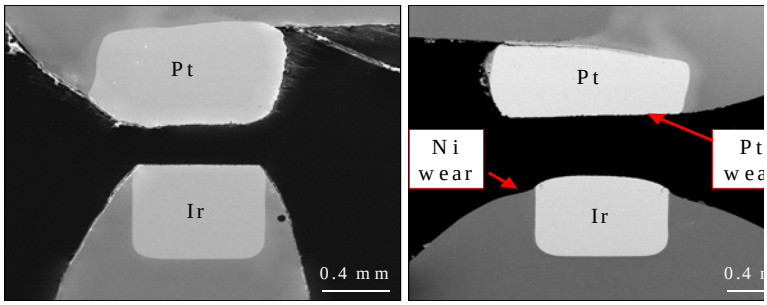

Figure 2. Micrograph showing the differences between a new and used spark plug; of note is the erosion of both the nickel base and the platinum electrode.

Efforts to increase spark plug lifetimes via the development of improved electrode alloys were also initiated during this reporting period. This subtask will be based on insights gained from the characterization of engine tested spark plugs, as well as on the manipulation and optimization of materials parameters that have been linked to improved erosion resistance (melting point, work function, hardness/strength, and oxidation/corrosion resistance, etc.). In support of this work, a simple bench top test rig for electrode materials screening is being assembled. This rig will be used to provide a rapid and economical way to screen and compare the sparking behavior/erosion resistance of developmental alloys, relative to baseline Ir and Pt alloys. Down-selected alloys will then be evaluated under increasingly more rigorous and representative test conditions using facilities at NTRC, with the goal of manufacturing prototype spark plugs for engine testing. Efforts will also be initiated to attract industrial collaborators from the alloy supplier and spark plug manufacture industries in support of the electrode alloy development work and to provide a mechanism for technology transfer of the developed alloys.

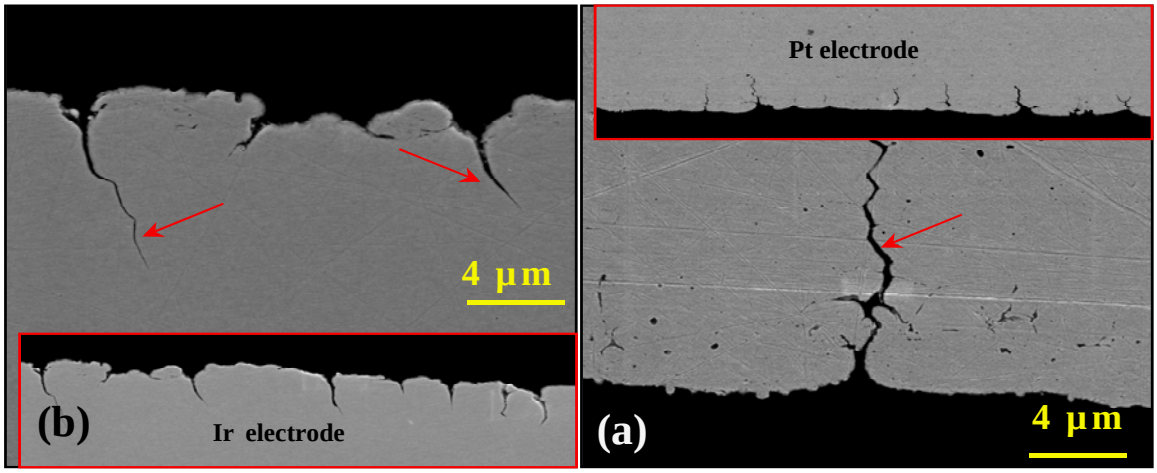

Figure 3. SEM micrograph of polished cross section of spark plug electrodes after 4368h engine test. a). Pt ground electrode, and b) Ir central electrode.

Status of Milestones – Spark Plug Erosion & Failure

Develop preliminary erosion/failure models (Sept 2004) – this milestone is on track for being met. The milestone will depend on obtaining suitable plugs from engine manufacturers.

Characterize used spark plugs metallurgically (Sept 2004) – this milestone is on-track to be met.

Problems Encountered – Spark Plug Erosion & Failure

None

Advanced Materials for Exhaust Components of Reciprocating Engines

P. J. Maziasz and N. D. Evans
Metals and Ceramics Division
Oak Ridge National Laboratory
P.O. Box 2008, Oak Ridge, TN 37831-6115
Phone: (865) 574-5082, E-mail: maziaszpj@ornl.gov

Objective

This program addresses the general high-temperature and performance limitations of various critical exhaust components (exhaust valve, exhaust manifold, turbocharger housing) for advanced natural gas reciprocating engine systems (ARES). It began by focusing on the Ni-based superalloy exhaust valves for ARES engines, but last year expanded to also consider other exhaust component materials (manifolds, turbochargers) for higher temperatures in advanced ARES engines. The program continues to assess the needs and priorities of ARES engine makers.

Highlights

ORNL completed detailed microcharacterization of Ni-based superalloy exhaust valves provided by Waukesha Engine, Dresser Inc. The Pyromet 31V Ni-Cr-Fe based valve contains a mixture of Ti- and Al-oxides beneath the surface of the combustion face of fresh valves, and more Ti-oxide particles form during service aging. Service aging produces large lath precipitates of α-chromium in the γ' hardened matrix, and increases the precipitation of Cr-rich $M_{23}C_6$ along the grain boundaries. This microcharacterization forms the basis for examination of similar valves exposed in advanced ARES engines. Some highlights of the creep-rupture resistance and microstructural behavior of the new CF8C-Plus cast austenitic stainless steel developed for advanced diesel engine exhaust component applications are also summarized, because that new steel is now being commercialized and may be applicable for similar components in ARES engines.

Technical Progress

Nickel-based superalloys like Nimonic 80A, 90, Pyromet 31 and Waspaloy are used to make exhaust valves for a variety of advanced diesel and ARES engines. These valves are complex systems, with weld-overlays on the valve seat, and coatings on the combustion face. The fillet region of the exhaust valve can see temperatures close to 700^{o}C, and those temperatures in valves of advanced ARES engines may be even higher. High-temperature engine exposure changes the base-metal microstructure and mechanical properties, as well as the structure at the coating and base-metal interface.

Microcharacterization of exhaust valves of Pyromet 31V (Ni-22Cr-15Fe alloy with Ti and Al for γ' precipitation hardening), provided by Waukesha Engine, Dresser Inc. and

TRW Automotive Division, TRW, Inc. was completed this quarter. Microcharacterization of the valves in the middle of the combustion face, comparing fresh and engine tested valves, is shown in Figs 1-3.

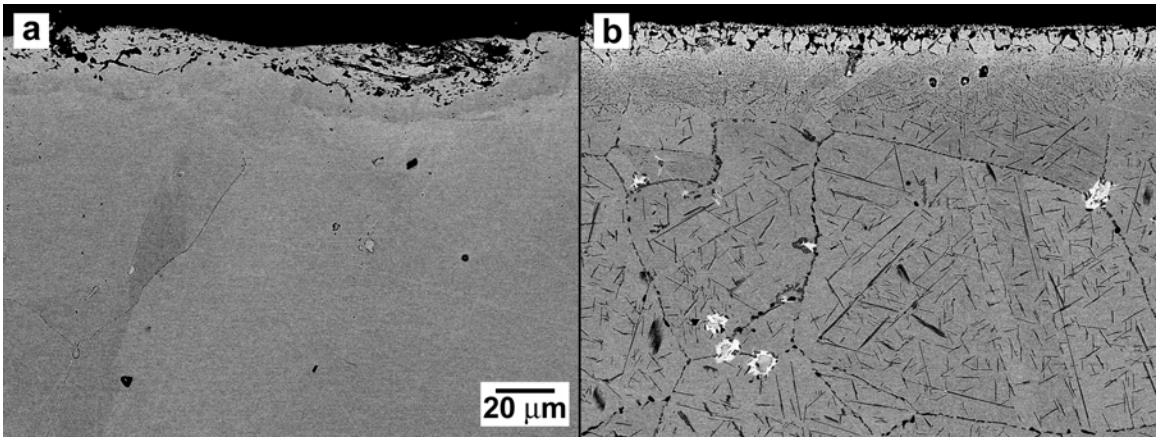

Figure 1 – Microcharacterization of the middle of the Pyromet 31V combustion face region, of a) a fresh valve, and b) a valve with several thousand hours of ARES engine service. Service aging produces significant precipitation along grain boundaries and within the grains, and there are clear differences between the metal just below the coated surface and the base-metal well below the surface.

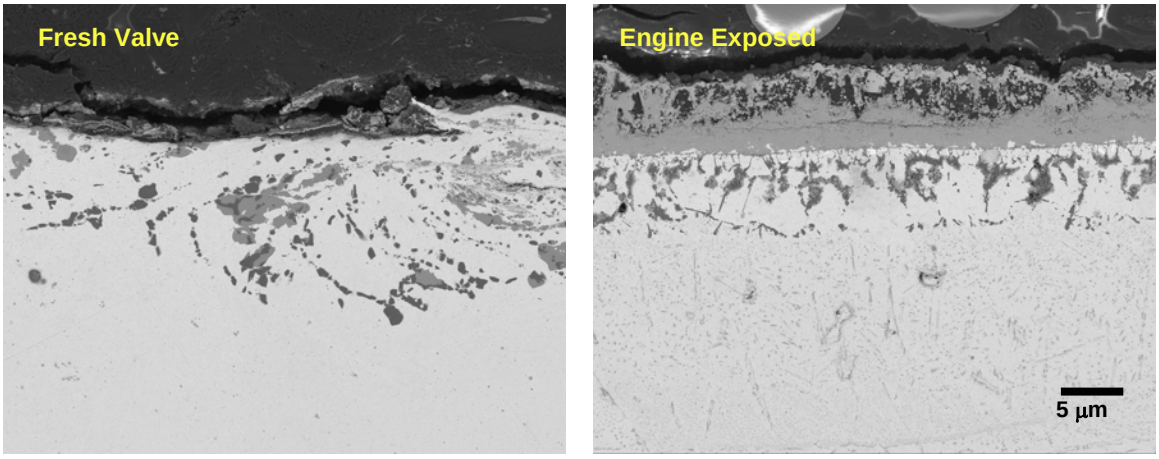

Figure 2 - Backscattered electron images from scanning electron microscopy (SEM) show the surface of the combustion faces of the valves (from Fig. 1) at higher magnification. There are non-uniform mixtures of coarse Al- and Ti-oxides beneath the surface of the fresh valve from prior processing. Those particles are entrained in the Cr-oxide scale that develops during service, and more Ti-oxides form beneath the scale.

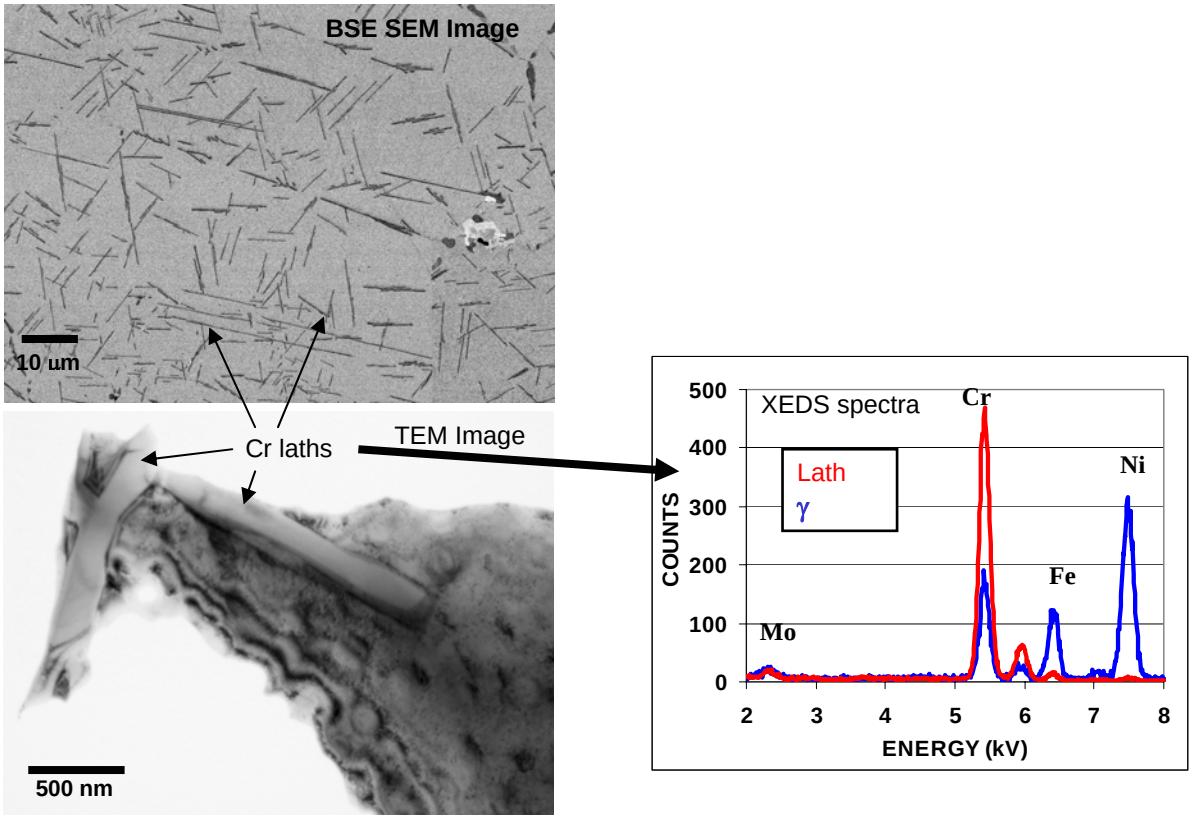

Figure 3 - Higher magnification SEM and transmission electron microscopy (TEM), including X-ray EDS from particles near the edge of the TEM foils, of typical matrix microstructure in a service aged valve. This analysis shows that new precipitate particles in the matrix are pure α-chromium particles, rather than Cr-rich oxides, carbides or intermetallic phases.

Aging during engine service produces significant changes in microstructure, causing additional precipitation in the matrix and along grain boundaries, as shown in Fig.1. including grain structure and the various precipitate phases. There are large TiO_2 and Al_2O_3 particles beneath the surface of the combustion face of the valve in the fresh valve due to prior processing or heat-treatments, as shown in Fig. 2. Some of these become entrained in the chromia scale that develops at the surface during service, and more oxide particles (mainly the Ti-oxides) develop underneath the scale during service. Figure 3 show that the uniform dispersion of needles that precipitate in the matrix of the valve body are pure α-chromium particles (confirmed by electron diffraction).

Last year, ORNL and Caterpillar developed a new cast austenitic stainless steel, CF8C-Plus, that has the potential for use as exhaust component applications in advanced diesel engines. Typical exhaust manifolds and turbocharger housings are made from SiMo cast iron, which has poor strength above 550-600^{o}C, and can be susceptible to thermal fatigue cracking during severe cycling after prolonged use. Standard CF8C steel (Fe-19Cr-9Ni-0.7Nb-0.07C), which has good castability and sufficient strength up to about 600-625^{o}C,

is not strong enough at higher temperatures. Moreover, it contains large (20-25 vol.%) of δ-ferrite, which transforms into σ-phase during aging at 600°C and above, and severely reduces ductility. CF8C-Plus steel was developed to be stronger and much more fatigue and thermal fatigue resistant for use in severe thermal cycling conditions, and its "engineered microstructure" contains no δ-ferrite in the as-cast microstructure, and hence no σ-phase forms during aging.

The creep-resistance of the new CF8C-Plus steel at 850°C is dramatically better than that found in the standard, commercial CF8C steel, and is similar to that of commercial CN-12 steel (Fig. 4). The 2 year creep rupture lifetime in air of the CF8C-Plus is also quite remarkable, since it has only 19%Cr compared to the 25% Cr of the CN12 steel. The CF8C-Plus should have much better performance at 600-800°C than SiMo cast iron or Ni-resist cast steel. The new CF8C-Plus steel is currently being commercialized, and may be applicable for exhaust components of advanced ARES engines.

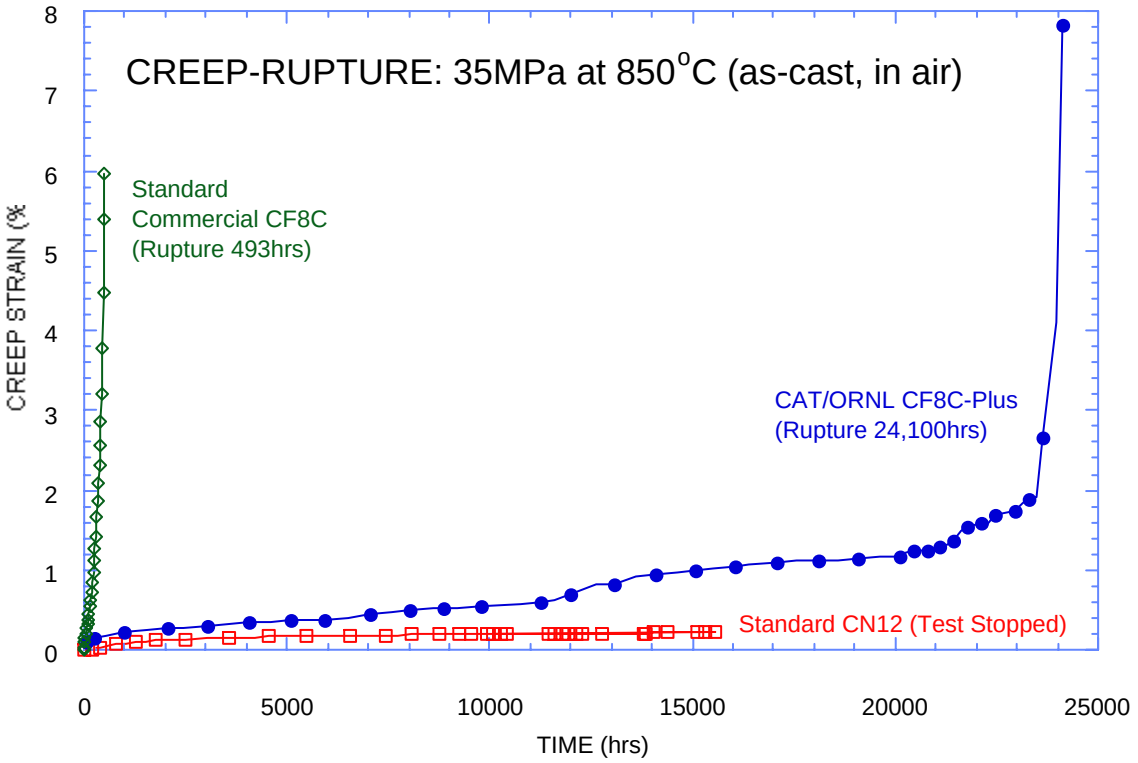

Figure 4 – Creep rupture testing of specimens of standard commercial heats of CF8C and CN12 stainless steels, and an ORNL lab-scale heat of the new CF8C-Plus stainless steel, all tested in air at 850°C and 35 MPa. The CF8C-Plus is nearly as creep resistant as the standard CN12 steel, which contains very high concentrations of both C and N, and dramatically more creep resistant than the standard CF8C steel.

Status of Milestones

FY 2004 – Complete characterization Ni-based superalloy (Pyromet 31V) valves to define aging effect during engine service. Define aging effects at weld overlay and coating bond regions (December 2003) – completed.

Industry Interactions

New discussions with Waukesha Engine, Dresser Inc. (Jim Drees, Joe Derra and others) about materials needs and interests for advanced ARES engines with ORNL (Tom King, Tim Theiss, Phil Maziasz and John Truhan) began this quarter, and will continue next quarter.

Problems Encountered

None

Publications/Presentations

None

Development of Catalytically Selective Electrodes for NOx and Ammonia Sensors

T. Armstrong, F. Montgomery, and D. West
Oak Ridge National Laboratory
P.O. Box 2008, Oak Ridge, TN 37831-6084
Phone: (865) 574-7996, E-mail: armstrongt@ornl.gov

Objective

To develop non-catalytic and catalytically selective electrodes for use in NOx and ammonia sensors and to build and test sensors using the materials and technology developed

Technical Highlights (NOx Sensor Development)

1. "NO-selective" behavior achieved with mulilayer (oxide on Pt) sensing element using Cr_2O_3/Pt, $CuWO_4$/Pt).
2. NO selective behavior appears to be related to the relative efficacy of Pt for the reduction/oxidation of O_2.
3. Little O_2 sensitivity is observed in these sensors.

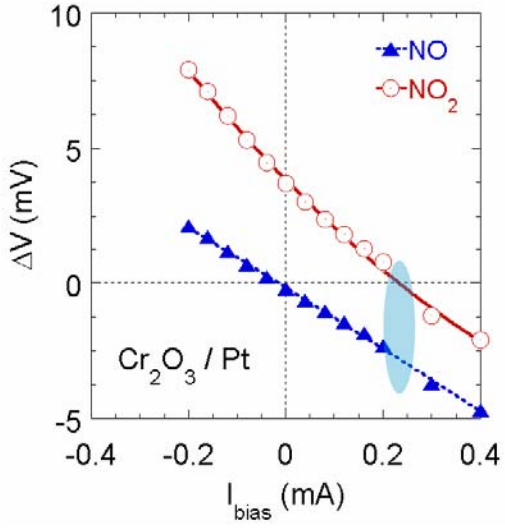

Figure 1. I-V curve for multilayer sensor. Highlighted region indicates that a bias current of 0. 22 mA will reduce the NO_2 signal to zero resulting in a sensor that measures only NO.

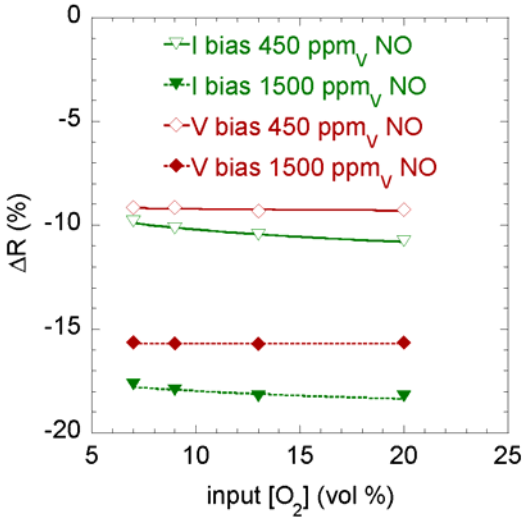

Figure 2. Plot showing oxygen insensitivity of multilayer NO sensor.

4. Single material sensing element gives "total NOx" behavior over a narrow biasing range

5. We have explored interdigitated designs with these sensing elements
    a. Irrespective of geometry, the single material design has a large O_2 sensitivity, increasing as the NOx concentration decreases
    b. The “interdigitated: designs give much larger signals (in terms of percent change in resistance) than the “original” design.
6. Non interdigited designs show a small O_2 sensitivity.

Status of Milestones

1. Determine kinetics of NO reaction on electrode as a function of temperature and environment.

    This is ongoing and will continue as new electrode materials are developed and tested as well as new sensor designs.

2. Fabricate and test a prototype NOx sensor (09/03)

    We are focusing on refining the NO and total NOx sensor. Testing of these sensors is ongoing. Complete results of the NO sensor tests will be reported on next quarter.

Communications/Visits/Travel

Cummings has expressed interest in our program and discussions are being initiated to brief them on our progress.

Problems Encountered

None

Inventions

1. Coplanar sensor for multiple species detection

Internal Distribution

B. L. Armstrong, 4515, MS-6063, armstrongbl@ornl.gov
T. R. Armstrong, 4508, MS-6084, armstrongt@ornl.gov
P. F. Becher, 4515, MS-6068, becherpf@ornl.gov
T. M. Besmann, 4515, MS-6063, besmanntm@ornl.gov
C. A. Blue, 4508, MS-6083, blueca@ornl.gov
M. P. Brady, 4500S, MS-6115, bradymp@ornl.gov
M. A. Brown, 4500N, MS-6186, brownma@ornl.gov
M. K. Ferber, 4515, MS-6069, ferbermk@ornl.gov
J. A. Haynes, 4515, MS-6063, haynesa@ornl.gov
D. R. Johnson, 4515, MS-6066, johnsondr@ornl.gov
M. A. Karnitz, 4500N, MS-6186, karnitzma@ornl.gov
J. O. Kiggans, 4508, MS-6087, kiggansjojr@ornl.gov
T. J. King, 4515, MS-6065, kingtjjr@ornl.gov
J. W. Klett, 4508, MS-6087, klettjw@ornl.gov
E. Lara-Curzio, 4515, MS-6069, laracurzioe@ornl.gov
H. T. Lin, 4515, MS-6068, linh@ornl.gov
R. A. Lowden, 4515, MS-6063, lowdenra@ornl.gov
P. J. Maziasz, 4500S, MS-6115, maziaszpj@ornl.gov
K. L. More, 4515, MS-6064, morekl1@ornl.gov
R. D. Ott, 4515, MS-6083, ottr@ornl.gov
S. D. Nunn, 4508, MS-6087, nunnsd@ornl.gov
B. A. Pint, 4500S, MS-6156, pintba@ornl.gov
D. T. Rizy, 3147, MS-6070, rizydt@ornl.gov
D. P. Stinton, 4515, MS-6063, stintondp@ornl.gov
R. W. Swindeman, 4500S, MS-6155, swindemanrw@ornl.gov
T. N. Tiegs, 4508, MS-6087, tiegstn@ornl.gov
P. F. Tortorelli, 4500S, MS-6156, tortorellipf@ornl.gov
I. G. Wright, 4500S, MS-6157, wrightig@ornl.gov
A. Zaltash, 3147, MS-6070, zaltasha@ornl.gov

External Distribution

ALLISON ADVANCED DEVELOPMENT CO., 1100 Wilson Blvd., Suite 1450, Arlington, VA 22209
J. Miles, r.jeffrey.miles@allison.com

ALM SYSTEMS, INC, 1920 N Street, NW, Suite 750, Washington, DC 20036
M. Kalin, mkalin@ibek.com

ARGONNE NATIONAL LABORATORY, 9700 S. Cass Ave., Argonne, IL 60439-4838
W. Ellingson, ellingson@anl.gov
J. P. Singh, jpsingh@anl.gov

BATTELLE MEMORIAL INSTITUTE, 505 King Avenue, Columbus, OH 43201
D. Anson, ansond@battelle.org

BAYSIDE MATERIALS TECHNOLOGY, 21150 New Hampshire Ave., Brookville, MD 20833
D. Freitag, dfreitag@ix.netcom.com

BCS, INC., 5550 Sterrett Place, Suite 216, Columbia, MD 21044
D. Bartley, dbartley@bcs-hq.com

BOWMAN POWER, 20501 Ventura Boulevard #285, Woodland Hills, CA 91364
T. Davies, tdavies@bowmanpower.co.uk
T. Hynes, ahynes.bowmanpower@att.net
D. Flaxington, dflaxington@bowmanpower.co.uk

CALIFORNIA ENERGY COMMISSION
A. Soinski, asoinski@energy.state.ca.us

CANNON-MUSKEGON CORP., Box 506, Muskegon, MI 49443-0506
J. Wahl, jwahl@canmkg.com

CAPSTONE TURBINE CORP., 6430 Independence Ave., Woodland Hills, CA 91367
P. Chancellor, pchancellor@capstoneturbine.com
K. Duggan, kduggan@capstoneturbine.com
M. Stewart, mstewart@capstoneturbine.com
J. Willis, jwillis@capstoneturbine.com
M. Rodrigues, mrodrigues@capstoneturbine.com
B. Treece, btreece@capstoneturbine.com

CERAMATEC INC., 2425 South 900 West, Salt Lake City, UT 84119
C. Lewinsohn, clewinsohn@ceramatec.com
B. Nair, bnair@ceramatec.com

CLEMSON UNIVERSITY, South Carolina Institute for Energy Studies, 386-2, Clemson, SC 29634-5180
L. Golan, glawren@clemson.edu
R. Wenglarz, rwnglrz@clemson.edu
J. Hinson, jhinson@clemson.edu

CONNECTICUT RESERVE TECHNOLOGIES, 2997 Sussex Ct., Stow, OH 44224
E. Baker, baker@crtechnologies.com
S. Duffy, sduffy@crtechnologies.com
J. Palko, jpalko@crtechnologies.com

DTE ENERGY, 37849 Interchange Dr., Suite 100, Farmington Hills, MI 48335
M. Davis, davism@dteenergy.com

ELECTRIC POWER RESEARCH INSTITUTE, 3412 Hillview Ave., Palo Alto, CA 94303
J. Stringer, jstringe@epri.com

ELGILOY SPECIALTY METALS, 1565 Fleetwood Drive, Elgin, IL 60123

T. Bartel, terryb@elgiloy.com

ELLIOTT ENERGY SYSTEMS, 2901 S.E. Monroe Street, Stuart, FL 34997
D. Burnham, dburnham@elliott-turbo.com
D. Dewis, ddewis@elliott-turbo.com

ENERGETICS, INC., 501 School St., SW, Suite 500, Washington, DC 20024
R. Scheer, rscheer@energeticsinc.com

ENERGY TECHNOLOGIES APPLICATIONS, 5064 Camino Vista Lujo, San Diego, CA 92130-2849
T. Bornemisza, borneger@ix.netcom.com

GAS TURBINE ASSOCIATION, 1050 Thomas Jefferson St., NW, 5th Fl, Washington, DC 20007
J. Abboud, abboud@advocatesinc.com

GENERAL ELECTRIC (GE) CR&D, 1 Research Circle, Building K1-RM 3B4, Niskayuna, NY 12309
S. Correa, correa@crd.ge.com
K. Luthra, luthra@crd.ge.com
M. VanDerwerken, vanderwerken@crd.ge.com
C. Johnson, johnsonca@crd.ge.com

GENERAL ELECTRIC AIRCRAFT ENGINES, One Neumann Way, Mail Drop M89, Cincinnati, OH 45215-1988
R. Darolia, ram.darolia@ae.ge.com

GENERAL ELECTRIC POWER SYSTEMS, One River Rd., 55-127, Schenectady, NY 12345
R. Orenstein, robert.orenstein@ps.ge.com

GENERAL ELECTRIC POWER SYSTEMS, Gas Technology Center, 300 Garlington Road, Greenville, SC 29615
P. Monaghan, philip.monagham@ps.ge.com

HAYNES INTERNATIONAL, INC., 1020 W. Park Avenue, P.O. Box 9013, Kokomo, IN 46904-9013
V. Ishwar, vishwar@haynesintl.com
D. Klarstrom, dklarstrom@haynesintl.com

HONEYWELL CERAMIC COMPONENTS, 2525 W. 190th St., Torrance, CA 90504
D. Foley, dan.foley@honeywell.com
C. Li, chien-wei.li@honeywell.com
D. Newson, danielle.newson@honeywell.com
M. Savitz, MaxineSavitz@aol.com
J. Wimmer, jim.wimmer@honeywell.com
M. Mitchell, michele.mitchell@honeywell.com

HONEYWELL COMPOSITES, 1300 Marrows Rd., PO Box 9559, Newark, DE 19714-9559
L. Connelly, liz.connolly@ps.ge.com
P. Gray, paul1.gray@ps.ge.com
D. Landini, dennis.landini@ps.ge.com

HONEYWELL ENGINES, SYSTEMS, & SERVICES 2739 E. Washington St., PO Box 5227, Phoenix, AZ 85010
B. Schenk, bjoern.schenk@honeywell.com
HONEYWELL POWER SYSTEMS, 8725 Pan American Freeway NE, Albuquerque, NM 87113
S. Wright, e.scott.wright@honeywell.com

HOWMET RESEARCH CORP., 1500 South Warner St., Operhall Research Center, Whitehall, MI 49461-1895
B. Mueller, bmueller@howmet.com
R. Thompson, rthompson@howmet.com

INGERSOLL-RAND ENERGY SYSTEMS, 32 Exeter St., Portsmouth, NH 03801
A. Kaplau-Colan, alex_haplau-colan@ingersoll-rand.com
M. Krieger, michael_krieger@irco.com
J. Johnson, jay_johnson@ingersoll-rand.com
J. Kesseli, jim_kesseli@ingersoll-rand.com
J. Nash, jim_nash@ingersoll-rand.com

KENNAMETAL INC. 1600 Technology Way, P.O. Box 231, Latrobe, PA 15650-0231
R. Yeckley, Russ.yeckley@kennametal.com

KINECTRICS NORTH AMERICA, 124 Balch Springs Circle, SW, Leesburg, VA 20175
B. Morrison, blake.Morrison@kinectrics.com

KRUPP VDM TECHNOLOGIES CORP., 11210 Steeplecrest, Suite #120, Houston, TX 77065-4939
D. Agarwal, dcagarwal@pdq.net

NASA GLENN RESEARCH CENTER, 21000 Brookpark Rd., MS 49-7, Cleveland, OH 44135
D. Brewer, david.n.brewer@grc.nasa.gov
J. Gykenyesi, john.p.gyekenyesi@lerc.nasa.gov
S. Levine, stanley.r.levine@lerc.nasa.gov
N. Nemeth, noel.n.nemeth@grc.nasa.gov
B. Opila, opila@grc.nasa.gov

NATIONAL RURAL ELECTRIC COOPERATIVE ASSOC., 4301 Wilson Blvd., SS9-204, Arlington, VA 22203-1860
E. Torrero, ed.torrero@nreca.org

NATURAL RESOURCES CANADA, 1 Haanel Drive, Nepean, Ontario, Canada K1A 1M1
R. Brandon, rbrandon@nrcan.gc.ca

PCC AIRFOILS, INC., 25201 Chagrin Blvd., Suite 290, Beachwood, OH 44122
C. Kortovich, ckortovich@pccairfoils.com

PENN STATE UNIVERSITY, Applied Research Laboratory, PO Box 30, State College, PA 16823
J. Singh, jxs46@psu.edu

RICHERSON AND ASSOC., 2093 E. Delmont Dr., Salt Lake City, UT 84117
D. Richerson, richersond@aol.com

ROLLS-ROYCE ALLISON, 2925 W. Minnesota St., PO Box 420, Indianapolis, IN 46241
S. Berenyi, steve.g.berenyi@allison.com
P. Heitman, peter.w.heitman@allison.com
F. Macri, francis.g.macri@allison.com
J. Oswald, jim.oswald@rolls-royce.com

SAINT-GOBAIN CERAMICS & PLASTICS, INC., Goddard Road, Northboro, MA 01532
B. LaCourse, Brian.C.LaCourse@saint-gobain.com
R. Licht, robert.h.licht@saint-gobain.com
M. Abouaf, Marc.Abouaf@saint-gobain.com
V. Pujari, Vimal.K.Pujari@saint-gobain.com
A. Vartabedian, Ara.M.Vartabedian@saint-gobain.com

SEBESTYEN, T., Consultant, 6550 Mission Ridge, Traverse City, MI 49686-6123
T. Sebestyen, sebestyen@chartermi.net

SIEMENS WESTINGHOUSE POWER CORP., 1310 Beulah Rd., Pittsburgh, PA 15235-5098
M. Burke, michael.burke@swpc.siemens.com
C. Forbes, christian.forbes@swpc.siemens.com

SOLAR TURBINES, INC., TurboFab Facility, 16504 DeZavala Rd., Channelview, TX 77530
B. Harkins, harkins_bruce_d@solarturbines.com

SOLAR TURBINES INC., 818 Connecticut Ave., NW, Suite 600, Washington, DC 20006-2702
R. Brent, solardc@bellatlantic.net

SOLAR TURBINES, INC., 2200 Pacific Highway, PO Box 85376, MZ R, San Diego, CA 92186-5376
P. Browning, browning_paul_f@solarturbines.com
M. Fitzpatrick, fitzpatrick_mike_d@solarturbines.com
P. Montague, montague_preston_j@solarturbines.com
M Van Roode, van_roode_mark_x@solarturbines.com
M. Ward, ward_mike_e@solarturbines.com
J. Price, jeffprice@solarturbines.com

SOUTHERN CALIFORNIA EDISON COMPANY, 2244 Walnut Grove Avenue, Rosemead, CA 91770

S. Hamilton, hamiltsl@sce.com

SOUTHERN COMPANY, 600 N. 18th Street, 14N-8195, P.O. Box 2641, Birmingham, AL 35291

S. Wilson

STEVEN I. FREEDMAN, Engineering Consultant, 410 Carlisle Ave., Deerfield, IL 60015

S. Freedman, sifreedman@aol.com

STAMBLER ASSOCIATES, 205 South Beverly Drive, Suite 208, Beverly Hills, California 90212

I. Stambler

THE BOEING COMPANY, Rocketdyne Propulsion & Power, 6633 Canoga Avenue
MC: GB-19, P.O. Box 7922, Canoga Park, CA 91309-7922

G. Pelletier, gerard.pelletier@west.boeing.com

TELEDYNE CONTINENTAL MOTORS, 1330 W. Laskey Rd., PO Box 6971, Toledo, OH 43612-0971

J. T. Exley, texley@teledyne.com

TURBEC

L. Malmrup, lars.malmrup@turbec.com

UCI COMBUSTION LABORATORY, U. of CA, Irvine, Irvine, CA 92697-3550

V. McDonell, mcdonell@ucic1.uci.edu

UDRI, Ceramic & Glass Laboratories, 300 College Park Ave., Dayton, OH 45469-0172

A. Crasto, allan.crasto@udri.udayton.edu
G. Graves, gravesga@udri.udayton.edu
N. Osborne, osborne@udri.udayton.edu
R. Wills, roger.wills@udri.udayton.edu

UNITED TECHNOLOGIES RESEARCH CENTER, 411 Silver Lane MS 129-24, East Hartford, CT 06108

H. Eaton, eatonhe@utrc.utc.com
J. Holowczak, holowcje@utrc.utc.com
T. Rosfjord, rosfjotj@utrc.utc.com
J. Smeggil, smeggijg@utrc.utc.com
G. Linsey, linseygd@utrc.utc.com
J. Shi, shij@utrc.utc.com
E. Sun, suney@utrc.utc.com
D. Mosher, mosherda@utrc.utc.com

UNIVERSITY OF CALIFORNIA, Department of Mechanical Engineering, Berkeley, CA 94720
R. Dibble, rdibble@newton.berkeley.edu

UNIVERSITY OF COLORADO, Department of Mechanical Engineering, Boulder, CO 80309-0427
R. Raj, rishi.raj@Colorado.edu

UNIVERSITY OF MARYLAND, Department of Mechanical Engineering, College Park, MD 20742-3035
R. Radermacher, rader@eng.umd.edu

UNIVERSITY OF WESTERN ONTARIO, Faculty of Engineering, London, Ontario, Canada N6G 4K1
B. E. Thompson, Thompson@eng.uwo.ca
A. G. Straatman, astraat@engga.uwo.ca

US DOE-NETL, P. O. Box 880, MSO-D01, 3610 Collins Ferry Rd., Morgantown, WV 26507-0880
C. Alsup, Jr., charles.alsup@netl.doe.gov
A. Layne, abbie.layne@netl.doe.gov
L. Wilson, lane.wilson@netl.doe.gov

US DOE-NETL, PO Box 10940, Pittsburgh, PA 15236
N. Holcombe, norman.holcombe@netl.doe.gov
U. Rao, rao@netl.doe.gov

US DOE CHICAGO OPERATIONS OFFICE, 9800 S. Cass Ave., Argonne, IL 60439
J. Jonkouski, jill.jonkouski@ch.doe.gov
J. Mavec, joseph.mavec@ch.doe.gov
J. Livengood, joanna.livengood@ch.doe.gov
S. Waslo, stephen.waslo@ch.doe.gov

US DOE-HQ, 1000 Independence Ave., S.W., Washington DC 20585
R. Fiskum, ronald.fiskum@ee.doe.gov
D. Haught, debbie.haught@ee.doe.gov
P. Hoffman, patricia.hoffman@ee.doe.gov
W. Parks, william.parks@ee.doe.gov
M. Smith, merrill.smith@ee.doe.gov
C. Sorrell, charles.sorrell@ee.doe.gov

WILLIAMS INTERNATIONAL, 2280 West Maple Rd., PO Box 200, Walled Lake, MI 48390-0200
G. Cruzen, g.cruzen@williams-int.com
W. Fohey, w.fohey@williams-int.com
C. Schiller, cschiller@williams-int.com

WRIGHT PATTERSON AIRFORCE BASE,

R. Sikorski, ruth.sikorski@wpafb.af.mil

CERAMIC RELIABILITY FOR MICROTURBINE HOT-SECTION COMPONENTS

Reliability Evaluation of Microturbine Components

H. T. Lin, M. K. Ferber, and T. P. Kirkland
Metals and Ceramics Division
Oak Ridge National Laboratory
P.O. Box 2008, Oak Ridge, TN 37831-6068
Phone: (865) 576-8857, E-mail: linh@ornl.gov

Objective

Evaluate and document the long-term mechanical properties of very small specimens machined from ceramic components (e.g., blades, nozzles, vanes, and rotors) in as processed and after engine testing at ambient and elevated temperatures under various controlled environments. This work will allow microturbine companies to verify mechanical properties of components and apply the generated database in probabilistic component design and lifetime prediction methodologies. The work also provides a critical insight into how the microturbine environments influence the microstructure and chemistry, thus mechanical performance of materials.

Highlights

Studies of dynamic fatigue properties of NT154 silicon nitride (Saint-Gobain Ceramics & Plastics, Northboro, MA) developed under the Task I efforts has been completed. Saint-Gobain was awarded by DOE under Microturbine Materials Program to re-develop NT154 silicon nitride for hot-section components for advanced microturbines. ASTM standard MOR bars were prepared with as-processed surface and also from the inner bulk region. Database generated has been provided to Saint-Gobain for further processing refinement, and to UTRC, GE, and Capstone for probabilistic component design and life prediction effort.

Technical Progress

Studies of dynamic fatigue properties for SiAlON ceramics (Kennametal Inc., PA) were initiated during this reporting period. Kennametal was awarded by DOE under Microturbine Materials Program to develop SiAlON ceramics for hot-section components for advanced microturbines. The SiAlON ceramics due to their superior wear resistance have been developed for metal cutting tool application, and might have potential for structural applications in microturbine systems. The purpose of this study is to generate a database for down-selecting the candidate composition(s) and also for probabilistic component design and life prediction efforts carried out by microturbine companies. Two batches of SiAlON ceramics (designated as 2308A and 2308E) were received from Kennametal. Both 2308A and 2308E contain a mixture of α- and β-SiAlON grain microstructure. The SiAlON ceramics were fabricated under the Phase I contract, and MOR bars were longitudinally machined per the revised ASTM C116 standard with 600 grit surface finish. The dynamic fatigue tests were carried out at 20 and 1204°C and at stressing rate of 30 and 0.003 MPa/s in air per ASTM C1465. The 30 MPa/s is used to evaluate the inert characteristic strength as a function of temperature, and 0.003 MPa/s is applied to measure the slow crack growth (SCG) susceptibility at temperatures.

Test results at 20°C and 30 MPa/s showed that both 2308A and 2308E material exhibited comparable flexural strengths as well as relatively low Weibull modulus with respect to various commercially available silicon nitride ceramics evaluated under DER Microturbine Materials Program and OTT Heavy Vehicle Propulsion System Materials Program. Also, when tested at 1204°C and 30 MPa/s both 2308A and 2308E material exhibited 31-38% decrease in inert characteristic strength as compared those generated at 20°C and 30 MPa/s (Table 1, and Fig. 1-4).

Table 1. Summary of uncensored Weibull and strength distributions for Kennametal SiAlON ceramic specimens with as-machined surface (longitudinally machined per the revised ASTM C1161 standard).

Material	# of Spmns. Tested	Stressing Rate (MPa/s)	Temp. (°C)	Uncens. Weibull Modulus	± 95% Uncens. Weibull Modulus	Uncens. Chrctstic Strength (MPa)	± 95% Uncens. Chrctstic Strength (MPa)
2308A	15	30	20	5.92	3.80, 8.55	651	589, 715
2308E	15	30	20	6.06	3.91, 8.73	783	710, 858
2308A	15	30	1204	9.79	6.52, 13.62	393	370, 415
2308A	15	0.003	1204	10.68	6.87, 15.38	415	392, 437
2308E	15	30	1204	7.45	4.67, 11.05	540	489, 582
2308E	14	0.003	1204	3.37	2.29, 4.55	440	369, 522

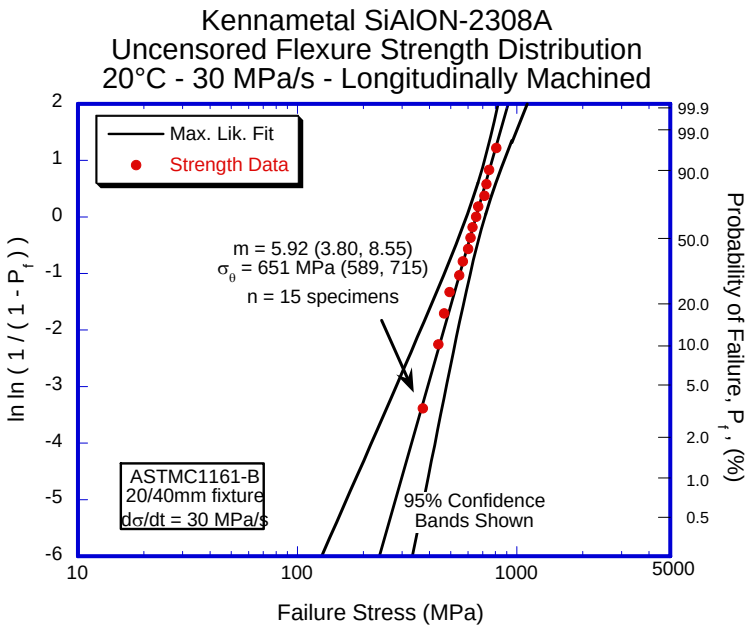

Figure 1. Uncensored flexure strength distribution at 20°C and 30 MPa/s of SiAlON-2308A ceramic with as-machined surface (bulk material).

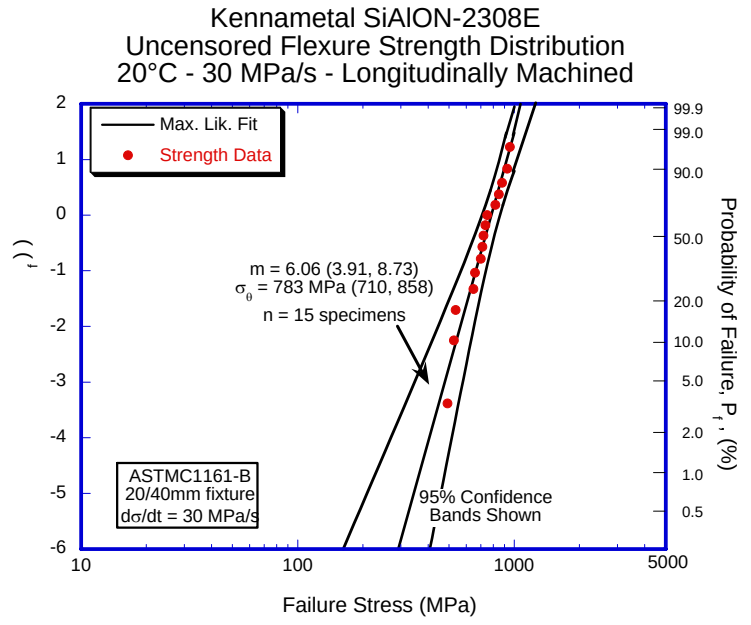

Figure 2. Uncensored flexure strength distribution at 20°C and 30 MPa/s of SiAlON-2308E ceramic with as-machined surface (bulk material).

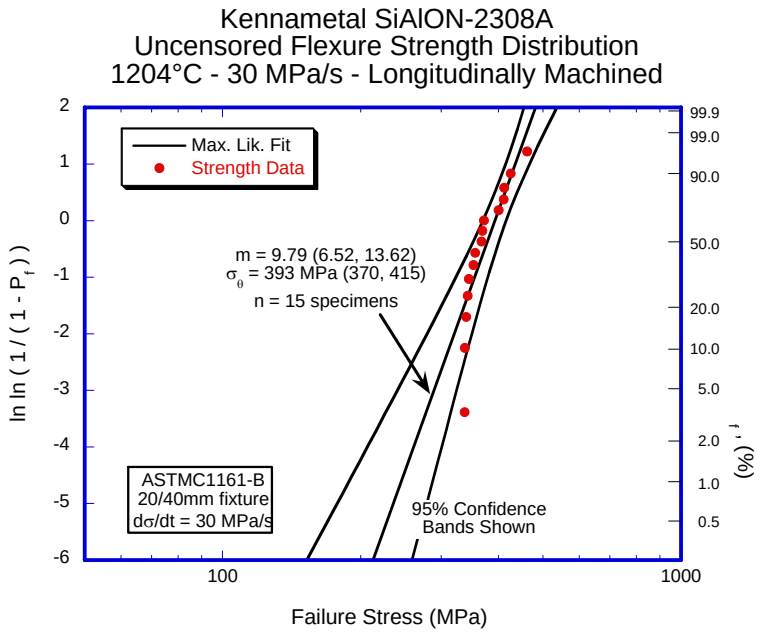

Figure 3. Uncensored flexure strength distribution at 1204°C and 30 MPa/s of SiAlON-2308A ceramic with as-machined surface (bulk material).

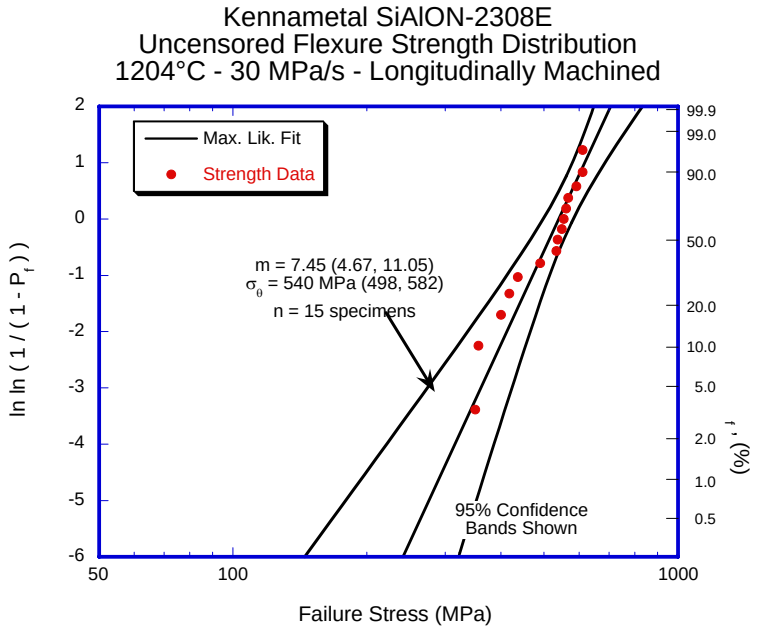

Figure 4. Uncensored flexure strength distribution at 1204°C and 30 MPa/s of SiAlON-2308E ceramic with as-machined surface (bulk material).

On the other hand, results showed there was minor change in inert characteristic strength accompanied with a high fatigue exponent for 2308A material when tested at 1204°C and 0.003

MPa/s. However, the 2308E material showed a 20% degradation in strength with a low fatigue exponent (~36) when tested at 1204°C and 0.003 MPa/s (Table 1 and Fig. 5, 6).

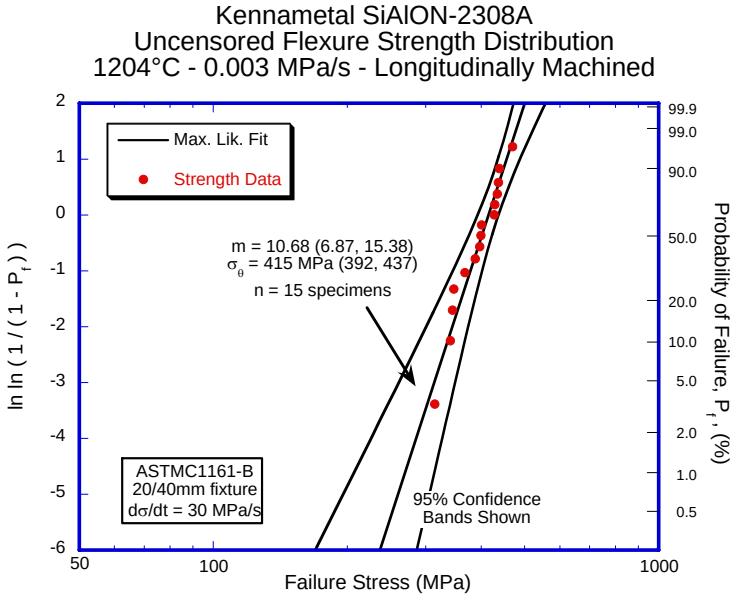

Figure 5. Uncensored flexure strength distribution at 1204°C and 0.003 MPa/s of SiAlON-2308A ceramic with as-machined surface (bulk material).

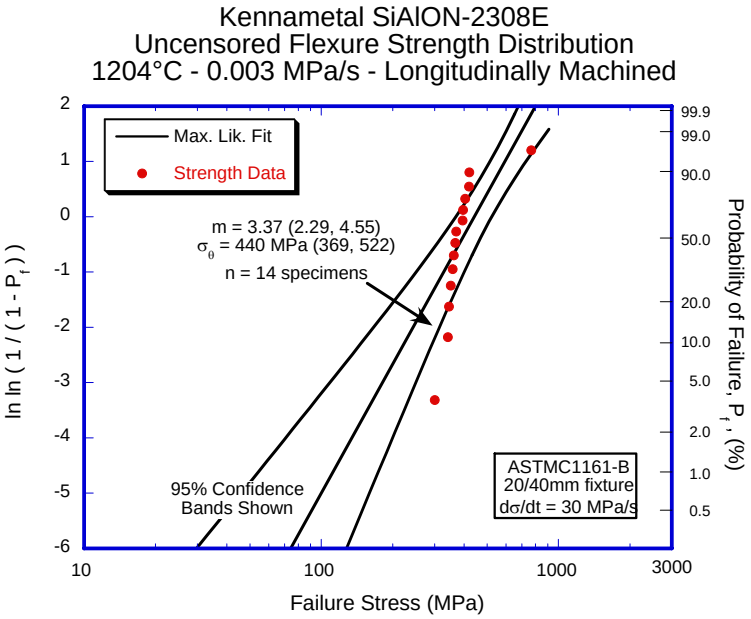

Figure 6. Uncensored flexure strength distribution at 1204°C and 0.003 MPa/s of SiAlON-2308E ceramic with as-machined surface (bulk material).

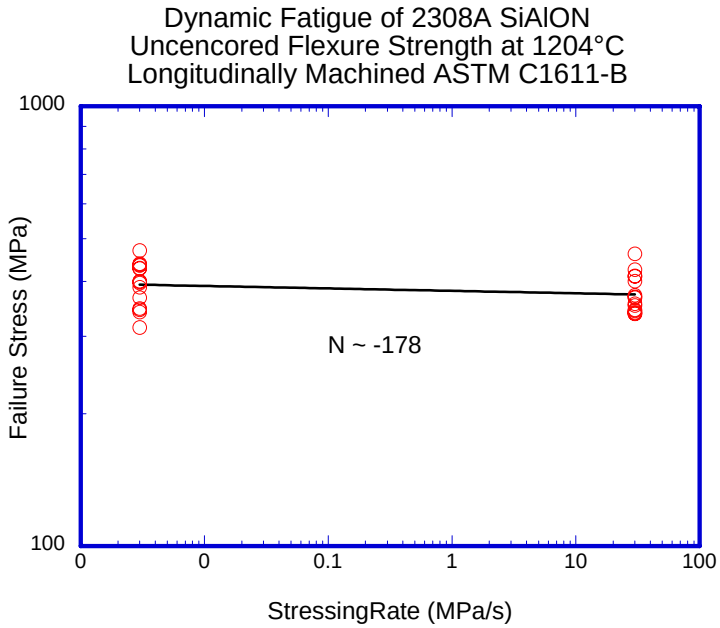

Figure 5. Flexure strength versus stressing rate for SiAlON-2308A with as-machined surface (bulk material) tested at 1204°C.

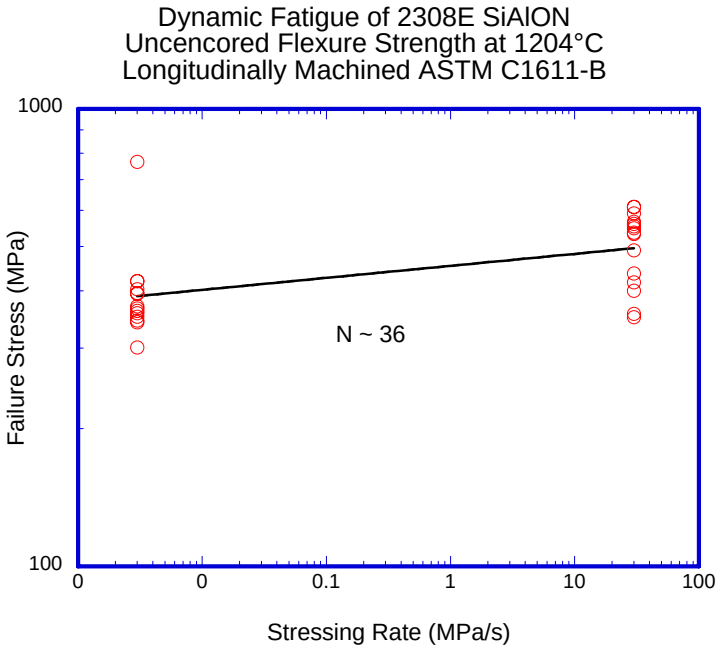

Figure 6. Flexure strength versus stressing rate for SiAlON-2308E with as-machined surface (bulk material) tested at 1204°C.

The low fatigue exponent at 1204°C, which is strongly dependent upon the chemical compositions used in the system, could be attributed to a high susceptibility to slow crack growth and/or creep process. The detailed fractography and SEM examinations will be carried out on fracture surfaces of selected bend bars to understand the cause of low fatigue exponent observed for 2308E material.

The second batch of SiAlON ceramic bars with 8 different compositions has been received from Kennametal. The MOR test bars will be machined and tested under the same conditions employed for the first batch of materials (i.e., 2308A and 2308E). Test results will be reported in the next quarterly report.

Status of Milestones

1. Complete evaluation of next generation Si_3N_4 with EBC from SMRC, Japan after long-term steam jet testing. September 2004. On schedule.

Industry Interactions

Communication with John Holowczak, Venkata Vedula, and Jun Shih at UTRC to discuss the mechanical database of Saint-Gobain NT154 silicon nitride as well as data generated from Kyocera SN237 microturbine rotor.

Communication with Vimal Pujari and Ara Vartabedian at Saint-Gobain Ceramics & Plastics on the updates of the testing status and results for NT154 silicon nitride materials manufactured during Task II effort under Phase I contract, and also the preparation status for the NT154 sintered with a diffusion barrier coating.

Communication with Russ Yeckley at Kennemetal on the test results of SiAlON ceramics manufactured during Task I effort.

Communication with Professor Rishi Raj at University of Colorado on the testing and evaluation of SiCN EBC materials under steam environments.

Problems Encountered

None

Publications/Presentations

H. T. Lin and M. K. Ferber, “Mechanical Properties of Silicon Nitride Ceramic Components.” Invited talk at the Composites at Lake Louise 2003, Lake Louise, Canada, October 19-24.

H. T. Lin, A. A. Wereszczck, M. K. Ferber, and T. P. Kirkland, “Effect of Materials Parameters on Mechanical Performance of Environmental Barrier Coatings,” talk presented at the 2003 EBC Workshop, Nashville, TN on November 18-19, 2003.

H. T. Lin and M. K. Ferber “Mechanical Properties of Silicon Nitride Ceramic Components” poster presented at the 2003 DER Peer Review Meeting, December 2-4, 2004, Washington DC.

Long-Term Testing in Water Vapor Enivronments

M. K. Ferber and H-T Lin
Metals and Ceramics Division
Oak Ridge National Laboratory
P.O. Box 2008, Oak Ridge, TN 37831-6069
Phone: (865) 576-0818, E-mail: ferberk@ornl.gov

Objective

The primary objective of this project is to evaluate the long-term mechanical and chemical stability of advanced materials of interest to the DER program. Currently the project is evaluating (1) structural ceramic, which are being considered for use as hot-section components in microturbines, and (2) thick thermal barrier coatings (TTBCs) being developed for thermal management in combustor liners used in industrial gas turbines. The structural ceramics effort focuses on the development and utilization of test facilities for evaluating the influence of high-pressure and high-temperature water vapor upon the long-term mechanical behavior of monolithic ceramics having environmental barrier coatings. In the case of the TTBCs, the primary focus is on the evaluation of changes in microstructure and thermal properties arising from long-term aging tests.

Highlights

Studies to evaluate the temperature sensitivity of recession of silicon carbide ceramics exposed in the steam injection rig were initiated.

Technical Progress

The steam injection system (Figure 1) described in the previous quarterly report was also used to evaluate the temperature sensitivity of recession of sintered alpha silicon carbide by exposing three specimens at 1100, 1200, and 1300°C. The recession was evaluated as a function of time by interrupting each test periodically and measuring the change in the gage diameter at several points in and around the injection site. The maximum loss in gage diameter was taken as the appropriate measure of surface recession. The results, which are shown in Figure 2, are compared with prediction based on the NASA recession equation. The velocity for each specimen was converting the rate of water consumption (in cc/h) to a linear rate of steam passing through the narrow gap between specimen and injection tip. With the exception of the results at 1300°C, the predicted and measured recession data were in good agreement. At 1300°C the experimental recession rate appeared to decrease below the predicted value after about 300 h. It is possible that the recession was affected by changes in the gap between steam injection tube and the specimen.

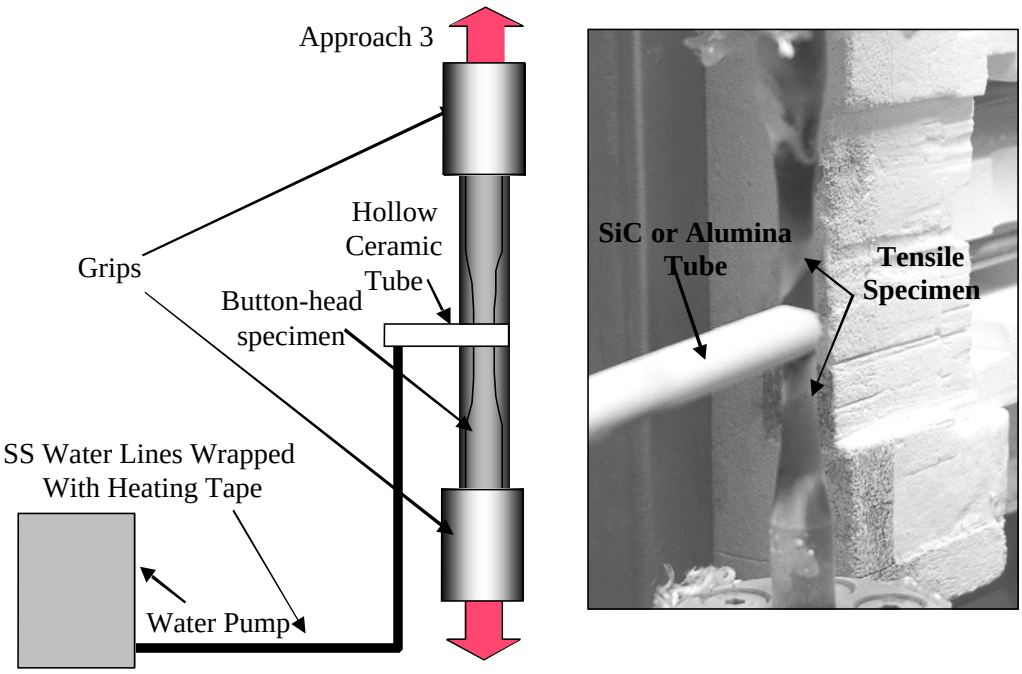

Figure 1: Direct Steam Injection System.

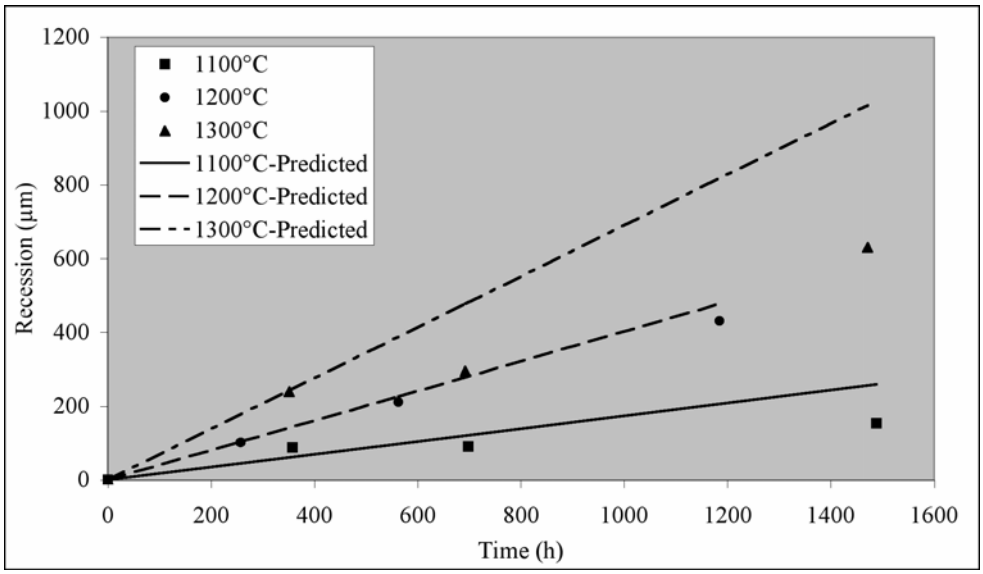

Figure 2: Recession data for SA silicon carbide.

A coordinate measuring machine was used to better quantify the recession of the specimens exposed at 1200 and 1300°C. Figure 3 compares the profiles obtained for these specimens with the reference profile of an unexposed specimen. Although the maximum reduction in gage diameters were similar for both specimens, the total amount of material loss was much larger for the specimen exposed at 1300°C. Differences in positioning of the steam injection tubes may have been responsible for the variation in recession profiles.

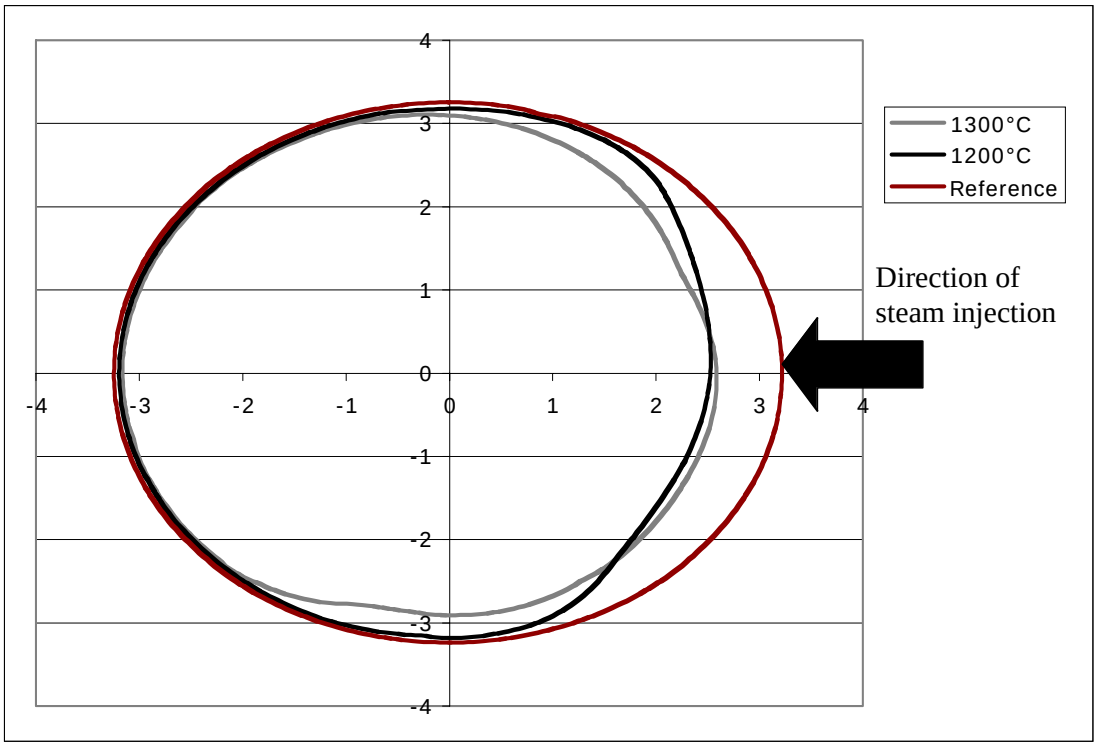

Figure 3: Surface profiles for specimens exposed at 1200 and 1300°C.

Status of Milestones

Complete the characterization of commercially available environmental barrier coatings and issue report. (September 2004)

Industry Interactions

Monthly teleconferences were held with UTRC to discuss results of ORNL activities conducted in support of their microturbine program.

Problems Encountered

None

Publications

None

References

None

Reliability Analysis of Microturbine Components

S.F. Duffy, E.H. Baker & J.L. Palko
Connecticut Reserve Technologies, LLC
2997 Sussex Court, Stow, Ohio 44224
Phone: 330-678-7328, E-mail: sduffy@crtechnologies.com

Objective

The objective of this project is to work closely with microturbine manufacturers and suppliers to provide technical expertise relative to component reliability analysis and statistical parameter estimation. This subcontract is separated into two tasks as outlined below:

Task 1 – Develop and enhance parameter estimation software (*WeibPar*).
Task 2 – Provide design support to companies involved in the DER project.

Task 1 is motivated by the materials needs of the various microturbine manufacturers to evaluate ceramic material provided by St. Gobain, Kennametals and Kyocera. The parameter estimation software is available to all participants in the DER program, and it is now interfaced with the NASA CARES reliability software. The second task is motivated by the need of the microturbine community to have the most up to date methods of analysis available in the design of components fabricated from ceramics.

Highlights

A cd-rom containing the most current version of the parameter estimation software algorithm *WeibPar* was distributed to participants at the EBC workshop in Nashville (November 2003).

Connecticut Reserve Technologies, LLC (CRT) has worked with Ingersoll Rand (IR) over the past year to analyze a CMT gasifier rotor. IR provided CRT with finite element models that captured both transient and steady state thermo-mechanical stress fields. CRT has provided reliability estimates of the rotor based on data generated by others in the DER program. CRT is currently in the process of developing and enhancing a methodology to ascertain Weibull distribution metrics for the IR rotor (see discussion on technical progress in the next section). The combination of service stress states and a requisite probability of survival for a Si_3N_4 microturbine rotor are being used to determine Weibull modulus - characteristic strength pairs for an arbitrary Si_3N_4. These data pairs will be provided relative to standard test coupons and methods (e.g., ASTM C1161B and the ORNL button head test specimens). The material characteristic strengths are determined for a range of Weibull moduli, and then are scaled to standard test coupons and test methods. The intent is to provide a methodology to define Weibull distribution metrics for Si_3N_4 vendors in terms of data generated from standard test specimens. These metrics will be associated with a specified probability of survival for the rotor. In essence, this effort is looking towards developing, in a practical way, the means to reverse engineer the material given a specific component application. The methodology was presented at the EBC workshop in Nashville (November 2003).

Technical Progress

Task 1 – Progress related to Task 1 is as follows:

- CRT continues to implement the capability of pooling failure data across multiple temperatures. The methodology for these routines has been used under separate contract for the ARMY Research Laboratory (ARL).

Task 2 –CRT in collaboration with ORNL research personnel has established a methodology to compute Weibull distribution parameter metrics. A material performance curve (see Figure 1) for a generic thin walled pressure vessel (see Figure 2) was developed relative to a four point bend specimen . The material performance curve demonstrates concept relative to a surface flaw analysis (volume flaw analyses were presented in the last report).

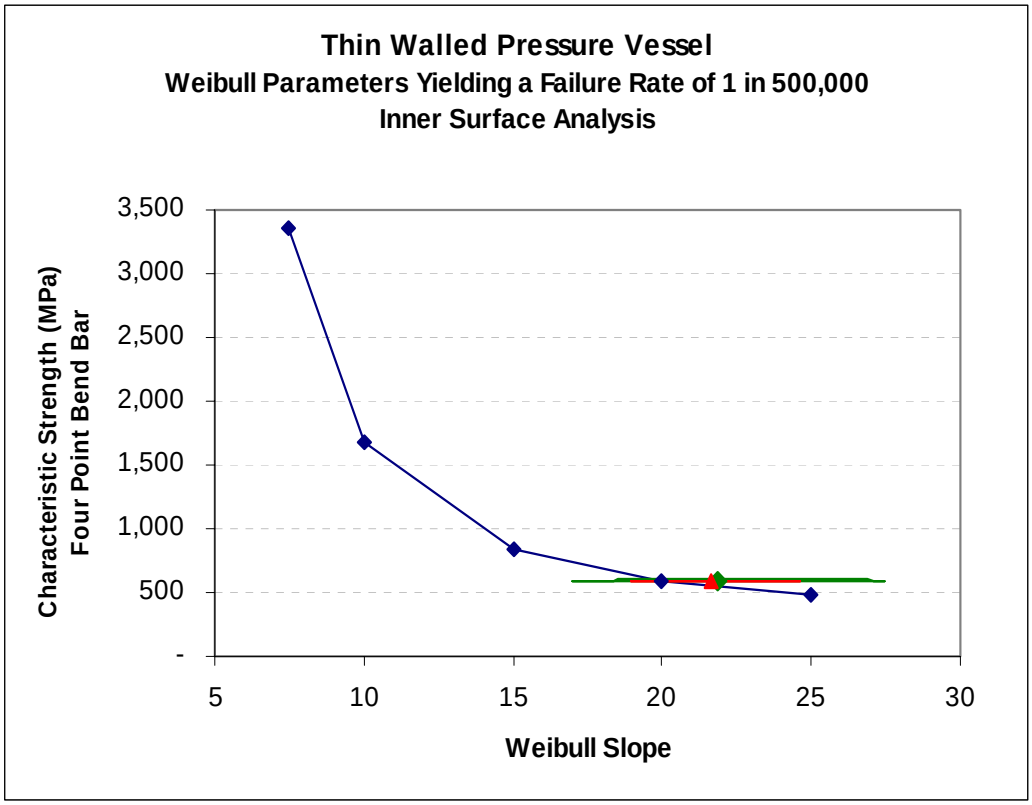

Figure 1 Material Characteristic Strength as a Function of the Weibull Modulus – Surface Flaw Analysis

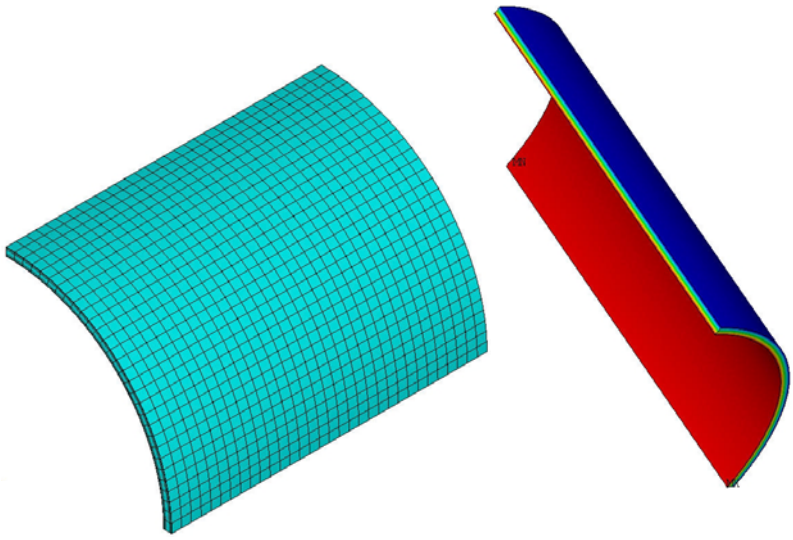

Figure 2 Thin Wall Pressure Vessel - Inner Radius = 100 mm; Thickness = 5 mm; Length = 400 mm; Applied Pressure = 10 MPa

CRT also indicated how the size of a data set can influence the ability to meet target values for the distribution parameters. Generic data sets were generated via Monte Carlo simulation using seed values of $m=20$ and $\sigma_\theta = 588$ *MPa*. These values were arbitrarily selected, and obtained from the blue material performance curve. An enlarged view of the simulation curves relative to the material performance curve is depicted in Figure 3.

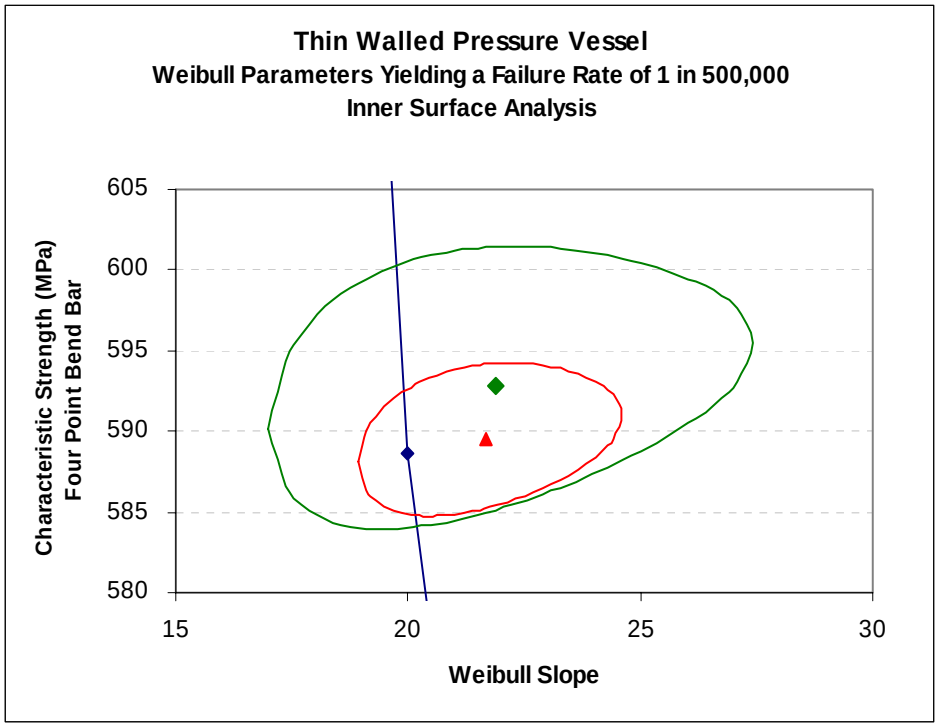

Figure 3 Confidence Bounds on Parameter Estimates Relative to the Size of the Data Set.

The green curve corresponds to a data set with 30 test specimens. The red curve corresponds to a data set with 100 test specimens. Both curves are associated with the *90th* percentile confidence interval. These confidence bounds encompass a region where one is *90%* confident of finding the true population parameters. The design engineer would be content to see parameter estimates to the right of the material performance curves. The figure above indicates that as the size of the data set is increased, the chance of true population parameters falling to the left of the material performance curve diminishes.

Status of Milestones

Complete the life prediction analysis of Ingersoll Rand's microturbine rotor utilizing a number of candidate materials (Kyocera's SN282 and SN237, Honeywell's AS800, archived St. Gobain's NT-154 from mid 1990s, improved St. Gobain materials, and Kennametal's new SiAlON. (November 2003) Complete

Industry and Research Interactions

CRT will visit St. Gobain in the near term to establish a closer working relationship between the two organizations. Preliminary discussions relative to establishing this relationship took place at the recent (January 2004) Cocoa Beach meetings.

Problems Encountered

None

Publications/Presentations

1. "Weibull Strength Parameter Requirements for Si_3N_4 Turbine Rotor Reliability," S. Duffy, E. Baker, J. Kesseli, A. Wereszczak, and C. Johnson, presented at the *Environmental Barrier Coatings Workshop*, November 18-19, 2003, Gaylord Opryland Resort & Convention Center, Nashville, Tennessee, USA

NDE Technology Development for Microturbines

W. A. Ellingson, R. Visher, C. Deemer, E. R. Koehl, and Z. Metzger
Argonne National Laboratory
9700 South Cass Avenue, Argonne, IL 60439
Phone: (630) 252-5058, E-mail: Ellingson@anl.gov

Objective

The objective of this project is development of low-cost, reliable nondestructive evaluation/characterization (NDE/C) technologies for: (1) evaluating low-cost monolithic ceramics for hot section components of microturbines or industrial gas turbines, (2) evaluating environmental barrier coatings (EBCs) for monolithic ceramics and ceramic matrix composites, and (3) evaluating other materials which are part of the technology to advance the programs for the Distributed Energy Resources (DER) technologies. The project is directly coupled to other Office of Distributed Energy and Electrical Reliability projects focused on materials developments.

Highlights

There are two main highlights this period. We successfully completed the addition of 4 more nodes, now up to 22 nodes, to the Beowolf cluster for high speed X-ray computed tomographic (CT) image reconstruction and we completed the installation of the 420 KVp X-ray head and are running it routinely.

Technical progress

Technical work this period focused on 3 areas: (1) developments towards volumetric, 3D, X-ray imaging for improving the reliability and processing methods of low-cost monolithic ceramic materials, (2) work on oxide-based ceramic composites, and (3) work to establish characteristics of new EBCs.

1.0 NDE development for on-line low-cost monolithics

Work this period focused on two areas: (1) fast image reconstruction of 3D X-ray data using the Beowolf cluster, and (2) continued investigations into the sensitivity of X-ray CT data for the detection of features in monolithic ceramic rotors.

High Speed Image Reconstructions using the Beowulf Computer cluster

As we have been reporting, in a cooperative effort with the Basic Sciences Division-Materials (BSD-M) here at Argonne, we are installing a new Beowulf computer cluster with a target of reaching 40 nodes by July 2004. The purpose of this cluster is to allow very high speed 3D X-ray image reconstructions using the massive data sets that are being collected from the large area flat

panel X-ray detectors that we use for the large hot section components. The goal is to reduce reconstruction time to less then 1 hour (more than 10x)

Flaw Delectability in Monolithic Ceramic Microturbine Rotors

To further investigate the capabilities of detection of flaws in monolithis ceramic mocroturbine components using new detectors, the gelcast Si_3N_4 AS800 rotor used previously was again used (see Fig 1). To again note the details, the three sections cut from the unbladed rotor had diameters of 67 mm, 112 mm, and 178 mm respectively. A series of three flat-bottom holes (having diameters of 0.4 mm, 0.6 mm, and 1.5 mm) were machined into each section using an ultrasonic drilling system. This time the detection study was done using the 450 kVp X-ray source (see 3rd Microturbine quarterly report from 2003) and two X-ray detectors were utilized; (1) an amorphous silicon flat panel area detector with a spatial resolution of 400 μm/ pixel, and (2) a linear CMOS based detector with a spatial resolution of 83 μm/ pixel. An example of a X-ray CT reconstruction from the CMOS linear detector is shown in Fig. 2. To quantify the detectability of the seeded defects using the two detectors, the relative 16-bit grey level from in the flat-bottom holes were compared to an undamaged region from each reconstruction. The grey scale difference was plotted and is shown in Fig. 3 for each flaw in each of the three sections. It is apparent that the flaw detectability of data from the high resolution CMOS detector is much better than the lower resolution area detector. It should be noted that the RID1620 detector with 400 μm pixels could not resolve the 0.4 mm diameter hole in the 178 mm diameter section, but the CMOS detector was able to resolve this easily with a 7000 grey scale difference in the 16-bit image.

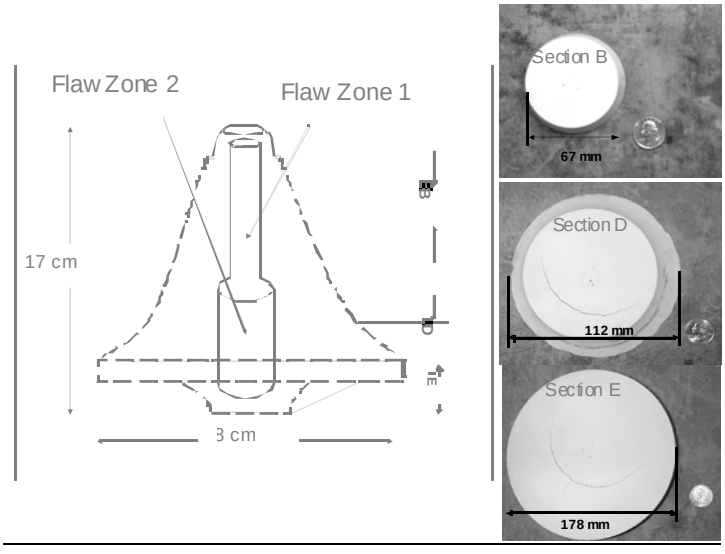

Fig. 1. Schematic diagram of unbladed gelcast AS800 microturbine rotor showing location of sections and digital photographs showing the seeded defects in sections.

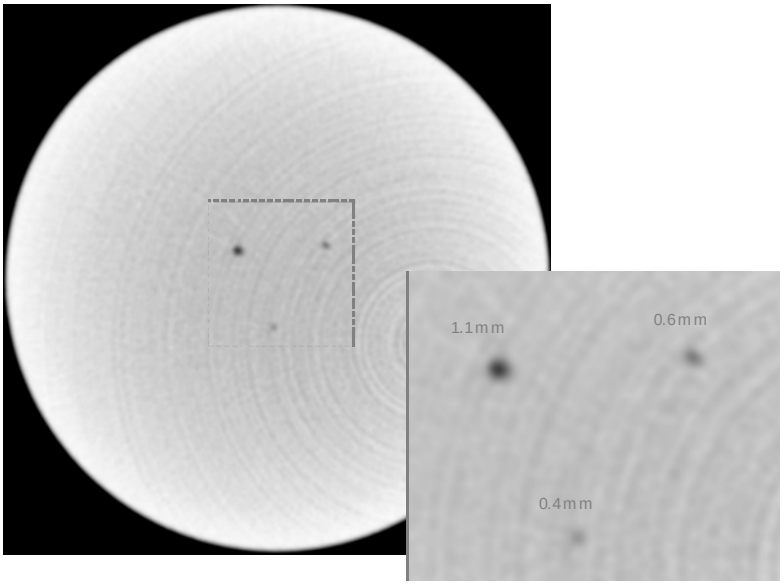

Fig. 2. CT reconstruction of the 67 mm diameter section showing the thee seeded defects.

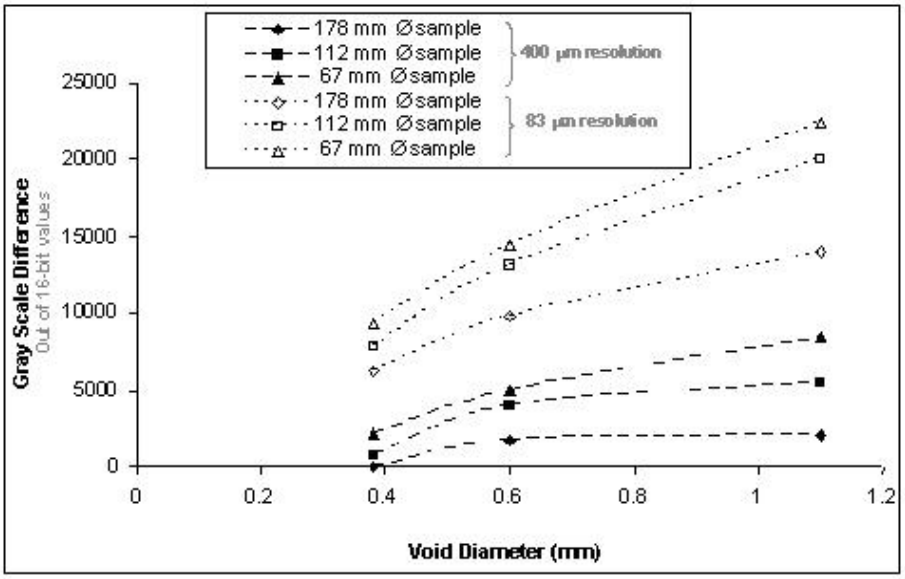

Fig. 3. Plot showing the detectability of the two detectors to resolve the seeded defects

Characterizing Machined Surfaces of Turbine Components

Discussions were held this period with staff of Saint-Gobain Industrial Ceramics and Plastics regarding use of various NDE methods to characterize the as-produced surfaces. It is expected that next period several test samples will be have been received and tested.

2.0 Oxide-based Composites

A limited amount of work continued this period relative to NDE technology development for oxide-based ceramic composites. However, based on the excellent results being attained in the Solar Turbine tests, oxide composites continue to be a material system of potential usefulness.

3.0 NDE Technology for EBCs

Work continued on development of the Optical Coherence Tomography NDE device for characterizing the thickness of EBC coatings. The OCT system that was acquired from Saint Gobain Ceramics and Plastics, Northboro, Massachusetts was used to investigate a BSAS EBC on a SiC/SiC substrate. The sample, shown in Figure 4, was thermally cycled until failure.

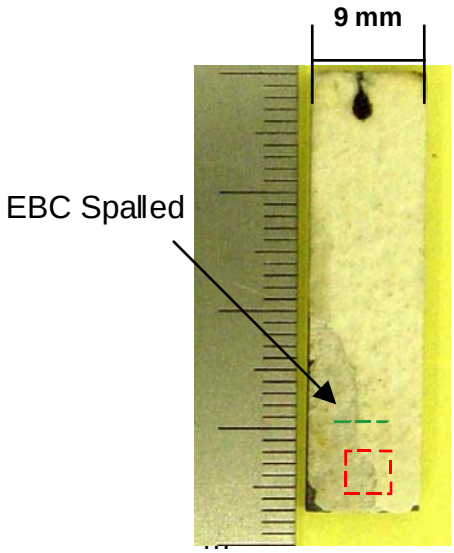

Fig. 4. EBC Test Sample with scan locations—vertical cross section indicated by green line, horizontal cross-sections indicated by red box

Three OCT images where acquired. A vertical cross-section was obtained in the approximate area of the green line in Figure 4. The OCT image is shown in Figure 5 and was compared to an optical micrograph cross section of the sample. The coating thickness measurement from the optical micrograph was about 0.29 mm as compared to the 0.25 mm measurement obtained from the OCT data.

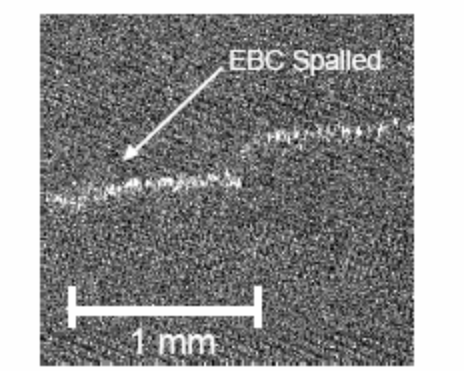

Fig. 5. Typical image obtained from OCT showing Vertical Cross-Section through BSAS EBC

Two horizontal cross-sections were obtained in the area approximated by the red box in Figure 4. One image, Fig. 6a, was obtained from a plane 20 µm below the surface and shows the EBC present in the right half of the image and the spalled region with no EBC present in the left half of the image. The second horizontal cross-section, Figure 6(b), was taken from the same location on the sample but from a plane 260 µm below the surface of the EBC. Using advanced signal processing methods to improve the signal-to-noise ratio, subsurface cracks were detected.

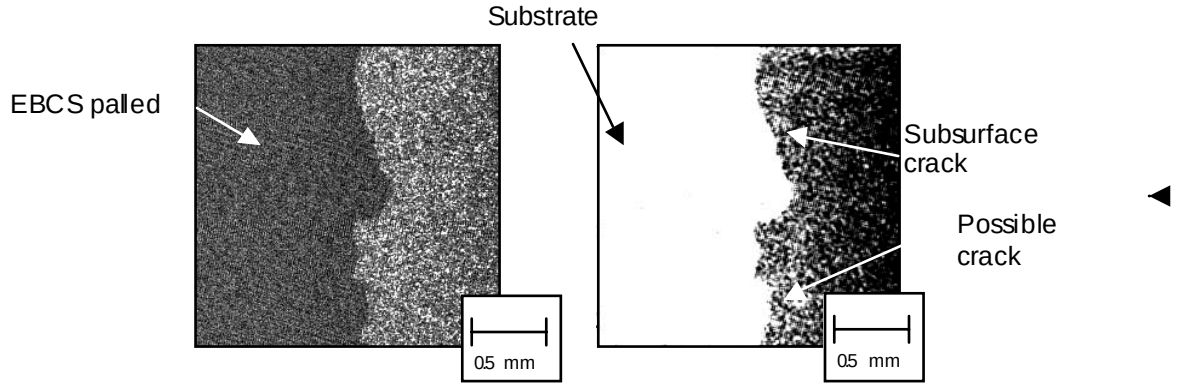

Fig. 6. OCT horizontal cross-sections taken of BSAS EBC.
(a) 20 µm below the EBC surface, and (b) 260 µm below the EBC surface.

Work continues on the OCT system to improve system robustness and signal-to-noise ratio for further investigation of EBCs.

Status of milestones

A. Demonstrate high-speed 3D-X-ray computed tomography to detect critical sized flaws in full-sized monolithic rotors. The new CMOS 80µm detector has allowed detection of necessary flaws. However, speed of reconstruction for 3D volumes is still too slow and work is progressing.

B. Complete installation of software for modeling laser scatter and demonstrate the ability to predict sensitivity of detection in EBCs. The software, Emflex, has been installed on a Sun Blade 100 computer. The "field-solver" software, based on Finite Element Analysis, is very complex and we are making headway.

C. Demonstrate detection of thermal shock damage for two A/N720 materials. This has not been done. Scheduled for 05/15/04.

Industry/National Lab Interactions

Additional discussions took place this period relative to interactions with others involved on the program. These included:

1. Discussions took place with staff from Saint-Gobain Industrial Ceramics and Plastics
2. Discussions continued with staff of Solar Turbines , Siemens-Westinghouse and COI relative to oxide/oxide composites
3. Discussions also continued with staff of Northwestern University relative to EBCs for monolithic materials

Problems encountered/resolved

The RID1620 large area x-ray detector has now been returned to service and is working well after repair and modification. We have also now have excellent results with the new large length, 36-inches, CMOS linear array detector.

Trips/meetings

1. W. A. Ellingson presented a paper to the DE sponsored meeting on Environmental Barrier Coatings for Microturbines and Industrial Gas Turbine Ceramics" held in Nashville, TN, November 18-19, 2003. The talk was titled " A Potential New NDE Tool for Characterizing EBCs and Reducing Engine Risk"

2. W. A. Ellingson gave an invited talk to the ASME International Mechanics Congress, held November 15-18, 2003, in Washington, DC. The paper was titled." Characterization of Thermally Cycled TBCs Using an Optical backscatter Method".

CHARACTERIZATION OF ADVANCED CERAMICS FOR INDUSTRIAL GAS TURBINE/ MICROTURBINE APPLICATIONS

Oxidation/Corrosion Characterization of Microturbine Materials

K. L. More and P. F. Tortorelli
Metals and Ceramics Division
Oak Ridge National Laboratory
P.O. Box 2008, Oak Ridge, Tennessee 37831-6064
Phone: (865) 574-7788, E-mail: morekl1@ornl.gov

Objectives

Characterization and corrosion analyses of Si_3N_4 materials provided to ORNL as part of the Hot-Section Materials/Component Development Program

Exposures of candidate Si_3N_4 materials to high water-vapor pressures (in Keiser Rig) to simulate high-temperature, high-pressure environmental effects associated with microturbines

Evaluate the reliability of environmental barrier coatings (EBCs) on silicon nitrides for selected microturbine applications

Highlight

During this reporting period, a second study of the microstructural stability of oxide/oxide composites in high water-vapor pressure environments was initiated for comparison with a similar set of exposures conducted at 1135°C. In this second study, the oxide/oxide composite material was subjected to long-term exposures (up to 3000 h) at 1200°C, 10 atm total pressure in a N_2-10%O_2-10%H_2O-6%CO_2 gas mixture used to simulate the combustion environment of a Capstone microturbine. Extensive microstructural and mechanical characterization will be conducted following each of 0, 1000, 2000, and 3000 h exposures.

Technical Progress

A furnace system that provides a high-temperature, high-pressure, low-flow-velocity (< 0.1 fps) mixed-gas environment (ORNL's Keiser Rig) is being used to conduct first-stage evaluations of ATK-COI Ceramic's (oxide fiber)/(oxide matrix) ceramic composite, A/N720. In a previous study, which was completed in FY 2003 (see DER Quarterly Reports for periods July 1, 2002 – September 30, 2002, October 1, 2002 – December 31, 2002, January 1, 2003 – March 31, 2003, and April 1, 2003 – June 30, 2003), the A/N720 was evaluated for Capstone Turbines in support of their Advanced Microturbine Systems Program. The oxide/oxide composite was subjected to long-term exposures (0-3000 h) in a simulated microturbine environment in the Keiser Rig at 1135°C, 10 atm total system pressure, and a N_2-10%O_2-10%H_2O-6%CO_2 gas

mixture. In the present work, the same oxide/oxide composite material is being exposed using the same parameters as used in the previous study except at a higher temperature of 1200°C.

For the study at 1200°C, 18 A/N720 specimens were submitted to ORNL for evaluation and exposure. Nine 1" X 7" bars (to be used for post-exposure tensile tests) and nine 1" X 2" coupons (to be used for post-exposure microstructural characterization and shear tests) were exposed in the first 1000 h exposure. The as-processed A/N720 was fully characterized (microstructurally and mechanically) in the previous study conducted at 1135°C (DER Quarterly Report January 1, 2003 – March 31, 2003). In addition, smaller samples were cut from the 1" X 2" coupons for TGA in both air and air+10% H_2O in the microbalance.

The first (1000 h) exposure of the A/N720 oxide/oxide composite material began on October 23, 2003 and ended December 5, 2003. At that time, all 18 exposed specimens were removed from the Keiser Rig, 6 specimens were selected and removed for the 1000 h microstructural characterization, and mechanical testing. The remaining 12 samples were put back in the Keiser Rig (in the exact same positions in tubes) for another 1000 h exposure (to accumulate 2000 h total on second set of samples). The second 1000 h exposure began on February 13, 2004 and will end on March 26, 2003 at which time another 6 samples exposed for 2000 h will be removed from the test for microstructural characterization and mechanical testing. The remaining 6 A/N720 coupons will be exposed for 3000 h in the Keiser Rig.

Results from A/N720 post-exposure mechanical testing in tension are shown in Figure 1. These data compare the tensile strength of the as-processed A/N720 to the A/N720 exposed for 1000, 2000, and 3000 h at 1135°C and A/N720 exposed for 1000 h at 1200°C. As can be seen from Figure 1, no statistical differences were observed for the tensile strength of any of the exposed material (either 1135°C or 1200°C) and no strength decrease occurred during exposure due to high water vapor pressure or elevated temperature.

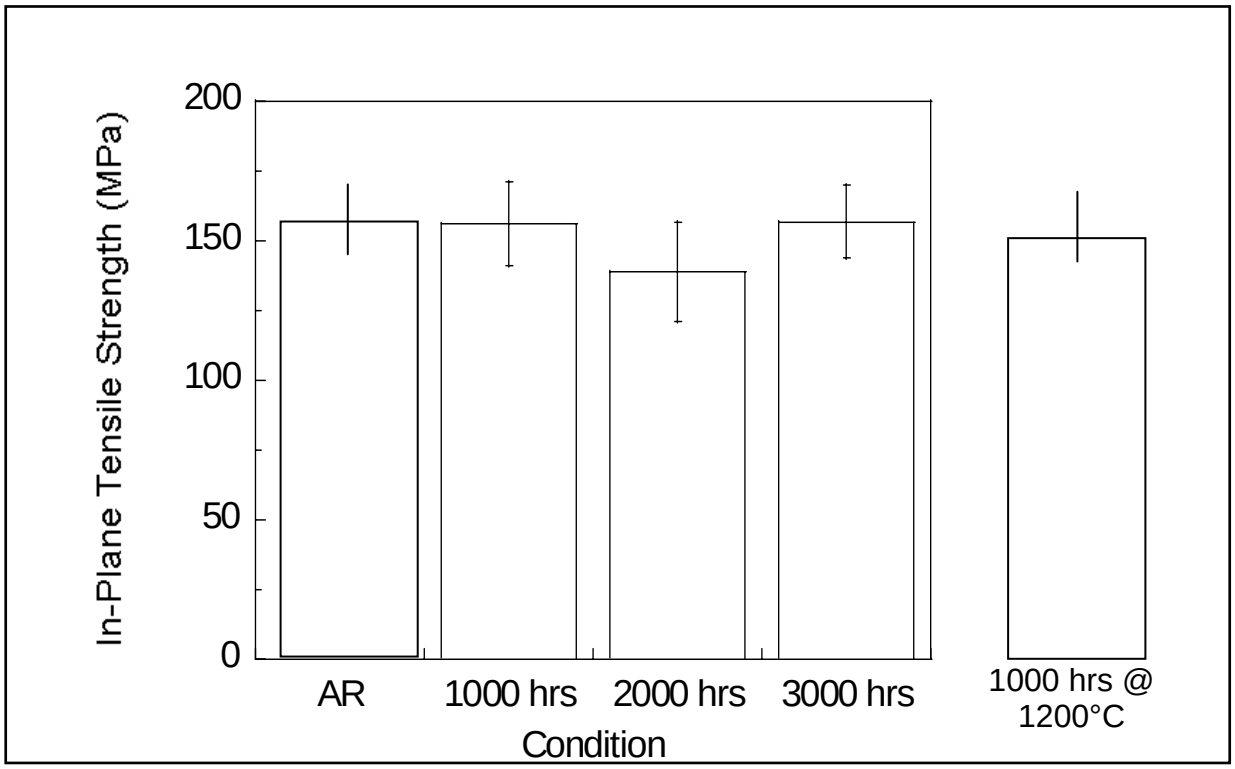

Figure 1. Tensile strength results for A/N720 oxide/oxide composites comparing as-processed to material exposed for up to 3000 h at 1135°C and 1000 h at 1200°C in ORNL's Keiser Rig.

Status of Milestones

08/2003 Report results of initial evaluation of "new" Si_3N_4 materials from Saint-Gobain and Kennametal exposed in the Keiser Rig for two temperatures and two water-vapor pressures.
Milestone is completed. Reports/summaries have been given to both Kennametal and St. Gobain regarding exposures of Si_3N_4 and Sialon materials in the Keiser Rig at 1200°C and two different water-vapor pressures.

07/2004 Compile and report the results of the evaluation and comparison of uncoated Si_3N_4 (manufactured by Honeywell, Kyocera, St. Gobain, and Kennametal) exposed in the Keiser Rig for two different temperatures and two water-vapor pressures after 1000 h exposure.
Work is currently in progress.

Industry Interactions

Initiated new exposures of ATK-COI Ceramics, Inc. A/N720 oxide/oxide composite material at 1200°C. Work is being done in collaboration with Andy Szweda of ATK-COI Ceramics, Inc.

Met with Ara Vartebedian (St. Gobain) and Russ Yeckley (Kennametal) to review data from Keiser Rig exposures of Si_3N_4 and Sialon materials. Meetings were held during the EBC Workshop in Nashville, TN, November 18-19, 2003.

Problems Encountered

None

Publications/Presentations

K. L. More and P. F. Tortorelli, "Evaluation of EBCs in ORNL's Keiser Rig," presented at the EBC Workshop in Nashville, TN, November 6-7, 2002.

K. L. More, P. F. Tortorelli, and L. R. Walker, "Verification of an EBC's Protective Capability by First-Stage Evaluation in a High-Temperature, High-Pressure Furnace," ASME Paper #GT2003-38923. Presentation made at IGTI Turbo Expo 2003 in Atlanta, GA from June 15-19, 2003.

P. F. Tortorelli and K. L. More, "Evaluation of EBCs in the Keiser Rig," presented at the EBC Workshop in Nashville, TN, November 18-19, 2003.

Mechanical Characterization of Monolithic Silicon Nitride Si_3N_4

R. R. Wills, M. Pierson, S. Hilton, and S. Goodrich
University of Dayton Research Institute
300 College Park, KL-165, Dayton, OH 45469-0162
Phone: (927) 229-4341, E-mail: roger.wills@udri.udayton.edu

Objective

The objective of this project is to work closely with microturbine materials suppliers to characterize monolithic ceramics and provide the data obtained to microturbine manufacturers via a Web site database. User-friendly software, that will allow prospective users to readily compare different silicon nitrides, will also be developed. This project consists of the following four tasks:

- Task 1: Evaluate Strength and Slow Crack Growth of New Materials
- Task 2: Modify Six Existing Creep Frames to Allow Introduction of Water Vapor
- Task 3: Evaluate the Effects of Water Vapor Upon Honeywell's Silicon Nitride Ceramics
- Task 4: Develop "User Friendly" Software for Searching Existing Mechanical Properties Database

Task 1 is motivated by the materials needs of Ingersoll-Rand (IR) Energy Systems, General Electric, and UTRC. The ceramic materials being considered by IR Energy Systems include Kyocera's SN-235 and SN-237 for which the required mechanical property data are somewhat limited. In the case of the UTRC microturbine, Si-SiC is a prime candidate for the combustor. Consequently, Task 1 will focus on the generation of key mechanical property data for these materials with emphasis on strength (and strength distribution), time dependent failure (evaluated using dynamic fatigue), elastic properties, and fracture toughness.

In FY 2003, baseline mechanical property data will be measured for materials supplied by Kennametal and St. Gobain Advanced Ceramics as part of their materials development effort funded by ORNL. The initial focus will be on measuring flexure strength as a function of temperature and stressing rate.

In Task 2, two approaches for environmental testing will be considered. The first method, which was previously used on two test frames, involves the uniform injection of steam into the furnace cavity. The primary advantage of this arrangement is that extensometry can still be used to evaluate creep deformation. The second approach utilizes a small ceramic tube to inject water directly onto the gage section of the buttonhead specimen. This approach will be evaluated in FY2003 using SN-281 buttonhead specimens.

Task 3 is currently on hold due to the unavailability of material.

In FY 2003 in Task 4 the data sets generated at ORNL will be added to the UDRI Web site.

Highlights

Very little work this period was done as the contract ended and a final report was written. Support work for General Electric was completed and Roger Wills attended the EBC workshop in Nashville. Input was obtained from General Electric and United Technologies on the proposed statement of work for the new contract.

Microstructural Characterization of CFCCs and Protective Coatings

K. L. More and P. F. Tortorelli
Metals and Ceramics Division
Oak Ridge National Laboratory
P.O. Box 2008, Oak Ridge, Tennessee 37831-6064
Phone: (865) 574-7788, E-mail: koz@ornl.gov

Objectives

Characterization of CFCC materials and CFCC combustor liners after exposure to simulated (ORNL's Keiser Rig) and actual (engine tests) combustion environments

Exposures of candidate environmental barrier coatings (EBCs) to high water-vapor pressures (in Keiser Rig) to determine thermal stability and protective capability

Work with CFCC and coating suppliers/manufacturers to evaluate new/improved ceramic fibers, protective coatings, and composite materials

Highlights

During this quarter, work was initiated in collaboration with UTRC to expand the use of the Keiser Rig by operating at very high H_2O pressures (~20 atm) to evaluate volatilization of candidate EBCs. This work is being undertaken primarily to understand the mechanism(s) of BSAS recession in gas turbine and microturbine combustors.

Technical Progress

Volatilization of ceramics can be the life-limiting factor for the use of these materials in combustion environments, where high temperatures, elevated oxidizing potentials, and significant gas-flow velocities exacerbate the process. This degradation mechanism has been shown to be of specific relevance for SiC and Si_3N_4, where SiO_2 forms by oxidation and then readily reacts with environmental H_2O to form volatile species.[1,2,3] Of the various volatilization reactions, the one forming $Si(OH)_4$,

$$SiO_2 + 2H_2O = Si(OH)_4, \quad (1)$$

has been shown to be predominant in combustion environments.[3] It is therefore of interest to examine the various factors involved in volatilization under oxidizing conditions as part of studies that are aimed at developing and characterizing materials that are stable at the high water-vapor pressures associated with various combustion conditions.

For the present purposes, it is assumed that the release of a volatile species is controlled by diffusion through a gaseous boundary layer adjacent to the solid oxide surface under laminar-flow conditions. These assumptions have been shown to be appropriate for combustion associated with moderate gas-flow velocities (order of 40 m/s) [3] and should also apply to the slow-flow, large-

diameter, flat-specimen conditions of the Keiser Rig. Thus, the mass flux associated with volatilization, **J**, can be described as [3]

$$\mathbf{J} \alpha (\rho' \nu L/\eta)^{1/2}(\eta/\rho' D)^{1/3}(D\rho/L) \quad (2)$$

where ν is the linear gas velocity, η is the gas viscosity, D is the interdiffusion coefficient of the volatile species in the major gas component, ρ is the concentration of the volatile species at the solid-gas interface, ρ' is the concentration of the major gas component, and L is the characteristic specimen length parallel to the flow direction and over which the volatility is averaged.

For the conditions associated with the Keiser Rig, eq. (2) reduces to

$$\mathbf{J} \alpha (\nu^{1/2} \bullet \Sigma p_{vol})/\sqrt{p_{tot}} \quad (3)$$

where p_{vol} is the partial pressure of a volatile species and p_{tot} is the total system pressure.

For the present case in which the primary interest is in volatilization of oxides in the presence of water vapor, the formation of a volatile hydroxide product, $A_xO_{y+z}H_{2Z}$, can be generally represented as

$$A_xO_y\,(s) + zH_2O\,(g) = A_xO_{y+z}H_{2Z}\,(g) \quad (4)$$

The equilibrium constant for this reaction, K_4, can be expressed in terms of the activity of the oxide, a_{AxOy}, and partial pressures as

$$K_4 = p_{A_xO_{y+z}H_{2z}}/(p^z_{H_2O} \bullet a_{A_xO_y}) \quad (5)$$

and is related to the free energy of formation of $A_xO_{y+z}H_{2Z}$, $\Delta G_{A_xO_{y+z}H_{2z}}$:

$$K_4 = \exp(-\Delta G_{A_xO_{y+z}H_{2z}}/RT) \quad (6)$$

where T is the absolute temperature and R is the gas constant.

Combining (5) and (6) yields

$$p_{A_xO_{y+z}H_{2z}} = \exp(-\Delta G_{A_xO_{y+z}H_{2z}}RT) \bullet p^z_{H_2O} \bullet a_{A_xO_y.} \quad (7)$$

Assuming the reaction shown in (4) generates the only volatile species and using eq. 3, the mass flux of volatile species can be described as

$$\mathbf{J} \alpha \nu^{1/2} \bullet \exp(-\Delta G_{A_xO_{y+z}H_{2z}}/RT) \bullet p^z_{H_2O} \bullet a_{A_xO_y}/\sqrt{p_{tot}} \quad (8)$$

A flux equation of the form shown in eq. 8 has been shown to describe measurements of SiC and Si_3N_4 recession controlled by volatilization of SiO_2 quite well.[1,2] However, at low gas-flow velocities and modest pressures, as employed in many laboratory experiments, specimen mass losses due to volatilization are small (eq. 8) and, thus, difficult to measure, particularly because of large mass gains

due to accelerated solid-state oxidation at elevated p_{H_2O}.[4] This was the case for experiments normally conducted in the Keiser Rig, which focused on the effects of elevated H_2O pressures (typically 1.5 atm., which is representative of those found in combustors) on oxidation of Si-based ceramics and environmental barrier coatings.[4,5,6] However, as shown by eq. 8, mass fluxes for a given ν can be increased substantially by using higher H_2O pressures, particularly if $z \geq 1$.

An example of how higher H_2O pressure can be used to generate more readily measurable mass fluxes can be gotten from the case of SiO_2 (eq. 1), where, from eqs. 4 and 8,

$$\mathbf{J} \overset{\alpha}{} \nu^{1/2} \bullet \exp\left(-\Delta G_{Si(OH)_4}/RT\right) \bullet p^2_{H_2O} \bullet a_{SiO_2}/\sqrt{p_{tot}} \qquad (9)$$

and $a_{SiO_2} = 1$. Relatively high fluxes of $Si(OH)_4$ can be achieved by increasing p_{H_2O} because **J** is proportional to the square of the water-vapor pressure. Therefore, if there is no change in mechanism, low gas-flow velocities can be offset by higher p_{H_2O}. This is illustrated in Fig. 1., which plots $\mathbf{J}/\mathbf{J}_o$ versus p_{H_2O} for the case represented by eq. 9 where $\mathbf{J}_o$ is the $Si(OH)_4$ flux for typical combustor liner conditions (ν = 35 m/s, p_{H2O} = 1.5 atm, T = 1200°C) and **J** is for the same temperature with $\nu = 6X10^{-4}$ m/s (typical gas-flow velocity in the Keiser Rig). Note from Fig. 1 that the normalized flux can be increased by approximately two orders of magnitude by increasing p_{H_2O} from 1.5 (pressure typically used in a Keiser Rig) to 20 atm.

The results shown in Fig. 1 show that the high-temperature, high-pressure capability offered by a Keiser Rig or similar exposure facility can be used to yield relatively high volatility fluxes by conducting experiments at substantially higher water-vapor pressures. As such, this approach can be used to screen the volatility resistance of candidate cermics for use in combustin environments as bulk mateirals or protective surface layers (such as needed in environmental barrier coating systems). However, such use is predicated on no change in the rate-controlling volatiilization mechanism as the water-vapor pressure is increased. Given the nature of the process described above (diffusion of volatile product across a laminar gas-boundary region), it is not expected that changes in pressures over the range indicted in Fig. 1 would result in a mechanism change.

Referring to eq. 8, it is important to note that the ability to use higher water-vapor pressures to screen the volatilization resistance of candidate materials in systems using low gas-flow velocities depends critically on z, the number of moles of H_2O needed to form one mole of volatile product (see eq. 4). A low z value would make it more difficult to achieve easily measurable volatile fluxes by increasing the water-vapor pressure over a reasonable range. As an example, the difference in the normalized flux between z=1 and z=2 is shown in Fig. 2 for $\nu = 6 \times 10^{-4}$ m/s and 1200°C. While there is about an order of magnitude increase in the volatile flux when p_{H2O} is increased from 1.5 to 20 atm, this enhancement is still about 10x less than for z=2. Therefore, it is important to understand the nature of the predominant volatility reaction (eq. 4) to determine if p_{H_2O} elevation will yield the desired measurements and to effectively compare relative results for J for different oxides.

Besides z, there are other factors that need to be considered in analyzing volatility results from such experiments. As shown in eq. 3, the total volatile flux is a sum of all potential reactions, so it is possible to have measured values that are not specific to one species if there are several products with comparable vapor pressures. This can be the case for complex mixed oxides with different z values and/or that form oxides as well as hydroxides with high vapor pressures. Strict interpretation of such results from such mixed oxides will also be complicated by uncertainties in the activities of the various components (see eq. 8) as these may be far from what is expected for regular or ideal solution behavior.

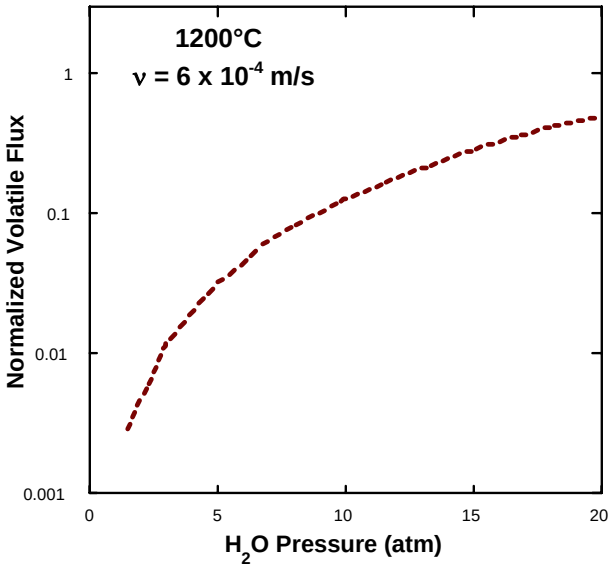

Fig. 1. Plot of flux of $Si(OH)_4$ due to volatilization of SiO_2 in an H_2O-containing environment at 1200°C, a total pressure of 20 atm, and a gas-flow velocity of 6 x 10^{-4} m/s as a function of the partial pressure of H_2O.

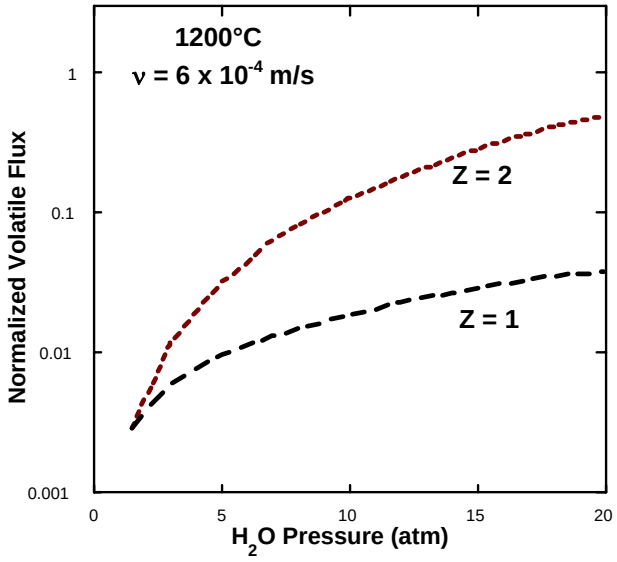

Fig. 2. Plot of flux of a volatile species in an H_2O-containing environment at 1200°C, a total pressure of 20 atm, and a gas-flow velocity of 6 x 10^{-4} m/s as a function of z and of the partial pressure of H_2O.

References:

1. J.L.Smialek, R.C. Robinson, E.J. Opila, D.S. Fox, and N.S. Jacobson, *Adv. Composite Mater*. **8** (1999) 33-45.

2. R.C. Robinson and J.L. Smialek, *J. Am. Ceram. Soc*. **82** (1999) 1817-25.

3. E..J. Opila, J.L.Smialek, R.C. Robinson, D.S. Fox, and N.S. Jacobson, *J. Am. Ceram. Soc.* **82** (1999) 1826-34.

4. K.L. More, P.F. Tortorelli, M.K. Ferber, L.R. Walker, J.R. Keiser, W.D. Brentnall, N. Miriyala, and J.R. Price, *J. Eng. Gas Turbines and Power* **122** (2000) 212-18.

5. P.F. Tortorelli and K.L. More, *J. Am. Ceram*. Soc. **86** (2003) 1249-55.

6. K.L. More, P.F. Tortorelli, and L.R. Walker, ASME Paper #GT2003-38923.

Status of Milestones

04/03 Milestone — Prepare a report and present results on the evaluation of the set of 15,000 h Malden Mills engine-tested combustor liners.

This milestone has been completed. Results from the study were presented at a closed meeting with Solar Turbines, United Technologies Research Center, Argonne National Laboratory, and ORNL during the 27th Annual Ceramics and Composites Conference in Cocoa Beach, FL on January 29, 2003. A manuscript was prepared by Solar Turbines, Inc., which summarizes these results. ASME Paper #GT-2003-38920, "The Evaluation of CFCC Liners After Field Testing in a Gas Turbine – IV," by J. Kimmel, J.R. Price, K.L. More, P.F. Tortorelli, E.Y. Sun, and G.D. Linsey, was presented at IGTI Turbo Expo 2003 in Atlanta, GA, June 15-19, 2003.

09/03 Milestone — Complete first-stage evaluations of the effects of water vapor on the oxidation of at least two new candidate compositions for protective coatings.

This milestone has been completed. EBCs supplied by UTRC, Honeywell Ceramic Components, Northwestern University, SMAHT Ceramics, Inc., and University of Colorado have been exposed in the Keiser Rig. Results from these exposures have been reported to the individual coating producers. Some results were published in paper by K.L. More, P.F. Tortorelli, and L.R. Walker, "Verification of an EBC's Protective Capability by First-Stage Evaluation in a High-Temperature, High-Pressure Furnace," ASME Paper #GT-2003-38923

06/04 Milestone — Prepare a report and present results on the evaluation of oxide/oxide composite materials exposed in the Keiser Rig for use as microturbine or stationary gas turbine combustor liners. (June 2004)

This milestone is in progress. ATK-COI Ceramics, Inc. oxide/oxide composite material, A/N720, is currently being exposed under simulated microturbine exhaust conditions in ORNL's Keiser Rig at 1200°C for 3000 h. Results are completed for exposure of the same material for 3000 h @ 1135°C.

Industry Interactions

Visited with T. Bhatia, G.D. Linsey, and J. Holowzak, at UTRC, East Hartford, CT, to discuss collaboration on expanding the use of the Keiser Rig to evaluate volatilization of BSAS EBCs (10/03). T. Bhatia also visited ORNL on Nov. 20, 2003 to discuss progress on this collaboration.

Attended 3rd Annual UEET Program Technology Forum in Westlake, OH.

Currently working with Andy Szweda of ATK-COI Ceramics, Inc. to expose A/N720 CFCC material in Keiser Rig at 1200°C.

Currently working with Rama Nageswaran of SMAHT Ceramics, Inc. on the exposure of candidate EBC compositions in the Keiser Rig.

Currently working with Rishi Raj, University of Colorado, on the exposure of SiCN EBCs in the Keiser Rig.

Problems Encountered

None

Publications/Presentations

1. K.L. More and P.F. Tortorelli, "Evaluation of EBCs in ORNL's Keiser Rig," presented at the EBC Workshop in Nashville, TN, November 6-7, 2002.
2. K.L. More, P.F. Tortorelli, L.R. Walker, H.E. Eaton, E.Y. Sun, G.D. Linsey, J.B. Kimmel, N. Miriyala, and J.R. Price, "Evaluating EBCs on Ceramic Matrix Composites After Engine and Laboratory Exposures," presented at IGTI Turbo Expo 2002, Amsterdam, June 3-6, 2002. ASME Paper #GT-2002-30630. Selected for publication in *Journal Engineering for Gas Turbines and Power*. This paper won the Best Paper Award for Ceramics Division.
3. K.L. More and P.F. Tortorelli, "The High-Temperature Stability of SiC-Based Composites in High Water-Vapor Pressure Environments," *Journal of The American Ceramic Society*, **86**[8] 1272-81 (2003).

4. P.F. Tortorelli and K.L. More, "Effects of High Water-Vapor Pressure on Oxidation of SiC at 1200°C," *Journal of The American Ceramic Society*, **86**[8] 1249-55 (2003).
5. K.L. More, P.F. Tortorelli, and L.R. Walker, "Verification of an EBC's Protective Capability by First-Stage Evaluation in a High-Temperature, High-Pressure Furnace," ASME Paper #GT-2003-38923. Presented at IGTI Turbo Expo 2003 in Atlanta, GA, June 16-19, 2003
6. J.B. Kimmel, J.R. Price, K.L. More, P.F. Tortorelli, E.Y. Sun, and G.D. Linsey, "The Evaluation of CFCC Liners After Field Testing in a Gas Turbine – IV," ASME Paper #GT-2003-38920. Presented at IGTI Turbo Expo 2003 in Atlanta, GA, June 16-19, 2003.
7. P.F. Tortorelli and K.L. More, "Evaluation of EBCs in the Keiser Rig," presented at the DER EBC Workshop, Nashville, TN, Nov. 18-19, 2003.